THESIS FOR THE DEGREE OF DOCTOR OF PHILOSOPHY IN NATURAL SCIENCE,
SPECIALISING IN CHEMISTRY

Formation and Transformation of Atmospheric Brown Carbon (BrC)

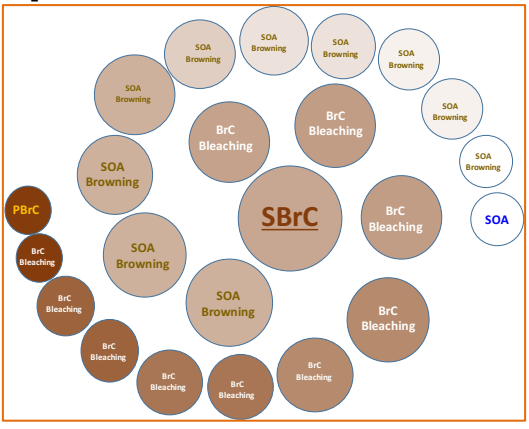

Kalyan Mitra

UNIVERSITY OF GOTHENBURG
Department of Chemistry and Molecular Biology
University of Gothenburg
Gothenburg, Sweden

Formation and Transformation of Atmospheric Brown Carbon (BrC)

Atmospheric Science,
Department of Chemistry and Molecular Biology,
University of Gothenburg,
SE-412 96 Gothenburg,
Sweden

ISBN: 978-91-8069-xxx-x (PRINT)
ISBN: 978-91-8069-xxx-x (PDF)

Printed by Stema AB
Borås, Sweden 2022

Cover picture: Drawing of atmospheric BrC formation and transformation processes

The comical story that always keeps me grounded

A scientist investigating behavior in bullfrogs notices that when startled by a loud noise the frog jumps.

Deciding to experiment further he yells "Jump" and notes that the frog jumps a distance of 4 feet.
He then cuts off a front leg, yells jump and the frog jumps 3 feet.
He cuts off the other front leg, yells jump; the frog jumps 2 feet.
He cuts off a back leg, yells jump; the frog barely manages to jump 6 inches.
Cutting off the last leg when he yells jump the frog doesn't move. He yells louder; the frog doesn't move.

In his notebook the scientist concludes: "A frog with no legs becomes deaf."

– ***Anonymous***

CONTENTS

List of Abbreviations

3C*	*Organic compounds in triplet excited states*
AAE	*Ångström absorption exponent*
ALW	*Aerosol liquid water*
AOD	*Aerosols' optical depth*
APM	*Aerosol Particle Mass Analyzer*
aqSOA	*Aqueous SOA*
AS	*Ammonium sulfate*
B_{abs}	*Absorption Coefficient*
BB	*Biomass burning*
BB-POA	*Biomass burning- Primary organic aerosol*
BC	*Black carbon*
BG	*Biogenic*
BrC	*Brown carbon*
B_{scat}	*Light Scattering Coefficient*
CIMS	*Chemical ionization mass spectrometry*
CPC	*Condensation Particle Counter*
CPS	*Count per second*
d/p ratio	*Diffusion-to-premixing air ratio*
DMA	*Differential Mobility Analyzer*
DT	*Dilution Tunnel*
FF	*Fossil fuel*
FIGAERO	*Filter Inlet for Gases and AEROsols*
Go:PAM	*The Gothenburg Potential Aerosol Mass Chamber*
HR-ToF-CIMS	*High-resolution chemical ionization mass spectrometry*
HULIS	*Humic like substances*
IGP	*Indo-Gangetic Plains*
IGP-CARE	*Indo-Gangetic Plains – Centre for Air Research and Education*
IMR	*Ion Molecule Reaction*
m/z	*Mass/Charge*
MAC	*Mass absorption cross-section*
MFC	*Mass Flow Controllers*
MSC	*Mass Scattering Coefficient*
MW	*Molecular weight*
NAC	*Nitro-aromatic compounds*
NOC	*Nitrogen-containing organic compounds*
NOx	*NO_2 + NO*
NP	*Nitrogen-poor*
NR	*Nitrogen-rich*
NTD	*No thermo-denuder*
OA	*Organic aerosol*
OFR	*Oxidation flow reactor*
PAH	*Polycyclic aromatic hydrocarbons*
PASS-3	*Three-wavelength photo acoustic soot spectrometer*
PBLH	*Planetary boundary layer height*
PBrC	*Primary brown carbon*
PMF	*Positive Matrix Factorization*
POA	*Primary organic aerosol*
ppb	*Parts Per Billion*
ppbv	*Parts Per Billion per volume*
PSCF	*Potential Source Contribution Function*
R^2	*Regression coefficients*
RH	*Relative Humidity*
SBrC	*Secondary brown carbon*
SLCPs	*Short-lived climate pollutants*
SMPS	*Scanning Mobility Particle Sizer*
SOA	*Secondary organic aerosol*
TD	*Thermo-Denuder*
UV	*Ultra Violet*
VOC	*Volatile Organic Compound*
VS	*Ventilation coefficient*
VTDMA	*Volatility tandem differential mass–mobility analyzer*
WS	*Wind speed in the boundary layer*
ΔHC	*Consumed Hydrocarbons*

List of Figures

List of Tables

Abstract

Atmospheric brown carbon (BrC) aerosol absorbs light in the UV-Vis spectrum and has poorly constrained but potentially large climate forcing impacts. Most current climate models lack detailed chemistry and interlinked properties of atmospheric BrC, that induce large uncertainties in radiative forcing predictions. BrC lifecycle and its atmospheric lifespan have not been fully explored. It is suggested that strongly light absorbing primary BrC (PBrC) may rapidly evolve into weakly light absorbing secondary BrC (SBrC) in the atmosphere, which is considered as bleaching of PBrC. Therefore, formation, transformation and optical properties of PBrC from biomass and fossil-fuel combustion system were investigated in lab and field studies. On the other hand, non-absorbing secondary/primary organic aerosol (SOA/POA) evolve into weakly light absorbing SBrC referred as browning of SOA/POA. The chemical processes underlying SOA aging and the subsequent formation and transformation of SBrC are not well understood. The presence of reactive nitrogen, acidity and water is also thought to further drive the chemistry of SBrC evolution and hence contribute to the global radiative forcing budget. These possibilities, and others, were explored in detail and are presented in this PhD thesis.

Biomass is a major source of PBrC emissions, but also it is an important renewable bioenergy source because of its economic and environmental advantages over fossil fuels. The formation of PBrC and its optical properties in a modern Swedish small-scale biomass burner were explored. The measured parameters include gas and particle concentrations, optical absorption and chemical characteristics of gases and particles. Positive matrix factorization (PMF) was performed to analyze data from a HR-ToF-CIMS equipped with FIGAERO and PASS-3. Results from the factor analysis were linked to the optical properties of the emissions, and lignin and cellulose/hemicellulose pyrolysis products were the most important sources of PBrC under the tested burning conditions.

Further, formation of PBrC and its atmospheric transformation was studied at a remote rural site, the Indo-Gangetic Plains – Centre for Air Research and Education (IGP-CARE) in India,in the Indo Gangetic Plain in India where some of the most severe air pollution episodes occur on Earth. The field measurements of short-lived climate pollutants including BrC, black carbon (BC) and ozone (O_3) were conducted over a period of one year. In this study, the elevated concentrations of BrC co-emitted BC were identified, which was mostly PBrC and can largely be attributed to the local biomass burning activities in the neighbouring rural communities. This study's most important finding is that the BrC concentration normalized by BC concentration (BrC/BC ratio) showed a very pronounced diurnal variation throughout the year with distinct morning and evening peaks in general and a minimum at around noon time i.e. boat shape pattern of BrC/BC. The profile of the BrC/BC ratio evolved astonishingly during the day-time. An extremely sharp decline in the BrC/BC ratio at the time of dawn each morning indicates the dominance of photochemical processes in the transformation of PBrC. This is hypothesized to be associated with daytime photochemical bleaching of the PBrC and transforming it into SBrC.

PBrC formation and its optical properties were investigated in three distinct premixed fossil-fuelled i.e. propane, flames. POA containing BrC constituted a high fraction (20–40% by mass) of aerosol mass and was predominantly (i.e., 92–97% by mass) internally mixed with soot particles. In these flames, aerosol mixture containing BrC, POA and BC was found to be highly light absorptive, i.e., an Ångström absorption exponent (AAE) value at 405/781 nm > 1.5. The mass absorption cross-section (MAC - 5 m^2g^{-1}) of POA containing BrC at 405 nm under a specific flame i.e. fuel-rich setting, was comparable to MACs of BC particles (8–9 m^2 g^{-1}).

SBrC formation, transformation and its optical properties were explored under the influence of reactive nitrogen (NOx, NH_3)-, acidity (H_2SO_4)-, and water-mediated chemistry during the photo-oxidation of toluene and subsequent aging of its SOA. The pattern of toluene SOA formation at [NOx]/[ΔHC] molar ratios 0.15 or below was distinctly different (i.e. constant SOA mass) than that was observed at [NOx]/[ΔHC] ratios higher than 0.15 (i.e. here, SOA mass decreased). These distinguish between SOA formed under nitrogen-poor (NP) conditions i.e. with low initial NOx concentrations, and nitrogen-rich (NR) SOA formed at higher initial NOx concentrations, which has a higher content of compounds such as organo-nitrates. This distinction is valuable for understanding trends in the formation and properties of SOA containing BrC in the presence of varying concentrations of NOx. Hereafter, NP SOA and NR SOA are referred to SOA formed under nitrogen poor and nitrogen rich conditions, respectively. The light absorption coefficient (B_{abs}) and mass absorption cross-section (MAC) of the SOA increased with [NO_x/ΔHC] under both the NP and NR regimes. For NP SOA, the MAC increased with [NO_x/ΔHC] independently of the relative humidity (RH). However, the MAC of NR SOA was RH-dependent. Under both NP and NR regimes, NH_3 and acidity promoted SOA browning. The highest MAC was observed at the lowest RH (20%) for acidic NR SOA, and it was postulated that the MAC of SOA depends mainly on the pH and the $[H^+]_{free}$/[SOA mass] ratio of the aqueous SOA phase.

In the same preceding experiments, I additionally analyzed data from HR-ToF-CIMS. I found that several m/z (i.e. mass to charge ratio of a chemically ionized molecule detected in mass spectrometry) mimicked the trend of observed bulk B_{abs} – against [NO_x/ΔHC] increase, of SOA containing BrC. These m/z hereafter termed BrC molecules containing chromophores. An interesting observation was that the key m/z contributing to the B_{abs} were distinct for each experiment. However, we found m/z 296 as a common dominant BrC chromophore (m/z), under several experimental conditions. The RH played a vital role in determining the BrC composition i.e. m/z distribution. The BrC molecules containing chromophores corresponding to various identified m/z are suggested to be nitro-aromatic compounds (NAC), which are primarily formed via OH oxidation of toluene followed by the nitration processing of the oxidized aromatic ring. The suggested key BrC molecules containing chromophores are the nitro-derivatives of the phenols, catechol, benzoic acid, benzaldehyde and benzonitriles.

Keywords: brown carbon (BrC), primary organic aerosol (POA), secondary organic aerosol (SOA), BrC bleaching, BrC browning, Toluene photo-oxidation, NOx, NH_3 and acidity effects, light absorption.

Abstract (in Swedish)

Atmosfäriska aerosolpartiklar som innehåller brunt kol (BrC) absorberar ljus i UV-Vis-området. Detta gör att deras klimatpåverkan potentiellt kan vara väldigt stor även om den idag är dåligt kvantifierad. I de flesta av dagens klimatmodeller saknas detaljerade kemin med koppling till dessa egenskaper för atmosfärisk brunt kol. Detta innebär en stora osäkerheter i modellernas förutsägbarhet att beskriva strålningsbalansen. BrC atmosfäriska livscykel, m.a.o. bildning och omvandling, kan inte beskrivas fullt ut. Å ena sidan har det påpekats att den stark absorberande primära BrC (PBrC) kan omvandlas i atmosfären till mindre absorberande sekundär BrC via så kallad blekning. Därför studerades bildning, omvandling och optiska egenskaper för PBrC emitterad från förbränning av biomassa och fossila bränslen. Detta genomfördes både i fält- och laboratorieförsök. Å andra sidan kan icke absorberade sekundär (SOA) eller primär organisk aerosol (POA) omvandlas till svagt ljusabsorberande SBrC via så kallad ”browning” av SOA/POA. De kemiska processerna som ligger bakom denna omvandling/åldring av SOA är inte så väl karakteriserade. Dock tror man att närvaro av kväve, surhet och fuktighet driver på kemin för BrC processerna och därmed påverka den global strålningsbalansen. De är dessa möjligheter tillsammans med andra faktorer som har utforskats och nu presenteras i denna doktorsavhandling.

Biomassaförbränning bidrar mycket till PBrC men har ekonomiska och miljömässiga fördelar framför fossila bränslen. Här studerades PBrC emissioner från en modern svensk biomassaförbrännare. De studerade parametrarna inkluderar gas- och partikelkoncentrationer, optisk absorption och kemiska egenskaper hos gaser och partiklar. Positiv matrisfaktorisering utfördes för att analysera data från en högupplöst kemisk joniseringsmasspektrometer (HR-ToF-CIMS) utrustad med ett filterinsläpp för gaser och aerosoler (FIGAERO) tillsammans med data från en fotoakustisk sotspektrometer med tre våglängder (PASS-3). Resultatet från faktoranalysen kopplades till emissionernas optiska egenskaper där lignin och cellulosa/hemicellulosa pyrolysprodukter var de viktigaste källorna till PBrC under de testade förbränningsförhållandena.

Bildningen av PBrC och dess omvandling studeras även vid Indo-Gangetic Plains – Center for Air Research and Education (IGP-CARE) som är en lantligt och avlägsen plats i Indien. Här påträffas oftast episoder med några av jordens mest extrema halter av luftföroreningar. Fältmätningar av kortlivade klimatföroreningar inklusive BrC, svart kol (BC) och ozon (O_3) genomfördes under ett år. Här identifierades förhöjda koncentrationerna av BrC och BC, vilket till stor del kan hänföras till den lokala biomassaförbränningen i närliggande landsbygdssamhällen. De viktigaste resultaten från studien är att den BC normaliserade BrC-koncentrationen (BrC/BC-förhållande) påvisade en mycket uttalad dygnsvariation under hela året med distinkta morgon- och kvällstoppar i allmänhet och ett minimum runt middagstid, dvs. en slags båtformsmönster över dygnet. Den extremt kraftiga minskningen av BrC/BC-förhållandet vid gryningen varje morgon indikerar betydelsen av fotokemiska processer i omvandlingen av BrC. Detta kan antas vara associerat med fotokemisk blekning av PBrC.

PBrC bildningen och dess optiska egenskaper studerades vid tre olika bränsleblandningar för en propanlåga. Emissionen av primär organisk aerosol (POA) utgjorde en hög andel

(20–40 viktprocent) vid förbränning av propan och den var övervägande (dvs. 92–97 viktprocent) internt blandad med BC.
För dessa förbränningsförhållanden var partikelemissionerna som innehöll BrC, POA och BC mycket ljusabsorberande, d.v.s. har en Ångström absorptionsexponent (AAE) vid 405/781 nm >1.5. Massabsorptionstvärsnitt (MAC) var 5 m^2 g^{-1} för POA vid 405 nm för en av sammansättningarna (fet bränsleblandning) vilket är jämförbar med MAC:er av BC-partiklar (8–9 m^2 g^{-1}).

BrC bildning, omvandlingen och optiska egenskapen studeras med avseende på inverkan av reaktivt kväve (NO_x, NH_3), surhetsgrad (H_2SO_4) och fuktighet för SOA bildad vid fotooxidation av toluen.
Bildningen av toluen SOA vid [NOx]/[ΔHC] molförhållande från 0.15 och nedåt skilde sig tydligt (var konstant) från molförhållanden över 0.15, där SOA massan ökade. Detta skiljer SOA bildade vid kvävefattiga (NR, låga NOx halter), och kväverika (NP, höga NOx halter) förhållanden vilka ger högre halter av organiska nitrater. Denna distinktion är ett värdefullt verktyg för att förstå och beskriva trender i bildning och egenskaper av BrC innehållande SOA vid olika NOx halter. Därför klassificeras SOA bildad vid kvävefattiga och kväverika förhållanden som NP SOA och NR SOA, respektive. Ljusabsorptionskoefficienten (B_{abs}) och massabsorptionstvärsnittet (MAC) av SOA ökade med [NOx/ΔHC] för både NP- och NR-regimerna. För NP SOA ökade MAC med [NOx/ΔHC] oberoende av den relativa fuktigheten (RH). MAC för NR SOA var emellertid RH-beroende. Under både NP- och NR-regimer främjade surhet SOA-"browning" medan NH_3 ökade B_{abs} och MAC vid 80 % RH. Den högsta MAC observerades vid den lägsta RH (20%) och pH för NR SOA. Det antogs därmed att MAC för SOA beror huvudsakligen på pH och förhållandet $[H^+]_{fri}$/[SOA massa] för den vatteninnehållande SOA-fasen

I samma försök som ovan analyserades även data från HR-ToF-CIMS. Jag noterade att vid flera m/z (detta är massa laddningsförhållanden av detekterade joner som bildas vid kemisk jonisation) var trenden för topparna samma som trenden för bulkljusabsorptionen B_{abs} vid ökad [NO_x/ΔHC] för BrC innehållande SOA. Dessa m/z namnges som BrC molekyler innehållande kromoforer. En intressant observation var att det var unika m/z som framförallt bidrog till B_{abs} för varje experiment. Dock var m/z=296 en av det vanligaste jonerna detekterad under flera av de utvalda experimentella förhållandena. RH spelade en viktig roll för m/z-fördelningen. De BrC-kromoforer som motsvarar olika identifierade m/z föreslås vara nitroaromatiska föreningar (NAC). Dessa bildas primärt via OH-oxidation av toluen följt av nitrering och/eller demetylering av den oxiderade aromatiska ringen. De föreslagna nyckel BrC-kromoforerna är nitroderivat av fenoler, katekol, bensoesyra, bensaldehyd och bensonitriler.

Nyckelord: brunt kol (BrC), primär organisk aerosol (POA), sekundär organisk aerosol (SOA), BrC-blekning, BrC-browning, Toluenfotooxidation, NOx, NH_3 och surhetseffekter, ljusabsorption

List of publications

Publications included in this thesis work

Paper I: Molecular Characterization of Emissions from a Residential Wood Burning Boiler
Xiangrui Kong, Christian Mark Salvador, Staffan Carlsson, Ravi K. Pathak, Kent O Davidsson, Michael Le Breton, Samuel Mwaniki Gaita, **Kalyan Mitra,** Åsa M. Hallquist, Mattias Hallquist, Jan B. C. Pettersson
Science of the Total Environment, 2021, 754, 142143.

Paper II: Characterization, sources, and atmospheric transformation of a few key short-lived climate pollutants (SLCPs) at a rural super-site in the Indo-Gangetic Plain (IGP) of India
Jai Prakash, Harsh Raj Mishra, **Kalyan Mitra,** Bhilok Chandra, Mattias Hallquist, Gazala Habib, Geetam Tiwari, Jan B. C. Pettersson, Johan Boman, Håkan Pleijel, Ravi K. Pathak
Environmental Science: Atmospheres, 2022, 2 (3), 517-538.

Paper III: Characterization of Propane Fuelled Flames: A Significant Source of Brown Carbon
Jai Prakash, **Kalyan Mitra,** Harsh Raj Mishra, Xiangyu Pei, Evert Ljungström, Ravi K. Pathak
Atmosphere, 2022, 13(8), 1270.

Paper IV Secondary Organic Aerosol (SOA) from Photo-Oxidation of Toluene: 1 Influence of Reactive Nitrogen, Acidity and Water Vapours on Optical Properties
Kalyan Mitra, Harsh Raj Mishra, Xiangyu Pei, Ravi K. Pathak
Atmosphere, 2022, 13 (7), 1099.

Paper V: Secondary Organic Aerosol (SOA) from Photo-Oxidation of Toluene: 2. Molecular Markers linking to Optical Properties
Kalyan Mitra, Harsh Raj Mishra, Yesh Rozera, Christian Mark Salvador, and Ravi K. Pathak
Atmosphere, 2022 manuscript submitted

Author's contribution

Paper I: The author operated the PASS-3 instrument during the measurements and participated in the evaluation of results.

Paper II: The author actively took part in the data analysis, and paper writing with the co-authors.

Paper III: The author took part in the data curation and formal analysis and writing and reviewing the paper.

Paper IV: The author is the main author of this paper with Ravi Kant Pathak. The author took lead in the planning of the study, conducted the measurements, performed the data analysis, and wrote the paper in collaboration with the co-authors.

Paper V: The author is the main author of this paper with Ravi Kant Pathak. The author took lead in the planning of the study, conducted the measurements, performed the data analysis, and wrote the paper in collaboration with the co-authors.

PART- I

Extended Summary

1 Chapter I: Introduction

Atmospheric aerosols markedly affect the radiative balance in Earth's atmosphere and play key roles in climatic processes [1]. However, current air quality and climate models cannot accurately describe the influence of aerosols on the radiative forcing of the planet. The uncertainties exist because their formation and transformation in the atmosphere are complex processes that strongly affect their composition and hence their properties. For instance, one common aerosol component, organic aerosol (OA) is thought to cool the planet [1]. However, some components of OA can absorb light and warm the planet. These warming components of OA are collectively referred as brown carbon (BrC). Atmospheric brown carbon aerosol absorbs light in the UV-Vis spectrum and has poorly constrained but potentially large climate forcing impacts. Most current climate models lack detailed chemistry and interlinked properties of atmospheric BrC, that induce large uncertainties in radiative forcing predictions. BrC has complex lifecycle and many unknown still remaining [2]. It is suggested that strongly light absorbing primary BrC (PBrC) may rapidly evolve into weakly light absorbing secondary BrC (SBrC) in the atmosphere, which is considered as bleaching of PBrC. On the other hand, non-absorbing secondary/primary organic aerosol (SOA/POA) evolve into weakly light absorbing SBrC referred as browning of SOA/POA.

The processes underlying the formation and transformation of primary BrC from both biomass and fossil fuel combustion systems are still unclear. Further, the SOA aging and the subsequent formation and transformation of secondary BrC in the atmosphere are also obscure. The presence of reactive nitrogen, acidity and water is also thought to further drive the chemistry of BrC evolution and hence contribute to the global radiative forcing budget. These possibilities, and others, were explored in the laboratory and field experiments and are presented here.

In this thesis, I tried to explore and improve the understanding of the formation and transformation of the atmospheric brown carbon - both the primary and secondary in nature and interlinked optical properties of the browning molecules. The thesis is a comprehensive summary of various articles that have been published or are in the process of publication.

Paper I: Concentrations, optical absorption and chemical characteristics of gases and particles emitted from modern Swedish small-scale biomass burner. Positive matrix factorization was performed to analyze data from a high-resolution time-of-flight chemical ionization mass spectrometer (HR-ToF-CIMS) equipped with a filter inlet for gases and aerosols (FIGAERO), which yield six well-interpreted factors. Ordinal analysis enabled the automatic identification of the most characteristic molecules for each individual factor. Correlations of factors and optical properties are discussed.

Paper II: In this paper, the sources and atmospheric processes of formation and transformation of key short-lived climate pollutants (SLCPs) - black carbon (BC), brown carbon (BrC), and ozone (O_3) were characterised at our long-term air pollution monitoring station in a remote rural IGP site, the Indo-Gangetic Plains Centre for Air Research and

Education (IGP-CARE) in India. The elevated BrC concentrations were identified, which can be attributed to the local and regional atmospheric events and processes, including very pronounced diurnal variation.

Paper III: In this paper, the formation of primary BrC in fossil fuelled flames was explored under several specific settings, e.g. fuel-rich to lean flames, and the BrC was characterized to understand its warming potential i.e. MAC of the POA. POA was found to be constituted of highly light absorptive BrC and interestingly, its mass absorption cross-section (MAC) at 405 nm for some testing conditions was comparable to BC.

Paper IV: In this paper, the influence of reactive nitrogen (NOx, NH_3)-, acidity (H_2SO_4)-, and water-mediated chemistry on SOA formed by the photo-oxidation of toluene, the subsequent formation and transformation of BrC, and its optical properties were investigated. A framework describing browning of toluene SOA with respect to NOx to reacted toluene [NOx/ΔHC] ratio, NH_3 to reacted toluene [NH_3/ΔHC] ratio, and aerosol acidity was developed.

Paper V: In this paper, the potential BrC chromophores i.e. m/z with some probable empirical formulas, were identified that mimic the light absorption (B_{abs}). The chemical pathways of specific BrC chromophore formation were explored in the purview of reactive nitrogen (NOx, NH_3)-, acidity (H_2SO_4)-, and water-mediated chemistry.

Studies of primary BrC formation and transformation are reported in Papers I, II and III: Paper I presents a characterization of gases and particles emitted from the biomass burning in a modern Swedish small-scale biomass burner. Results from the PMF analysis were linked to the optical properties of the emissions, and lignin and cellulose/hemicellulose pyrolysis products were assessed to be the most important sources of PBrC under the tested burning conditions. Paper II outlines that the BrC formed during biomass burning and transformed subsequently in the atmosphere is highly photosensitive i.e. photobleaching is significantly noticeable during daytime. While Paper III underlines the BrC formed in the propane fuel-rich flames was highly absorptive and its MAC was comparable to BC.

Studies of secondary BrC formation and transformation are reported in Papers IV and V: Paper IV outlines the browning of toluene SOA under the influence of reactive nitrogen (NOx, NH_3)-, acidity (H_2SO_4)-, and water-mediated chemistry. Contrary to Paper II the SOA was transformed into darker BrC as NOx concentration was increased. Paper V describes the key SOA chromophores that mimic the bulk optical absorption properties under the influence of reactive nitrogen (NOx, NH_3)-, acidity (H_2SO_4)-, and water-mediated chemistry. This paper may have far reaching implications for mitigating the negative impact of key SOA chromophores on human health, biodiversity ecosystems and climate.

The above papers constitute a knowledge that enriches the understanding of atmospheric processes involved in the formation and transformation of BrC in lab and field. The new findings improve the understanding of BrC contribution to estimate the radiative forcing in

the atmosphere and finally culminate in the paper V that describes the molecular nature of secondary BrC and thus it might contribute towards mitigating the negative impacts of BrC. Thus, this thesis altogether provides a holistic picture of both PBrC and SBrC of sources and formation and transformation processes in the atmosphere.

2 Chapter II: State-of-the-art

2.1 Atmospheric sources and processes of BrC

Atmospheric BrC has two major sources: (i) primary BrC aerosol directly emitted due to incomplete combustion of either fossil fuels [3] or biomass [4,5] and (ii) secondary BrC produced via aging of SOA in the atmosphere involving carbonyl and/or aromatic compounds [6]. The formation of strongly light-absorbing primary OA-containing BrC has been observed in open biomass fires, combustion chambers and flames [7,8], and secondary BrC is also formed by the oxidation of precursor VOCs and further aging of both primary and secondary organic aerosol (POA and SOA) [7,9].

Recent studies suggest that aerosol components from biomass burning are more prevalent than previously thought [10] and may strongly contribute to observed high background BrC [11]. Since there is a thrust to reduce fossil fuel consumption, warming climate increases risk of more wild fires, increasing population that burns biomass for sustenance and burn crop wastes, increases the relative and total impacts of biomass burning on air quality and climate forcing [12]. There is a growing body of evidence that atmospheric primary BrC evolves differently from non-absorbing SOA/POA due to production of BrC from SOA and loss of BrC from photo bleaching [13-15], volatilization, or aerosol-phase reactions. For instance, the photo- induced bleaching of SBrC – produced by limonene ozonolysis in presence of ammonia, was much faster with an effective half-life of <0.5hr [16]. Understanding the sources, formation, atmospheric evolution, and environmental effects of BrC requires molecular identification and characterization of light-absorption properties of BrC chromophores. Identification of BrC components is challenging due to the complexity of atmospheric aerosols composition, chemistry and dynamics. The key BrC evolution processes are illustrated in Figure 1.

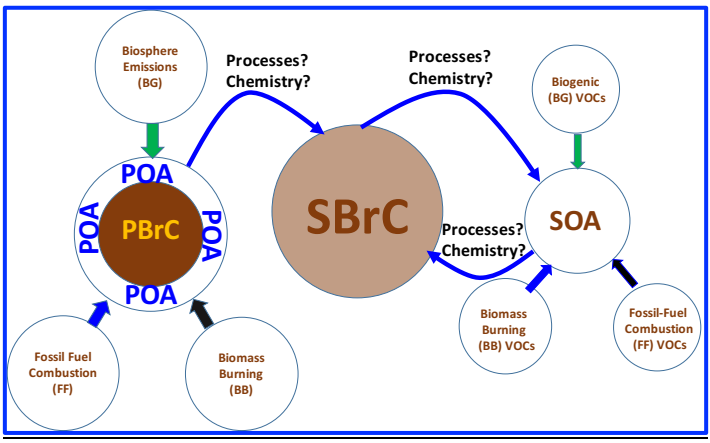

Figure 1: Summary of formation and transformation processes of BrC in the atmosphere: Strongly light absorbing primary BrC (PBrC) aerosol from FF/BB/BG emissions evolve into weakly light absorbing secondary BrC (SBrC) as it ages in the atmosphere; while non-light-absorbing SOA/POA from various sources is transformed into weakly light absorbing SBrC and vice-versa (SBrC→SOA)

2.2 Primary BrC formation and transformation

Primary BrC is directly formed and emitted to the atmosphere mostly during the combustion process or insignificantly through direct anthropogenic/biogenic aerosol emissions. As outlined in Figure 1, PBrC comes from fossil fuel (FF), biomass burning (BB) and biogenic (BG) sources. BB is estimated to contribute about 62% of the global POA and SOA budget annually [17]. Therefore, BB emissions significantly affect air quality and the climate system. Primary BrC is a component of POA and may be constituted of many light absorbing molecules called chromophores. A major class of chromophores from BB includes lignin-pyrolysis products, which are typically substituted aromatics with a high degree of unsaturation, such as conifer-aldehyde [18-20]. Another class is nitroaromatics, such as nitro-catechols, which are readily produced in the presence of NOx and strongly absorb light at lower wavelength i.e. 340nm [16,21]. Large polycyclic aromatic hydrocarbons (PAHs) resulting from incomplete combustion processes can be significantly light-absorbing at the near-UV-vis range [22]. Sulfur-containing species result from pyrolysis of fern and peat, and are thought to be formed via acid-catalyzed heterogeneous reactions [18]. Tar balls from BB are largely externally mixed aggregates produced from smouldering combustion or through multiphase chemical processes [23,24]. Tar balls are thought to be composed of oxygenated organic compounds [23,25-28].

BrC components undergo photochemical transformations i.e. photobleaching or browning, during its atmospheric aging. For instance, a substantial decay in aerosol UV light absorption in biomass burning plumes was observed within half a day time span in the atmosphere [2,16,29]. However, there can be a recalcitrant fraction of BrC that may persist even after long aging times. It is likely that lower-weight chromophores (< 500 Da) evolve into higher-molecular-weight chromophores (> 500 Da) within plume transport time, on the order of hours to days [30]. Further, primary BrC is thought to evolve in the atmosphere via processes including heterogeneous photooxidation (exposure of particles to gaseous OH and other oxidants), aqueous photooxidation (exposure of BB-POA compounds to OH within cloud/fog water droplets), direct photolysis (exposure of particles or their aqueous extracts to actinic UV radiation), and indirect photolysis (photosensitized reactions between BB-POA molecules and electronically excited triplet states of photosensitizers). Several studies have characterized changes in the UV–Vis spectra of nitrophenols commonly found in BB-POA [15,31,32]. Lignin pyrolysis products and other lignin derived molecules can be heterogeneously oxidized into more light absorbing compounds [33-36]. In Kaur et al. [37], five BB-POA model compounds were irradiated and hydroxyl radicals, singlet molecular oxygen, and triplet excited-state molecules were detected with probe molecules and all model compounds decayed on the order of hours from indirect photooxidation. The photodegradation of PAHs on ice surfaces, ocean water mimics, and soil has been studied significantly [38-40].

Biomass fuel type and their combustion condition determine the composition of BrC, and which in-turn determines the lifetimes of individual BrC molecules. UV photodegradation of BB with lignin and flavonoid sources mostly has longest lifetimes [41]. While individual

BrC chromophores may not survive for many days, the net light absorption by the sample normally persists longer due to slow condensed-phase photochemistry leading to photobleaching of BB-POA. Therefore, competing chemical aging mechanisms, such as heterogeneous oxidation by OH, may be more important for controlling the rate of BrC photobleaching in BB-POA [41].

The photochemical transformation of real mixtures of BB-POA compounds, not just model compounds, have also been widely investigated [42,43]. BB-POA after irradiation to UV/sunlight enhanced the light absorption initially, and then decreased significantly [14,43,44]. These indicate that BrC in BB-POA evolved through photo-enhancement and photobleaching processes to produced secondary brown carbon (SBrC). During these PBrC transformation processes, the low-molecular-weight BrC chromophores (< 400 Da) were quickly formed and subsequently photo-degraded, giving yield to a photo-enhancement due to the formation of high-molecular weight species (> 400 Da) and this high molecular-weight fraction was responsible for long-lived light absorption [44]. Sumlin et al. [45] found that the mass absorption coefficient of BB-POA upon Photo-oxidation decreased roughly 45% at 375 nm after an equivalent of 4.5 days of photochemical aging.

Modeling studies have also demonstrated that BrC can have large positive effects on the radiative forcing [46-50]. However, field measurements to date indicate that BrC has a short lifetime of 10 h, which would considerably reduce its impact if included in models [2,29]. Light absorption by BrC can also result in a significant decrease in the photolysis rates of photochemically active gases, such as HONO and NO_2, which affect the mixing ratios of atmospheric oxidants [51,52]. To better quantify the effect of BrC on climate, the chemical composition and lifetimes of individual BrC chromophores, as well as the effect of photochemical aging on the optical properties of BrC particles, should be studied. Further, for a comprehensive understanding, we should consider the diversity of BrC, spanning nonpolar to polar molecules, and BB-POA from a range of sources.

2.3 Secondary BrC formation and transformation

Secondary BrC is generated via complex oxidation reactions of volatile organic compounds (VOCs) in anthropogenic and biogenic BB emissions [9,43,53,54]. The secondary BrC sources are straightforward to identify. However, the mechanisms that generate light-absorbing SOA are highly uncertain [55]. Candidates include: nitration of polycyclic aromatic hydrocarbons, yielding light-absorbing nitrophenols [56,57]; reactions of NH_3, NH_4^+, or amino acids with condensed-phase carbonyl products [6,49,58-61]; acid-catalyzed aldol condensation of volatile aldehydes [62,63]; reactions of OH radicals with aromatic hydroxyacids and phenols in cloud water [33,64]; heterogeneous reactions of isoprene on acidic aerosol particles [65]; aqueous photochemistry of pyruvic acid in the presence of atmospheric electrolytes (e.g., SO_4^{2-} and NH_4^+) [66,67]; and reactions of isoprene epoxydiols on sulfate aerosol forming absorbing oligomers [68]. The complexity of resultant light-absorbing organic compounds and variations in their relative concentrations complicate attempts to characterize the molecular composition of BrC and identify the molecules or aggregates governing its optical properties. Despite these analytical difficulties, several classes of compounds have been identified as potential contributors to

BrC's light absorption, including nitroaromatic compounds, such as nitrophenols, imidazole-based and other N-heterocyclic compounds, and quinones. Less is known about the molecular composition of light-absorbing oligomers produced through condensation reactions and humic like substances (HULIS) [49]. It has also been proposed that supramolecular aggregates and complexes of organic molecules with transition metals may be responsible for BrC's observed optical properties. However, it is unclear if typical BrC includes a few strong chromophores or diverse weak chromophores. The latter would be more consistent with the featureless UV−visible spectra of BrC observed in most field studies. However, analyses of BrC's spectra in some field studies have identified clear peaks in the visible range [69-71], indicating that both molecular and supramolecular chromophores may coexist in ambient BrC. Several laboratory proxies of BrC, have also been shown to exhibit distinct absorption spectra (such as the 510 nm band in the aged limonene SOA shown in Figure 1. The identification and structural characterization of BrC chromophores clearly require highly sensitive molecular approaches capable of detecting both strongly and weakly absorbing species. Quantifying BrC's contribution to light absorption is critically important for accurate interpretation of aerosols' optical depth (AOD), the atmospheric column's light extinction due to both scattering and absorption

2.4 Aqueous phase SBrC formation and transformation

Dark and photochemical processes of the aqueous-phase reactions can promote the optical spectra of organic aerosols, and are also the important process of secondary BrC formation [72-75]. Formation and light absorption of BrC are affected by many environment factors such as concentrations and compositions of VOCs and oxidants, aerosol aqueous phase acidity, and meteorological conditions.

In recent years, increasing laboratory and field observational studies have shown that aqueous inorganic-organic reactions in the atmosphere can be major sources of SBrC [15,76,77]. For example, light-absorbing substances can be generated from water-soluble carbonyl compounds' interactions with ammonium sulfate (AS) and amine compounds in aqueous phase.

Formation of aqueous SOA (aqSOA) via photochemical reactions involves oxidation reactions, in which the hydroxyl radical ($^{\bullet}OH$) usually considered to be the primary oxidant [78,79]. For example, organic compounds in triplet excited states ($^3C^*$) generated by irradiation of light-absorbing organics (e.g. non-phenolic aromatic carbonyls), oxidized phenols at higher rates and with greater aqSOA yields than $^{\bullet}OH$ [79-82]. Thus, they strongly enhance SBrC production.

As well as being an oxidant, $^3C^*$ can also be a precursor of singlet oxygen ($^1O_2$), superoxide ($O_2^{\bullet-}$) or hydroperoxyl ($^{\bullet}HO_2$) and $^{\bullet}OH$ (via $HO^{\bullet}_2$ /$O_2^{\bullet-}$ formation) radicals upon reactions with O_2 and substrates such as phenols [83]. The estimated $^3C^*$ concentration in typical fog water is >25 times higher than that of $^{\bullet}OH$, indicating that it is the primary photo-oxidant for BB-generated phenolic compounds [37,84]. However, recent studies on triplet-driven oxidation of phenols have mainly focused on changes in physicochemical properties (e.g., light absorption) and aqSOA yields [36,79,85], with few reports on reaction pathways and products [72,86,87].

BB is a significant atmospheric source of both phenolic and non-phenolic aromatic carbonyls [88-91]. Upon exposure to sunlight, aromatic carbonyls in BB emissions are excited to triplet excited states, which (as mentioned) can initiate oxidation leading to aqSOA formation [36,79,85]. Inorganic salts such as ammonium nitrate are major components of aerosols and cloud or fog water, and frequently co-exist with BB emission products [92-94]. In cloud and fog water, inorganic nitrate levels can vary from 50 to 1000 μM, and are typically higher in polluted conditions [95-100]. Upon photolysis [82,101,102], inorganic nitrate in cloud and fog water can contribute to SBrC [103] and aqSOA formation [73,104,105] by generating $^{\bullet}OH$ and $^{\bullet}NO_2$ (also a nitrating agent). For example, aqSOA yields from photo-oxidation of phenolic carbonyls in ammonium nitrate are twice as high as yields in ammonium sulfate solution [73]. Thus, nitration is a significant process in the formation of light-absorbing organics or SBrC in the atmosphere [5,49,56,76,106-108].

The effects of NO_2 on secondary BrC formation were also studied in laboratory studies. A scientific assessment on the optical role of BrC [109] indicated that the wavelength dependent absorptive component (k) values of secondary organic aerosols (SOA) formed in the presence of NO_2 are greater than those without NO_2, and the nitrogen-containing organic compounds (NOCs) are the key components enhancing light absorption. Liu et al. [109] and Xie et al. [110] reported that the light absorption of SOA generated in the presence of NO_2 is higher than in presence of hydrogen peroxide (H_2O_2), and the mass absorption coefficient (MAC) of nitro-aromatic compounds is more than twice as that of the whole SOA.

2.5 Current knowledge gaps and challenges

Understanding the environmental effects of BrC, its sources, formation, and atmospheric aging mechanisms requires robust description of relationships between its molecular composition and light absorption properties. Available evidence suggests that even a very small weight fraction of strongly absorbing BrC chromophores may substantially affect OA's optical properties [55]. Because of the low concentrations of light-absorbing molecules in the complex organic mixtures present in both laboratory-generated and ambient OA, identifying BrC chromophores is highly challenging [55]. A recent review [49] clearly indicates that various BrC chromophores may be present in both POA and SOA originating from diverse sources. However, knowledge of their chemical identities, light-absorbing properties, concentrations, and atmospheric stability is fragmentary. Thus, we have insufficient understanding for practical parametrization of BrC properties in atmospheric and climate models. To obtain sufficient observations and scientific knowledge for constraining and validating future models there it is a need to do investigations that include fundamental molecular level studies of BrC chromophores, including characterization of their chemical composition and optical properties, sources, formation mechanisms, and atmospheric degradation.

However, due to its complex chemical composition, analytical obstacles and other factors, there is still very limited knowledge and theoretical understanding of its sources, formation, degradation mechanisms, and the chromophore transformations involved.

3 Chapter III: Experimental methods

Advanced and the state-of-the-art experimental techniques are required to understand BrC formation and transformation processes. This section briefly introduces the experimental methods used to characterize and investigate different formation and transformation processes and properties of PBrC and SBrC.

3.1 Experimental methods

3.1.1 Molecular characterization and optical properties of primary emissions from a residential wood burning boiler

The residential wood burning boiler testing facility at the Research Institute of Sweden AB accessed to study the BrC formation and properties from various type of wood and pellets commonly used in Swedish homes. The configuration of the experimental setup is shown in Figure 2. Details of the experiments are available in attached paper I.

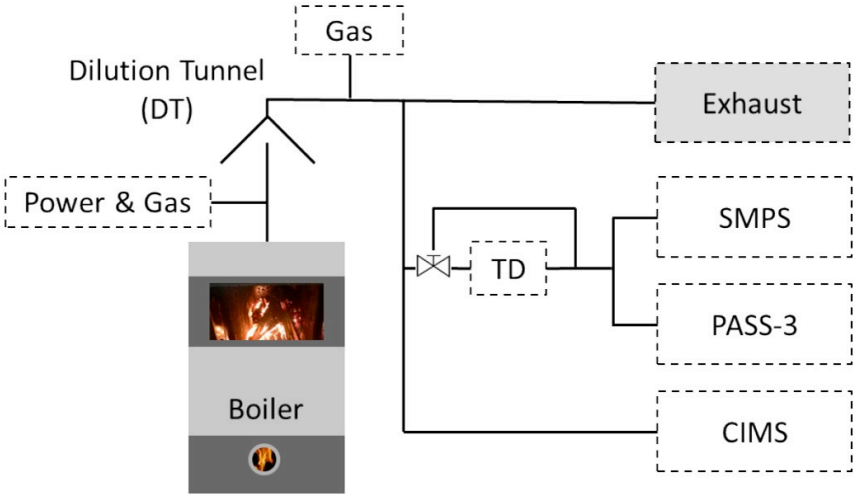

Figure 2: Schematic view of the experimental setup for paper I

3.1.2 Sources and characterization of BrC at a rural site in the Indo-Gangetic Plain (IGP) of India

To facilitate long-term measurement of SLCPs in the IGP region, a new monitoring site was established in 2016 in a rural area. This site, the Indo-Gangetic Plains - Centre for Air Research and Education (IGP-CARE), is situated in agricultural fields adjacent to a forest by the River Burma (a tributary of the River Betwa) surrounded by six villages in the Hamirpur district of Uttar Pradesh (25° 48’ 55.5” N; 79° 55’ 07.5” E), India (Figure 3). Real-time long-term measurements of SLCPs (e.g., O3, NOx, CO, black carbon, brown carbon) have been conducted continuously at the IGP-CARE site since January 2017. The

dataset examined in this study covers the period from January 2017 to December 2017. Details of the experiments are provided in the paper II appended with this thesis.

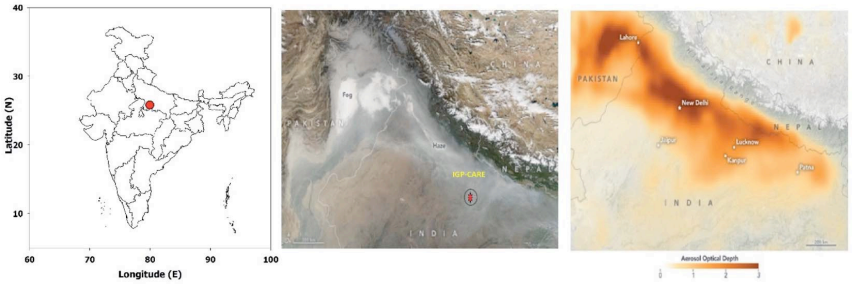

Figure 3: The rural Indo-Gangetic Plains Centre for Air Research and Education (IGP-CARE) monitoring station (red circle) in the IGP region, Hamirpur, India (left panel). A satellite view of haze spread over the IGP region, India, and the IGP-CARE location (middle panel), and a map of the AOD (right panel) over the IGP region (source: https://earthdata.nasa.gov/).

3.1.3 Formation and characterization of PBrC in fossil fuel flames

To perform controlled experiments in the laboratory, a propane burner was designed and built to generate submicron particles with adjustable (albeit interdependent) particle size distributions, BC fractions, BrC fractions, and mixing states with POA. The experimental setup used to characterize lab-scale flame emissions is shown in Figure 4. I have provided details of these experiments in the paper III appended with this thesis.

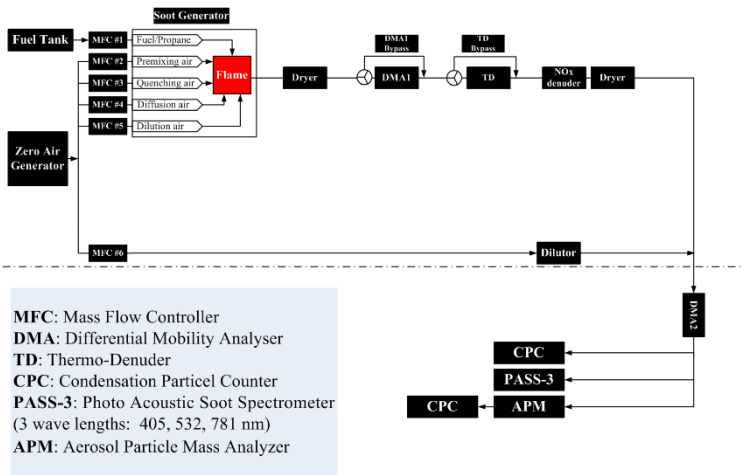

Figure 4: Schematic of the experimental setup for characterizing soot from lab-scale flames for Paper III

3.1.4 Formation and transformation processes, characterization and optical properties of Toluene photo-oxidation SOA

The experiment was designed to generate conditional SOA and has three serial zones as in Figure 5: (i) the reactants input control zone, (ii) the reaction zone, and (iii) the

instrumentation and measurement zone. Detailed description of these experiments are provided in the paper IV and V appended with this thesis.

Experimental Matrix

The experiments performed in this study are summarized in Table 1 Controlled experimental variables included the toluene concentration (ΔHC), the initial ozone concentration, the relative humidity, the NOx ramp and initial concentration (31 ppb to 362 ppb for experiments Tol-1 to Tol-4 and 30 ppb to 351 ppb for experiments Tol-7 to Tol-9), and the NH_3 ramp (42 ppb to 203 ppb for experiments Tol-5 and Tol-6).

Table 1: The experimental input matrix for paper IV and V

Exp.ID	Reacted Toluene (ΔHC) Concentration (ppb) [§]	NOx ($NO: NO_2$ Ratio = 1:1) Range (Initial to Final, ppb)	O_3 (Initial, ppb)	RH%	NH_3 Ramp Range (Initial to Final, ppb)	H_2SO_4 (μg m^{-3})	OH_{expo} (Calculated) × 10^{11} (cm^{-3}.s)	Remarks
Tol-1	1161	31 to 362	999	80	No	No	2.8	NOx ramped
Tol-2	1064	31 to 362	999	65	No	No	2.3	NOx ramped
Tol-3	870	31 to 362	999	35	No	No	1.6	NOx ramped
Tol-4	774	31 to 362	999	20	No	No	1.3	NOx ramped
Tol-5	1161	61	999	80	42 to 203	No	2.8	NH_3 ramped and NOx constant
Tol-6	1161	360	999	80	42 to 203	No	2.8	NH_3 ramped and NOx constant
Tol-7	1161	30 to 351	999	80	No	Yes (22.3)	2.8	NO_x ramped
Tol-8	1161	30 to 351	999	65	No	Yes (22.3)	2.8	NO_x ramped
Tol-9	780	30 to 351	999	20	No	Yes (22.3)	1.6	NOx ramped

[§]: Toluene reacted is calculated by measuring residual toluene from Go:PAM outlet with a VOC monitor with and without reaction at Go:PAM.

3.2 Instrumentation

This subsection describes the key components of the setups and apparatus used for field and lab measurements and formation and transformation of PBrC and SBrC.

3.2.1 FIGAERO-HR-ToF-CIMS

In Paper I, IV, and V, the mass/charge (m/z) spectrum was measured using a FIGAERO instrument of Aerodyne Research Inc., Billerica, Massachusetts, USA and by HR-ToF-CIMS, (Aerodyne Research Inc. and Tofwerk AG) as shown in Figure 6 and Figure 7 and discussed in details in many literatures [111,112]. In Figure 7: A) FIGAERO overview. The main manifold (green) and the movable tray (red) are made of Teflon. The movable tray switches between the two modes. The two sampling ports (gas phase inlet and aerosol inlet) and the thermal desorption port connected to the heating tube are mounted at the inlet plate. B) FIGAERO during gas phase sampling and particle collection. The desorption port is blocked by the tray. C) FIGAERO during desorption. The filter holder moves under the heated N_2 stream while the gas sampling port is blocked by the tray. The Figure 7 is *reproduced from* [111].

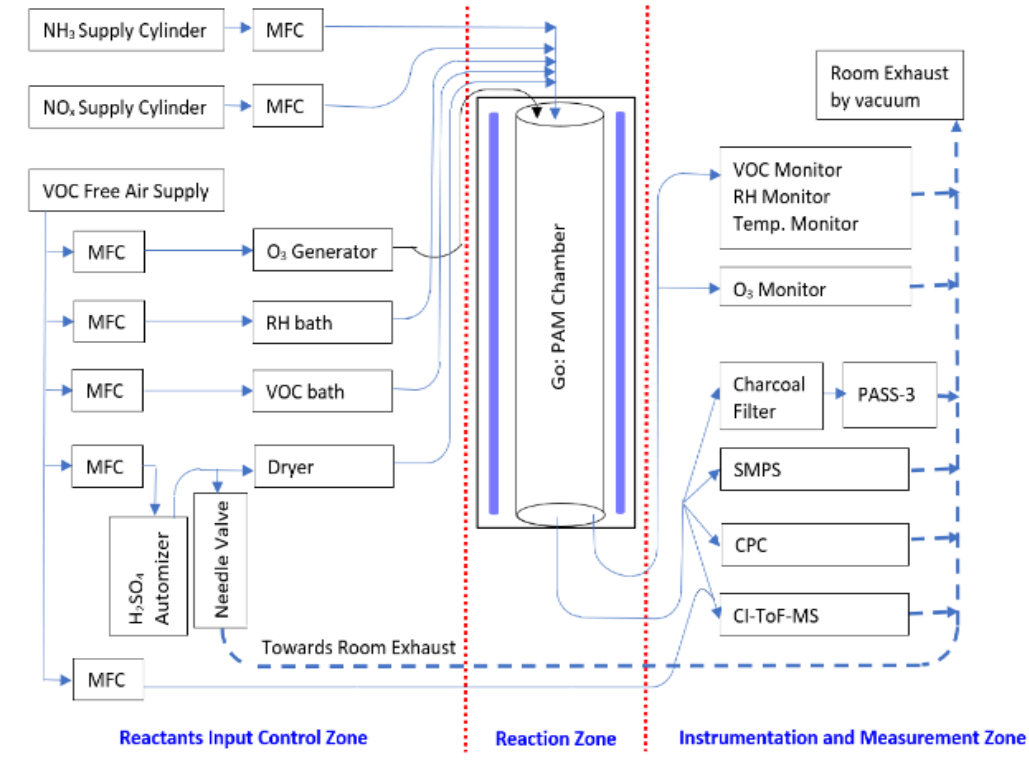

Figure 5: Process flow diagram of the experimental setup for Paper IV and V

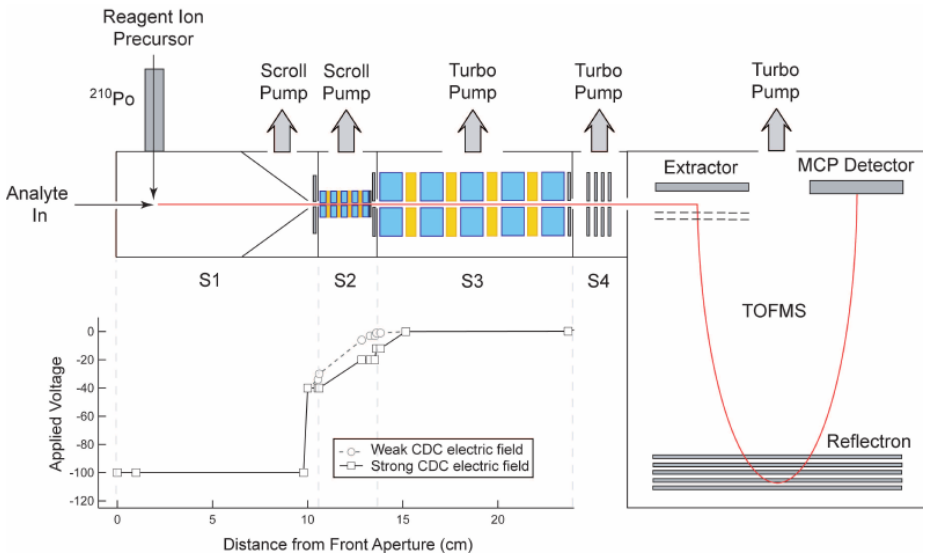

Figure 6: Schematic of the ToF-CIMS [113]

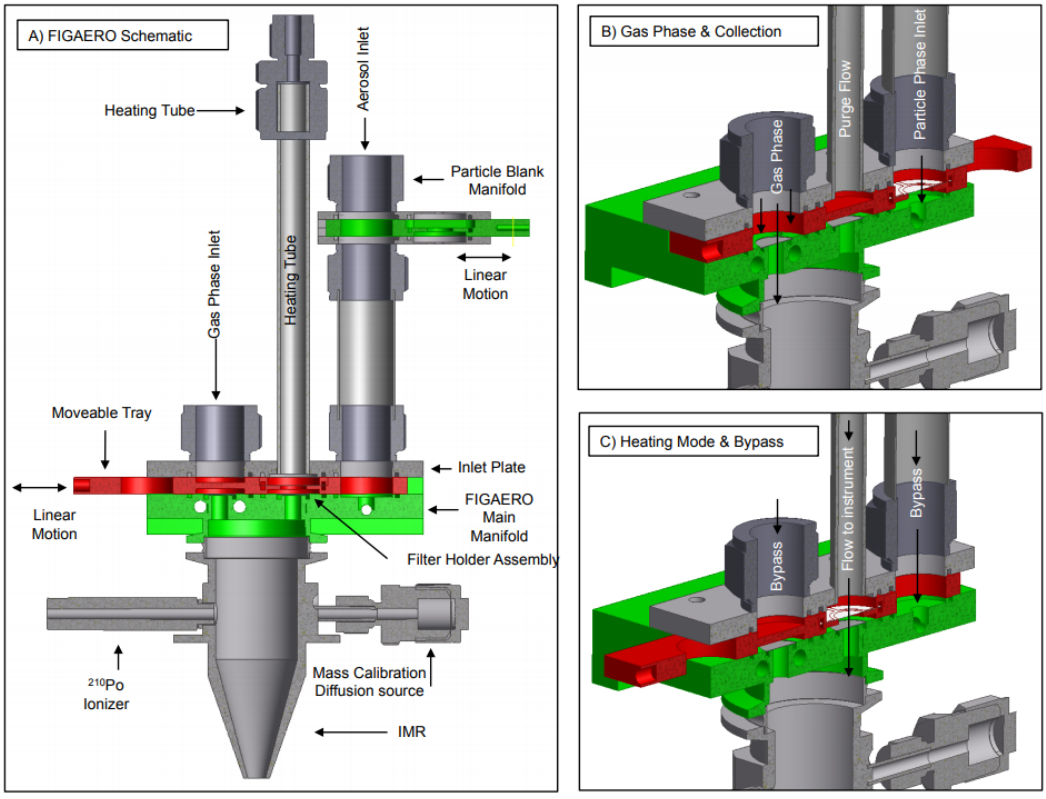

Figure 7: FIGAERO schematics [111]

3.2.2 Go:PAM

The Potential Aerosol Mass (PAM) reactor as show in Figure 5, is an oxidation flow reactor (OFR), which provides a highly oxidizing environment, enabling simulation of atmospheric oxidation processes of timescales ranging from one to several days, in a few minutes in the laboratory [114]. The Gothenburg Potential Aerosol Mass (Go:PAM) reactor has been developed in the University of Gothenburg and is described in the study by [115].

3.2.3 Absorption measurement with a PASS-3

PASS-3 shown in Figure 8 (Droplet Measurement Technologies) [116] is a sensitive, high-resolution, fast-response commercially available instrument for measuring the absorption coefficient of aerosol particles. In Papers I, III, IV, and V, a PASS-3 instrument was used to measure particles in-situ light absorption coefficients simultaneously at wavelengths of 405, 532, and 781 nm with a time resolution of 2s.

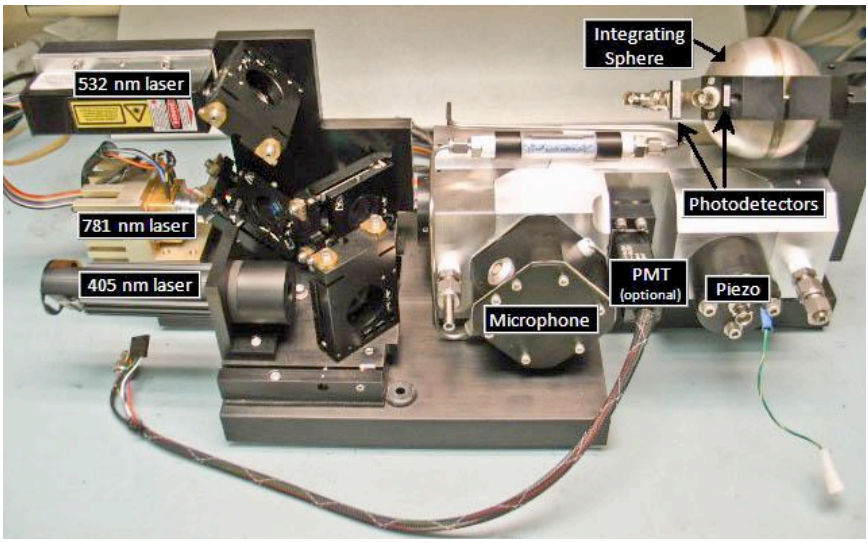

Figure 8: Main components of the PASS-3

3.2.4 Scanning mobility particle sizer (SMPS) spectrometer

The measurement of the particle number size distribution of the aerosol particles was performed with a scanning mobility particle sizer (SMPS) spectrometer, which is a combination of a DMA and a CPC in series.

3.2.5 Size Distribution with DMA + CPC

A DMA (DMA2) (Vienna type, length 280 mm, inner/outer radius 25.0/33.3 mm, aerosol flow rate 1.6 L min^{-1}, and sheath flow rate 10.0 L min^{-1}) and a CPC were used to measure the number size distributions (9–430 nm) of both fresh soot particles and thermo-denuded samples.

3.2.6 Particle mass mobility relationship using a DMA-APM system

The particle mass mobility relationship and, hence, the effective density were determined using the DMA2, an APM, and a CPC in series followed by previous literature *McMurry et al.* (2002) [117].

3.2.7 Other instruments

A few auxiliary instruments were utilized during the experiments. Briefly, the following instruments were used: an ozone monitor (2B Technologies, USA, model 205), VOC monitor (ALPHASENSE LIMITED, UK, model: PID AH2), CO Monitor (Ecotech, ACOEM Group, model:Serinus® 30), O_3 monitor (Ecotech, ACOEM Group, model: Serinus® 10), NOX (Ecotech, ACOEM Group, model: Serinus® 40), BC monitor (Met One Instruments, Inc, USA, Model: BC 1050 series).

3.3 Data analysis

Details of the methods used for data analysis can be found in Papers I-V. The most important parameters considered in these studies are briefly discussed below.

3.3.1 Data Processing

All results obtained using the SMPS and PASS3 instruments as well as the acidity values and concentrations of NOx and NH_3 presented in this work are average of 30 min measurements data. Molecular speciation of toluene SOA was performed by analysing gas and aerosol samples drawn from the GO:PAM flow tube outlet at a rate of 4 litres per minute by the FIGAERO-HR-ToF-CIMS, operating in particle collection mode. The FIGAERO-HR-ToF-CIMS was operated in this mode in 30-min intervals.

The potential m/z that absorbed light were identified and selected as the following: (i) m/z must mimic the trend of bulk light absorption i.e. B_{abs} against the [NOx/ΔHC] increase; (ii) for the straight line trends, the correlation regression coefficient (R^2) must be significantly high (> 0.75) between the m/z signal (counts per second – CPS) and [NO_x/ΔHC] ratio. Further, for non-linear patterns of B_{abs} against the [NO_x/ΔHC] increase, I visually selected the m/z, which exactly matched the B_{abs} trend (see Figures 1S to 42S in *Supplementary Information of the paper V*).

It is to be noted that in the Ion Molecule Reaction (IMR) chamber of a mass spectrometer (MS), ionization of any molecule can occur in any of the following ways: (i) proton transfer, (ii) electrophilic addition, (iii) anion abstraction, and (iv) charge exchange due to (a) electrochemical potentials of reactants, (b) energy available for ionization and (c) other multiple parameters at various maintenance cycles of an MS. However, predicting the exact m/z obtained from the MS is challenging. The exact empirical formula of an obtained m/z when cannot be estimated without isotopic analysis, it must be complemented with chromatography and/or spectroscopy and calibrated with internal standards.

Here, I must acknowledge that I translated several m/z data into probable empirical formulae and molecular structures without validating them through above procedure. My motivation for doing the same is to narrow down the search of m/z empirical formula and structure with the aid of published literature for the similar set up.

4 Chapter IV: Results and discussion

The scientific content of this thesis includes sources, formation and transformation processes and characterization of BrC i.e. primary and secondary BrC. The results were obtained from: (i) the characterization of primary BrC from the emissions of modern Swedish residential biomass burner and laboratory scale fossil fuelled flames, (ii) the field measurements of ambient BrC from anthropogenic open biomass burning at the IGP-CARE; (iii) the characterization of secondary BrC from the aging of toluene SOA using state-of-the-art laboratory facilities at the University of Gothenburg.

The above experiments pertaining to formation and transformation processes of PBrC and SBrC provided the following data: (i) size and number distributions, molecular mass-spectra, light absorption coefficients of POA containing PBrC from the modern Swedish residential biomass burner; of toluene SOA containing BrC from GO:PAM; (ii) light absorption of ambient $PM_{2.5}$ containing BrC, ambient O_3, NOx, CO at the pristine rural site in the IGP region, (iii) light absorption coefficient of PBrC particles of five different sizes (75, 100, 150, 200 and 250 nm) from three lab-scale propane premixed flames.

The key findings are presented in five major sections:

4.1 Characteristics of PBrC from combustion of several wood types under the designed test conditions in the residential biomass burner;
4.2 Characteristics and transformation processes of ambient BrC from local biomass burning at the IGP-CARE;
4.3 Formation and characteristics of PBrC from lab scale fossil fuelled flames;
4.4 Formation, transformation and characterization of SBrC from the photooxidation of toluene under the influence of reactive nitrogen, acidity and water-mediated chemistry;
4.5 Key SBrC molecules containing chromophores i.e. m/z in the SBrC from the photooxidation of toluene under the influence of reactive nitrogen, acidity and water-mediated chemistry;

4.1 Characteristics of PBrC from the residential biomass burner

4.1.1 Factor profile and time series of PMF solution of HR-ToF-CIMS Data

Mass to charge ratio (i.e. m/z) intensity (arbitrary unit – a.u.) data obtained from the HR-ToF-CIMS were analyzed by PMF. The number of factors were varied to find the optimal solution, and the allocations for solutions using from two to seven factors shown in Figure 9. A seven-factor solution was concluded to produce physically and chemically meaningful results. These seven factors were identified based on their temporal behaviour and molecular properties. The representative names for these factors are: *cellulose* – products of cellulose/hemicellulose pyrolysis; *lignin 1* – products of lignin pyrolysis; *N-compounds* – nitrogen-containing compounds, volatile – characterized by volatile nature of the compounds; semi-volatile – characterized by semi-volatile compounds, and a separate

factor termed *filter* was associated with compounds formed on the filter used to collect particles in the FIGAERO inlet. An additional factor was also associated with decomposition of lignin (*lignin 2*). The time series and chemical properties of the two lignin-related factors showed similar chemical properties and time series but did not merge into one factor when using a six-factor solution instead of seven factors. Therefore, in this thesis, I combined the two lignin factors into one, which provided the six interpretable factors. In the five measurement days with three different woods (birch, spruce and aspen), these factors were repeatedly identified indicating the robustness of the PMF solutions.

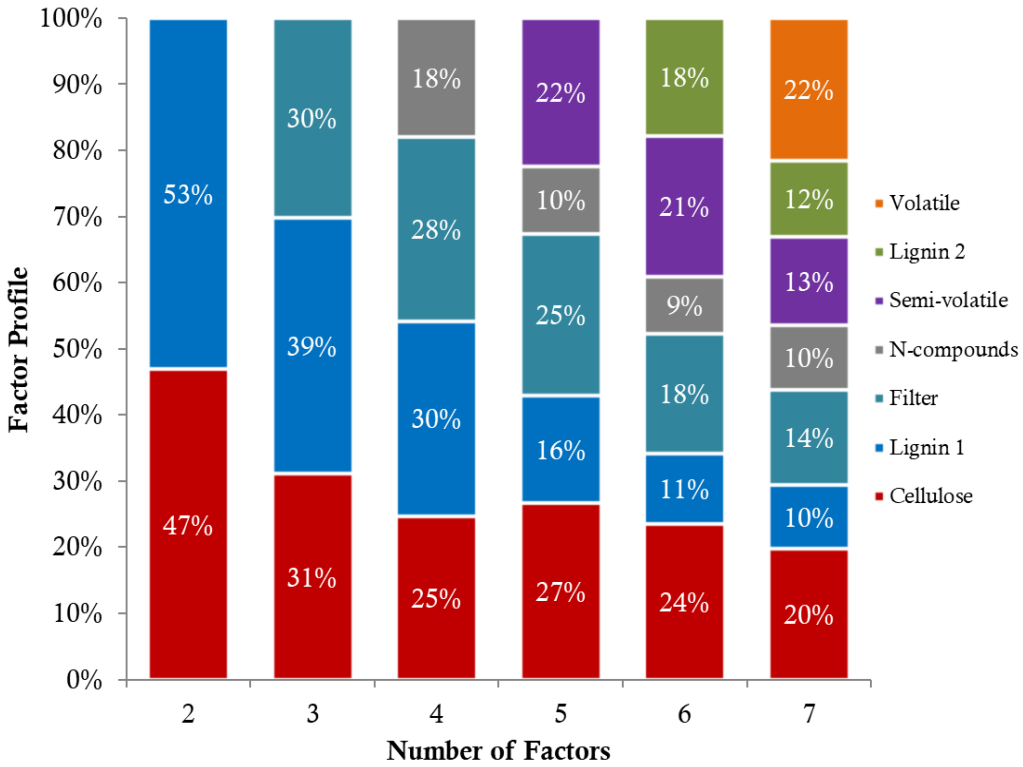

Figure 9: Factor allocations of the PMF solutions with 2-7 factors. The indicated names for individual factors correspond to the seven-factor solution.

The emission characteristics of these six factors based on the measurements performed on 15th May 2018 are shown in Figure 10 and summarized here. The signal intensity of factors including *lignin, cellulose, volatile, N-compounds* and *semi-volatile* exhibited sharp rises during the start-up stage i.e. ignition (IG) phase, of the burning cycle. The intensity of the *volatile* factor remained steady throughout the combustion cycle, while the *N-compounds* factor exhibited a peak that was broader than *lignin* and *cellulose* peaks and occurred later in the burning cycle. Lignin, volatile and N-compounds were dominant in the gas phase, while cellulose, semi-volatile and filter factors showed their dominance in particle phase. Nevertheless, significant fraction of particle phase was also observed in the *lignin* and *N-compound* factors. Therefore, these five factors were considered in the BrC analysis. The

same factors were repeatedly identified between days and for different fuels under the tested conditions.

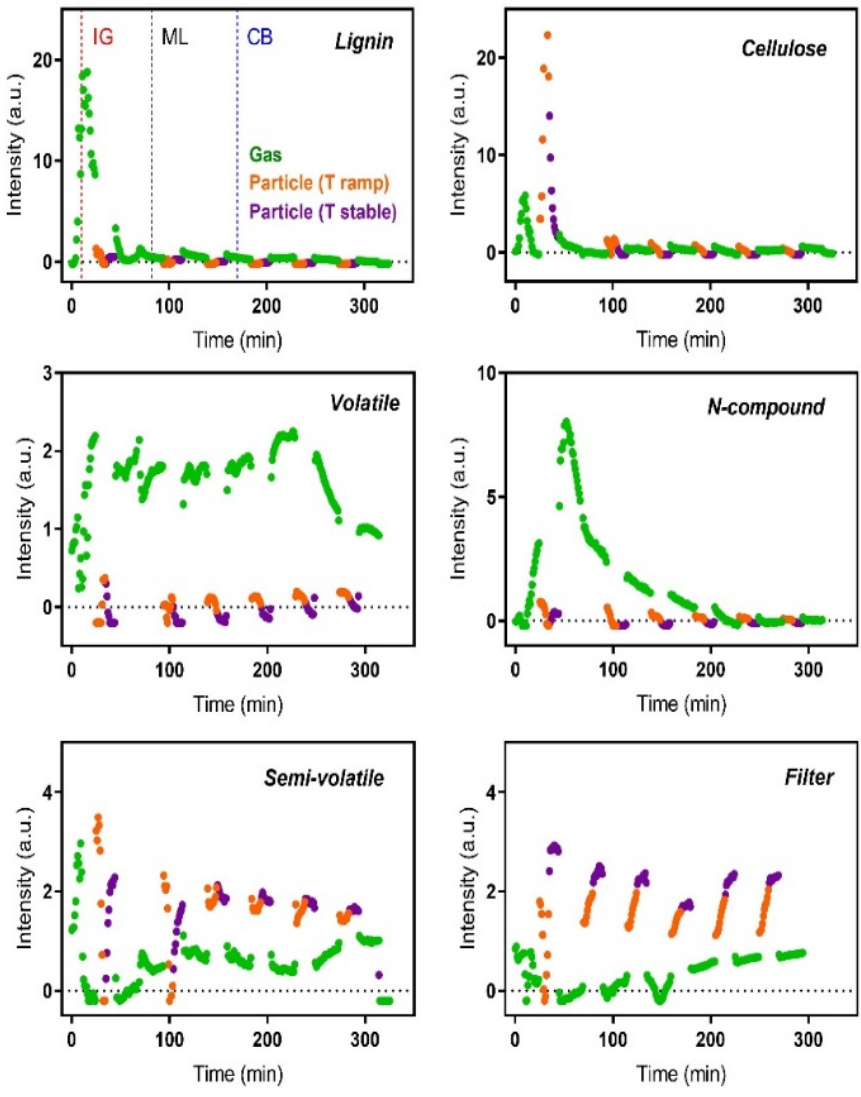

Figure 10: Example time series of the six PMF factors during birch combustion. The gas and particle phase measurements are indicated by different colors, including separate periods with temperature ramping and stable temperature of the filter in the FIGAERO inlet. The moments of ignition (IG), main load (ML) and char burning (CB) are marked in the panels

4.1.2 Molecular composition of the factors

An ordinal analysis was carried out to rank and identify the major molecular components i.e. mass to charge (m/z) observed for each factor. The most significant masses for each

factor i.e. those with highest factor fractions and an excellent fuel-independent reproducibility, were used for the data evaluation. The HR-ToF-CIMS spectra of the highest ranked masses were deconvoluted and the corresponding molecules were identified. The composition of key factors linking to the optical properties of BrC particles are discussed here and listed in Tables 1,2,3 and 4 in the *paper I*, appended to this thesis.
These include: (i) a cluster of masses around m/z = 270 was consistently observed for *lignin*, which consists mainly of iodide adducts of methoxyphenols and phenols released from lignin during pyrolysis [118-127] (ii) the compounds associated with the *cellulose* factor formed early during the start-up (IG) with relatively high m/z values and are known to be products of cellulose and hemicellulose pyrolysis e.g. levoglucosan (LG) – a tracer for biomass burning in the ambient atmosphere [22,128-132] and its isomers mannosan, and galactosan [133], saccharides (e.g. methyl galacturonate, ethylidene glucose and mannoheptulose), phenolic derivatives (e.g. trimethoxybenzaldehyde, benzal diacetate and acetate vanillin), and nitrophenazine.

4.1.3 Optical properties of the factors

The light absorption due to the aerosol particles was measured at wavelengths of 405 nm and 781 nm using PASS-3. The absorption Ångström exponent (AAE), which describes the optical properties of aerosol particles and served as an indicator of the fractions of BrC and BC, was calculated using eq.1 [134-136].

$$AAE = -\frac{ln(b_{\lambda 1}/b_{\lambda 2})}{ln(\lambda_1/\lambda_2)} \quad (1)$$

Time series of AAE and other optical properties can be found in Figure 11. The absorption enhancement at 405 nm (E_{405}) is due to the BrC content [137] which is

$$\boldsymbol{E_{405}} = \frac{\boldsymbol{b_{405}^{total}}}{\boldsymbol{b_{405}^{BC}}}. \quad (2)$$

The BrC absorption fraction (f_{BrC}) is calculated as

$$\boldsymbol{f_{BrC}} = \frac{\boldsymbol{b_{405}^{BrC}}}{\boldsymbol{b_{405}^{total}}}. \quad (3)$$

For pure graphite soot, AAE is approximately 1 [47,138]. By assuming that the absorption at 781 nm (b_{781}) is exclusively due to BC the 781 nm signal is directly related to the BC concentration, and eq.4 is used to compute the equivalent BrC concentration based on the measured values of b_{781} and b_{405}.

$$C_{BrC}^{eqv} = \frac{b_{405}}{MAC_{405}} - C_{BC} \quad (4)$$

The PMF solutions show excellent reproducibility between experiments and when using different wood fuels. Figure 12 shows that during the start-up stage both BC and BrC levels increased rapidly, and the AAE ranged from 2 to 3. Values in this range are typical for biomass burning [135,136]. The bursts of BC and BrC observed upon ignition match the profile of the *lignin* factor well. The *cellulose* factor probably also shares this profile, although detection of the corresponding compounds would have been delayed by the applied FIGAERO filter mode. This suggests that primary pyrolysis products are potentially significant contributors to BrC from wood burning, which is in agreement with what has been proposed in early BrC studies [139]. Moreover, nitro- and aromatic

compounds are known to absorb strongly at wavelengths of 400 - 600 nm [140] and have therefore traditionally been regarded as major contributors to BrC [5,56,141,142]. However, no significant correlation between the N-compounds factor and BrC levels was observed in this study.

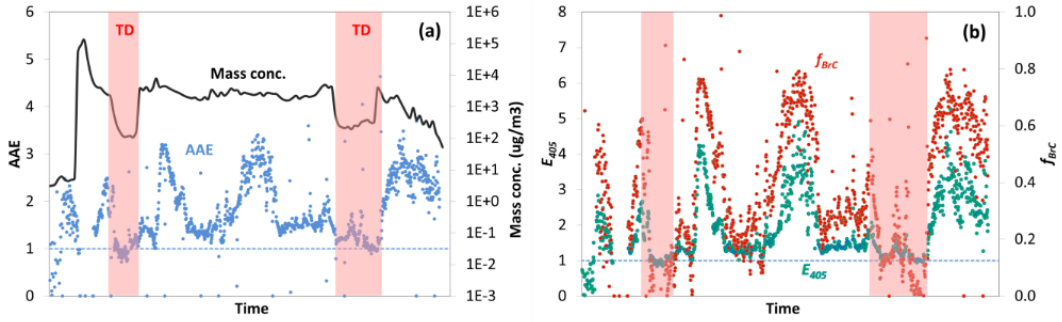

Figure 11: Times series of (a) AAE and SMPS mass concentration, (b) E_{405} and f_{BrC}. The red time periods indicate when the aerosol flow went through the TD.

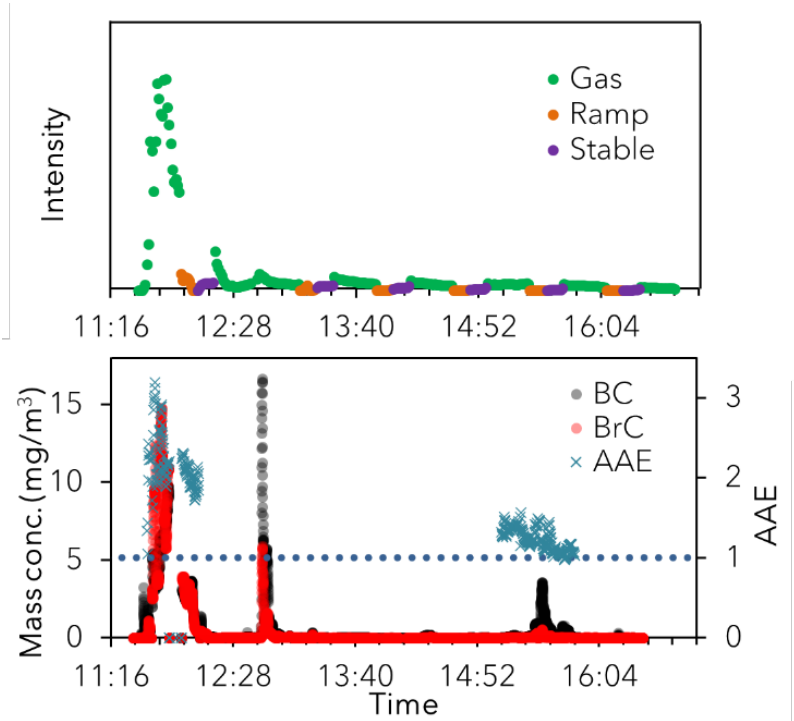

Figure 12: Time series for Factor Lignin (upper panel), and AAE values and concentrations of BC and BrC (lower panel) measured during birch wood combustion. The large spike amid the burning cycle at around 12:40 was due to the main loading of wood. The measurement was performed on 15th May 2018.

Based on the optical properties and factor time series, the lignin and cellulose factors were the main contributors to BrC emissions from biomass burning under the tested conditions.

4.2 Characteristics of ambient BrC at the IGP-CARE

The key short-lived climate pollutants measured at the IGP-CARE include BC, BrC, O_3, NOx and CO. During Jan-Dec 2017, the BC concentration ranged from 2.1 to 16.6 μg m^{-3} with an overall mean of 5.1 ± 2.2 μg m^{-3}, while the BrC concentration ranged from 0.5 to 32.3 μg m^{-3} with an overall mean of 2.6 ± 1.3 μg m^{-3}. The overall mean concentrations of O_3, CO, and NO_X were (31.0 ± 23.1) ppbv, (659 ± 437) ppbv, and (8.6 ± 3.5) ppbv, respectively.

The BC was moderately positively correlated with BrC in all seasons except monsoon (r^2 = 0.61 in autumn; r^2 = 0.56 in summer; r^2 = 0.52 in winter; and r^2 = 0.32 in monsoon). Both BC and BrC had moderate to high association with CO in winter and autumn seasons. This is an indication of similar sources of emissions of BC, BrC, and CO, such as biomass burning in autumn and winter and local burning (mud-brick firing or crop residue burning etc.) in summer. Both BC and BrC had moderate and positive association with NO_2 in the autumn season. BC and co-emitted species from biomass burning e.g. BrC, NOx and CO are considered primary pollutants.

4.2.1 Temporal trends of BrC

Figure 13 shows a time series of concentration of BC (top panel), BrC (middle panel), and regional fire counts (bottom panel). To outline their sources, characteristics, and processes at the IGP-CARE site, multiple episodic events were selected for further investigation, which also highlights thirteen episodic events using green shading in the Figure 13. Episodic events (E1 to E13) were defined as events during which the BC and BrC concentration was at least three times the hourly mean (3×hourly mean) for the study period. The episodic hourly mean BC and BrC levels along with the corresponding BrC/BC ratios, atmospheric process data, and their physical interpretations are summarized in *Table 2 of Paper II*. BrC/BC ratio in the atmosphere signifies the abundance of BrC relative to BC, types of emission sources, and atmospheric formation and transformation of organic aerosol. In this study, a higher (larger than the annual hourly mean) BrC/BC ratio is used as an indicator of biomass burning, while lower BrC/BC ratio (less than the annual hourly mean) are hypothesized to be contributed from non-local sources and atmospheric transformation of organic aerosol. In addition, some studies have used the BrC/BC ratio to identify dominant contributions from biomass burning and other fossil fuel combustion sources [143-146]. The ventilation coefficient ($VC = PBLH \times WS$) is used as an indicator of the capacity for dilution of pollutants via atmospheric processes, during the episodic events [147].

These episodic events showed the following characteristics of BrC: (i) BrC was mostly well correlated with BC, indicating that they originated from the same source e.g. all episodes except E13 (refer to *Figure S3 to Figure S7 in Paper II*); (ii) BrC concentrations showed both the seasonal and dial variability during the episodic events, e.g. winter (E1-E6: 8 - 3 μg m^{-3}); summer (E7: ~2 μg m^{-3} and E8: ~5 μg m^{-3} due to local brick firing) (*refer to Table S4 and Table S5 in Paper II*); (iii) BrC concentrations sometime correlated well with daily fire counts i.e. fire radiative power (FRP) indicating influence of regional

agriculture residue burning at the site e.g. E2, E7, E11; (iv) BrC/BC ratios during the episodic events varied significantly depending upon their sources and season, e.g. BrC/BC was high during the winter and autumn episodic events (E1- E6 : ~1 to 0.4) than summer episodic events (E7: ~0.3); however, E8 had a huge local biomass burning event from brick firing leading high BrC/BC ratio(~1.5), (v) BrC concentration and BrC/BC ratio usually showed a strong peak of concentration in the morning and evening linked to the morning and evening biomass burning for cooking.

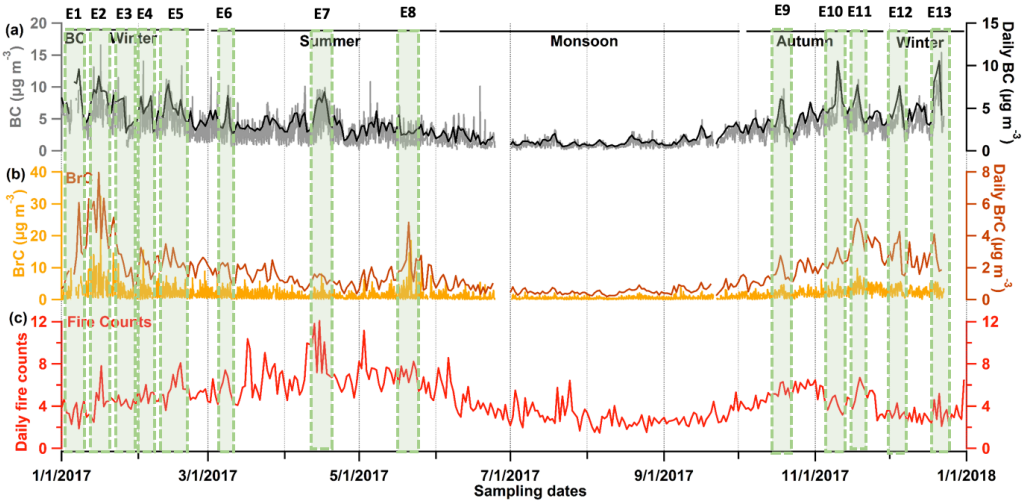

Figure 13: Hourly and daily variations in BC (top panel), BrC (middle panel), and daily fire counts (bottom panel) over IGP-CARE during the sampling period (January 2017 to December 2017). The light-green shaded areas correspond to episodic events, i.e. events during which the concentrations of BC and BrC were at least three times the hourly mean (3×hourly mean) over the sampling period.

Overall, episodic events of elevated BC and BrC concentrations can be attributed to the local biomass burning activities in the neighbouring rural communities. Therefore, it is suggested that high concentrations of BrC were mostly primary in nature and thought to be co-emitted with BC from biomass burning activities. However, above results showed that the observed episodic events are complex and influenced by several factors including sources and meteorological conditions as well as interlinked atmospheric process such as dilution and dispersion of pollutants, condensation-evaporation of organic species due to interlinked thermodynamics, heterogeneous chemical reactions, and photo-chemical processes. The influence of meteorology on the BrC at the IGP-CARE is discussed in the *section 3.7 of the paper II*.

4.2.2 Diurnal variation of BrC

The diurnal profile of BrC, BrC/BC ratio, along with BC and NO_X/BC ratio in different seasons are shown in Figure 14(a-d). In winter, BC and BrC concentrations had a bimodal diurnal distribution with concentrations peaking in the early morning (6.0 and 4.0 µg m^{-3} for BC and BrC) and night (6.5 and 4.4 µg m^{-3} for BC and BrC, respectively) and being lowest during the daytime (4.2 and 1.8 µg m^{-3}). The t-test indicated that the BC concentration in the mornings in winter was significantly higher ($p < 0.05$) than in other seasons. The low VC and calm winds during winter suggest that the regularly observed

high peaks of BC and BrC in the morning and evenings can be attributed to local biomass burning for cooking and heating. During morning hours (6:00-8:00 AM), low PBLH and VC, limited solar radiation, low temperature, and low wind speeds all favoured substantial increases in BC concentrations, as shown in Figure 14(a). During evening and late at night, BrC concentrations increased gradually due to the low VC and low temperature, especially in winter and autumn seasons. However, the morning and early night peaks were less prominent during monsoon season than in other seasons due to the wash-out effect (Figure 14(b)). The diurnal variation of BC and BrC from other studies was similar to the present study [148,149].

The BrC/BC ratio can suggest the formation process of BrC and/or BC and their sources, e.g., biomass burning, fossil fuel combustion sources, and SOA formation etc. [143-146]. The low BrC/BC ratio in combination with higher NOx to BC ratio indicates fossil fuel combustion [150] e.g diesel vehicles (11-47); gasoline vehicle (1940-4407), while high BrC/BC ratio suggests the dominance of biomass burning with low NOx to BC ratio (0.9-2.5) [151]. This is because high temperature in fossil fuel combustion systems emit higher NOx and low BrC. In these lights, an interesting diurnal variation of the BrC/BC ratio was also observed at IGP-CARE. The humps of BrC/BC ratio in the morning and evening in all seasons were clearly observed (see Figure 14(c)). These humps were not associated with NO_X/BC ratio, however similar CO humps were observed in mornings of all seasons indicating CO and BrC were co-emitted from biomass burning (see Figure 14(d); and *Figure 5b in paper II*). These suggest BrC, BC, and CO were co-emitted from local biomass burning from cooking and/or heating activities. Further, BrC/BC ratio decreased sharply during daylight hours and increased at night (see Figure 14(c)). The BrC/BC ratio was higher in winter and autumn than in summer and the monsoon season. This can partially be attributed to more BrC partitioning to gas phase, photo-bleaching, and interlinked atmospheric chemistry during the latter two seasons.

4.2.3 Ambient BrC transformation chemistry

In general, the BrC time series indicates that BrC, BC, CO, and NOx followed similar patterns in various seasons (see Figure 13 and Figure 3 in paper II). This suggests that BrC was co-emitted with BC from the local biomass burnings for cooking and heating needs. Thus, mostly the measured BrC in this study was primary in nature, which is hypothesized to be transformed significantly during the day-time. As shown in Figure 14(b and c), the profile of BrC/BC ratio evolved astonishingly during the day-time. An extremely sharp decline in BrC/BC ratio at the time of dawn each morning indicates the dominance of photochemical processes in the transformation of BrC. This transformation of ambient BrC was observed to decrease the attenuation of light absorption at 375 nm in this study. The decrease in the ability to absorb light by organic aerosol in reference to BrC was termed as bleaching. To investigate the bleaching of brown carbon, I analyzed the variability of BrC, BC, and O_3 levels during the daytime and the night-time at IGP-CARE as functions of temperature and solar radiation. BrC bleaching reduced the BrC/BC ratio, as shown in Figure 14(c) and was strong during the daytime. Recent studies have suggested that strongly light-absorbing primary BrC may rapidly evolve into weakly light-absorbing

secondary BrC in the atmosphere; this process is known as BrC bleaching [2]. Several factors could potentially explain the day-time decrease in the BrC/BC ratio, including photochemical processes (which would be consistent with the sharp decrease in the BrC/BC ratio during the early morning hours), radical chemistry (i.e. reactions with OH and/or O_3) and the volatilization of BrC compounds at elevated temperatures during the midday hours. Interestingly, temperature correlated better with BrC/BC during the daytime than at night.

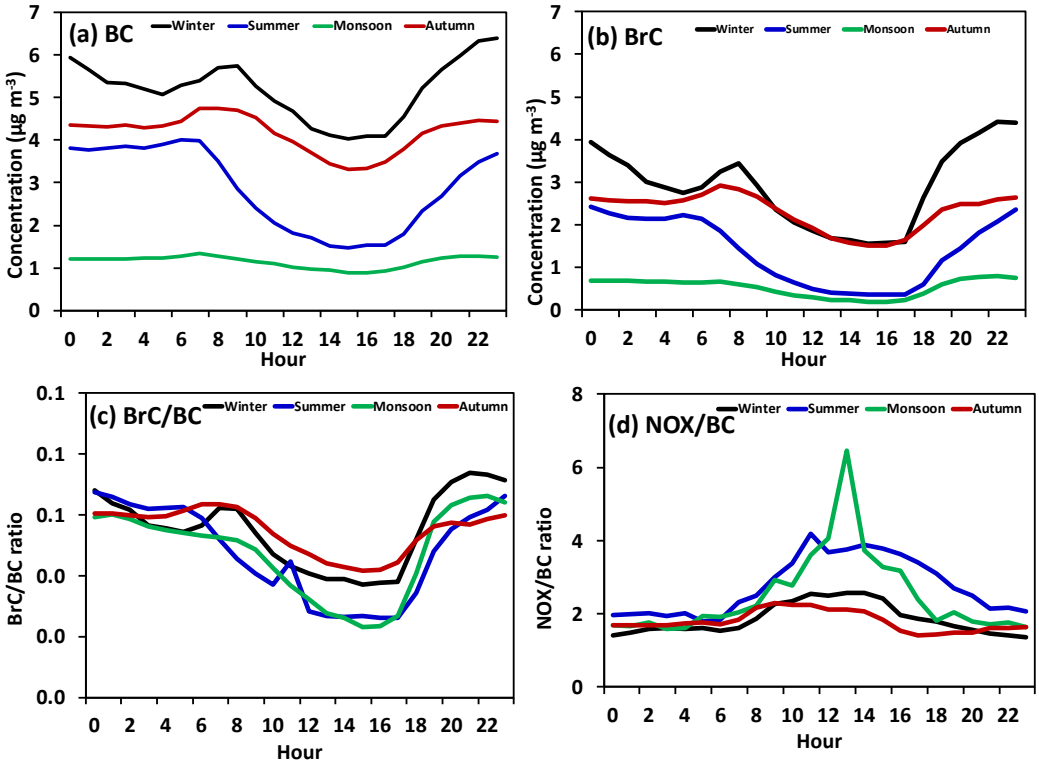

Figure 14: (a-d). Diurnal variation of BC, BrC, BrC/BC ratio, and NOx/BC ratio in four seasons at the IGP-CARE site during the sampling period 2017. The black, green, blue, and brown lines show results for the winter, summer, monsoon, and autumn seasons.

4.3 Characteristics of primary BrC in lab-scale flames

4.3.1 Composition and mixing state of BrC in fossil-fuelled premixed-flame emissions

In this PhD thesis, emissions from three propane-fuelled premixed flames were examined to characterize primary BrC co-emitted with soot. Here, five different particle sizes (75, 100, 150, 200 and 250 nm) from three lab-scale propane flames (Exp. F1, Exp. F2 and Exp. F3, refer *Table 1 in Paper III*) were studied. Two main components were found in particles of all five sizes i.e. BC and POA. The mass fraction of POA contributed 20–40% of the

total particle mass in soot (BC+POA) from all three flames. The results have been discussed in detail in the Paper III appended in this thesis and are summarized as following:

The diffusion-to-premixing air ratio (d/p ratio) may have affected the mechanism of POA formation and their size dependence of the POA mass fraction because the POA mass fraction was strongly size-dependent when the d/p ratio was small (13.8) but negligibly size-dependent when the d/p ratio increased to 19.9 (refer to *Figure 3 in paper III and Figure S2 in its Supplementary Information*). This suggests that the formation of smaller POA particles may have been favoured by reductions in the d/p ratio. The POA mass fractions in the largest (250 nm) soot particles were very similar for all three flames, indicating that POA of this size was not significantly influenced by changes in the proportions of premixing air and diffusion air.

The size-resolved mixing state of POA and BC was determined by measuring the number concentration and mass of particles from the flame exhaust using the Non-Thermal Desorption (NTD) at 25 °C and Thermal Desorption (TD) at 400 °C setups with VTDMA [152]. Figure 15(a-f) shows the number size distributions of particles in the three flames at 25 °C and 400 °C, and the mass concentration and mixing states of the size-resolved soot in all three flames at 25 °C.

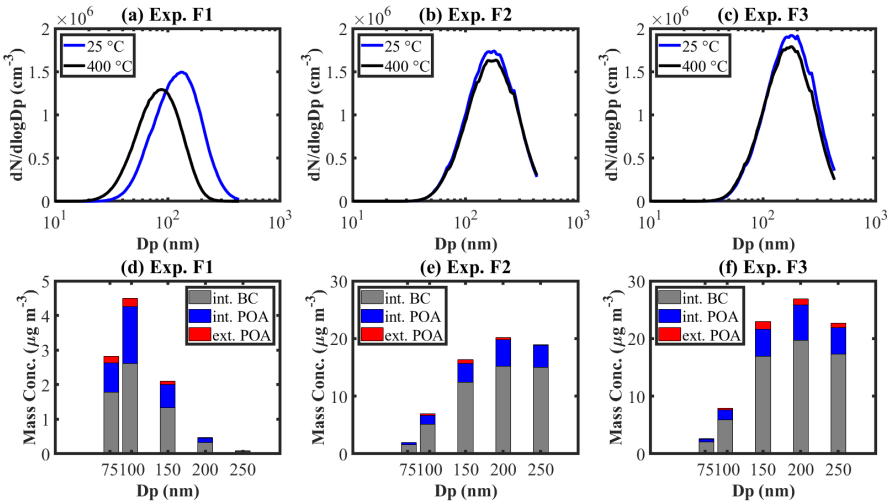

Figure 15: Top: Number size distributions of particles in (a) Exp. F1, (b) Exp. F2 and (c) Exp. F3 flames at 25 °C and 400 °C. Bottom: Mass concentrations and mixing states of size-resolved soot particles in (d) Exp. F1, (e) Exp. F2 and (f) Exp. F3 flames at 25°C

Figure 15(a-c) clearly demonstrate that: (i) POA and hence BrC was significantly internally mixed with BC in all flames; (ii) the fraction of internally mixed POA and hence BrC exhibited a strong size dependence; (iii) size dependence of fraction of internally mixed POA influenced by the flame settings, e.g. in F1, fraction of internal mixing of POA with BC was higher in the 75 and 100 nm particles, while in F2 and F3 it was higher in the particle larger than 100nm. However, previous studies had reported that POA was only

formed in small particles of 1-10 nm by homogeneous nucleation of organic vapors or hydrocarbon combustion reactions [153,154], and grew by condensation of PAH vapors, making it difficult for these externally mixed POA particles to grow appreciably. These findings suggest that the formation of internally mixed BrC with soot can also be important in fossil fuel combustion systems..

4.3.2 Light absorption properties of BrC

The AAE is a parameter that describes the wavelength-dependence of light absorption for particles of various sizes. The average $AAE_{405/781}$ values (calculated from absorption measurements at 405 and 781 nm) for BC+POA from the Exp. F1, Exp. F2 and Exp. F3 flames were 2.06±0.11, 1.65±0.08 and 1.84±0.06, respectively; the corresponding values for BC alone were 1.01±0.12, 1.08±0.11, and 1.28±0.07. These results indicate that all sizes of soot particles in all three flames had significant contents of light-absorbing POA (i.e. BrC). Hence, it is concluded that BrC existed in the from POA and was internally mixed with soot particles.

The estimated mass absorption cross-section (MAC) values of POA containing BrC in all three flames at all three wavelengths i.e. 405 nm, 532 nm and 781 nm, were significant as shown in Figure 15. However, at the wavelength of 405 nm, the MAC value of BrC (5 $m^2 g^{-1}$) under a certain flame setting (Exp. F2) was comparable to that of BC (8–9 $m^2 g^{-1}$). The MAC values and the corresponding imaginary part of the RI for POA (k_{POA}) derived from equation given at [140] for all three flames are shown as functions of the wavelength in Figure 16, together with literature data for POA formed during propane combustion (Kim et al. [155] and Lu et al. [156] and extracted from biomass samples Kirchstetter et al.[134]). At the short wavelength of 405 nm, POA from all three flames examined in this study exhibited strong absorption, which decreased significantly at longer wavelengths. The particles in the Exp. F1 and Exp. F3 flames had the same MAC at 405 nm, which was lower than that for Exp. F2 flame particles. This indicates that the flame conditions had a significant influence on the MAC of POA. Differences in the molecular composition of POA originating from different emission sources could cause differences in MAC and k_{POA} values at wavelengths below 530 nm [156,157]. The absorption of POA increases almost continuously with the extent of π-system conjugation [139], indicating that the particles from the Exp. F2 flame may have had higher contents of polycyclic aromatic hydrocarbons (PAH) or PAH-like materials than those from the Exp. F1 and Exp. F3 flames.

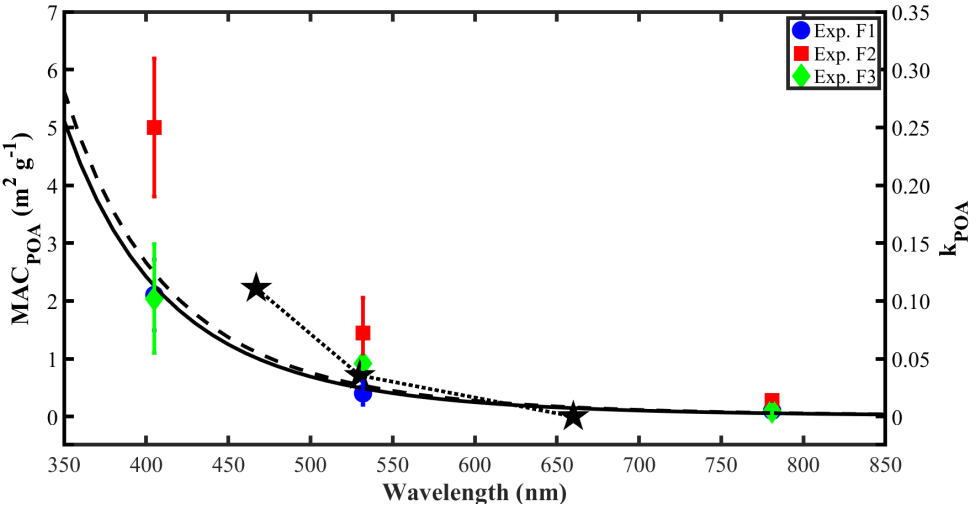

Figure 16: MAC values and estimated imaginary refractive indices of POA (k_{POA}) as functions of the wavelength

4.4 Influence of reactive nitrogen, acidity and water-mediated chemistry on the SBrC of toluene SOA

4.4.1 Summary of key results

The pattern of toluene SOA mass formation at [NOx]/[ΔHC] molar ratios at or below 0.15 was distinctly different (i.e. higher and constant) than that was observed at higher [NOx]/[ΔHC] ratios. The SOA mass decreased as the [NOx]/[ΔHC] ratio increased above 0.15 (*see Figure 1 in paper IV*). These distinguish between SOA formed under nitrogen-poor (NP) conditions i.e. with low initial NOx concentrations, and nitrogen-rich (NR) SOA formed at higher initial NOx concentrations, which has a higher content of compounds such as organo-nitrates [158,159]. Therefore, this distinction is valuable for understanding trends in the formation and properties of SOA under the variable NOx conditions. Hereafter, NP SOA and NR SOA are referred to SOA formed under nitrogen poor and nitrogen rich conditions, respectively. The main experimental results obtained in this work are summarized in Table 2 and described in *section 3.1 of paper IV*.

Table 2: Summary of experimental results for Paper IV

Exp. ID	SOA Type	SOA Mass µg m^{-3}	$B_{abs.\ 405}$ Mm^{-1}	$B_{abs\ 781}$ Mm^{-1}	$B_{scat\ 405}$ Mm^{-1}	$B_{scat\ 781}$ Mm^{-1}	MAC $_{405}$ m^{2}g^{-1}	MSC $_{405}$ m^{2}g^{-1}	OH (Molecules cm^{-3}s) x 10^{11}; [SOA Aging in Days]	Average Mobility Diameter (nm)
Tol-1	NP	552	11.8	0.320	1259	66.5	0.021	2.29	2.8; [1.61]	65.0
	NR	520	25.2	0.112	1258	67.4	0.048	2.38		64.7
Tol-2	NP	372	8.15	0.000	805	39.1	0.022	2.13	2.3; [1.33]	60.8
	NR	358	14.5	0.000	788	38.3	0.040	2.20		62.8
Tol-3	NP	261	5.31	0.937	516	22.3	0.020	1.88	1.6; [0.93]	58.8
	NR	223	10.3	0.195	451	20.3	0.045	1.95		57.7
Tol-4	NP	162	3.73	0.000	318	14.0	0.024	2.05	1.3; [0.77]	57.0
	NR	134	6.10	0.042	258	11.4	0.041	1.77		55.0
Tol-5	NP	465	13.3	0.246	2958	285.8	0.029	6.39	2.8; [1.61]	94.6
Tol-6	NR	432	40.1	0.025	1500	0.000	0.093	3.48	2.8; [1.61]	64.5
Tol-7	NP	375	11.5	0.000	1582	113.8	0.030	4.19	2.8; [1.61]	63.9
	NR	416	25.6	0.626	1950	139.6	0.061	4.57		64.5
Tol-8	NP	348	12.4	0.085	1747	127.4	0.035	5.05	2.8; [1.61]	91.2
	NR	321	21.4	0.987	1632	117.9	0.068	5.06		89.3
Tol-9	NP	192	7.86	0.000	807	55.2	0.041	4.14	1.6; [0.93]	87.8
	NR	182	10.3	0.000	738	51.4	0.058	4.05		88.1

4.4.2 Influence of NOx and RH on SBrC formation and properties (Exp. Tol-1 to Tol-4)

As discussed above, in Exp. Tol-1 to Tol-4, SOA mass was independent of [NOx]/[ΔHC] under NP conditions ([NOx]/[ΔHC] ≤ 0.15) but decreased with increasing [NOx]/[ΔHC] under NR conditions ([NOx]/[ΔHC] > 0.15). Conversely, the light absorption of the SOA (measured in terms of the aerosol absorption coefficient at 405 nm, i.e., $B_{abs,405}$) increased with [NOx]/[ΔHC], irrespective of NP or NR regimes as shown in Figure 17. These trends confirm the formation of SOA chromophores due to toluene-OH-NOx-water mediated chemistry. These indicate that [NOx]/[ΔHC] has two opposing effects on SOA formation; higher [NOx]/[ΔHC] levels promote the formation of light absorbing chromophores (browning of molecules) but reduce that of molecules contributing to SOA mass.

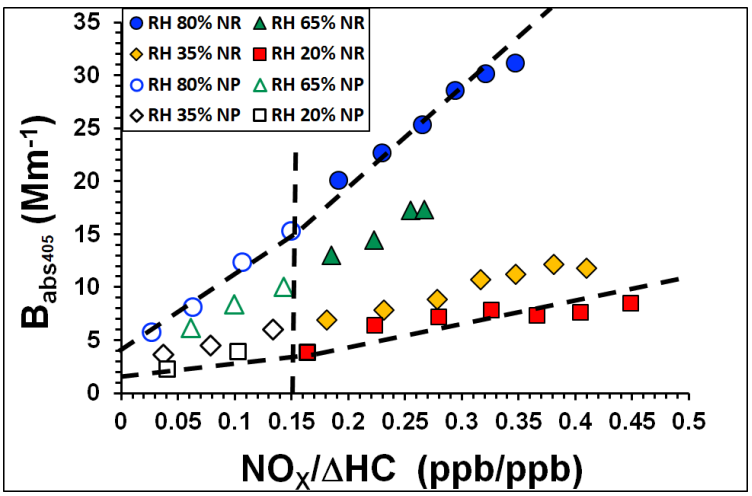

Figure 17: The aerosol absorption coefficient B_{abs} as a function of [NOx]/[ΔHC] at 80% RH, 65% RH, 35% RH and 20% RH. Empty and filled symbols show results for NP and NR SOA, respectively. Dashed lines are included to guide the eye.

As outlined above, NOx enhanced the formation of BrC in SOA. Similarly, at the higher RH, both the absolute values of B_{abs} and the slope of the plot of B_{abs} became higher as the NOx increased as shown in Figure 17. The trend towards higher B_{abs} values at higher RH is consistent with the trends observed for SOA mass (see *Figure 3 and Figure 1 in paper IV*). These results indicate that toluene-OH-NOx-water-mediated chemistry promoted the both SOA mass and BrC formation at high RH values (e.g., 80%) due to the synergistic effects of water vapour and high OH concentrations.

The mass absorption cross section (MAC) of the SOA was estimated by normalizing B_{abs} against the SOA mass (see *Table S2 in the Supplementary Information of Paper IV and* Table 3). Alike the B_{abs}, MAC of the SOA increased with [NOx]/[ΔHC] under all RH conditions, with a clear "*switching point*" at [NOx]/[ΔHC] = 0.15 as shown in Figure 18. However, MAC of NP SOA showed no influence of RH when [NOx]/[ΔHC] increased, while slope of MAC increase against [NOx]/[ΔHC] was steeper at higher RH under NR conditions (See Figure 18).

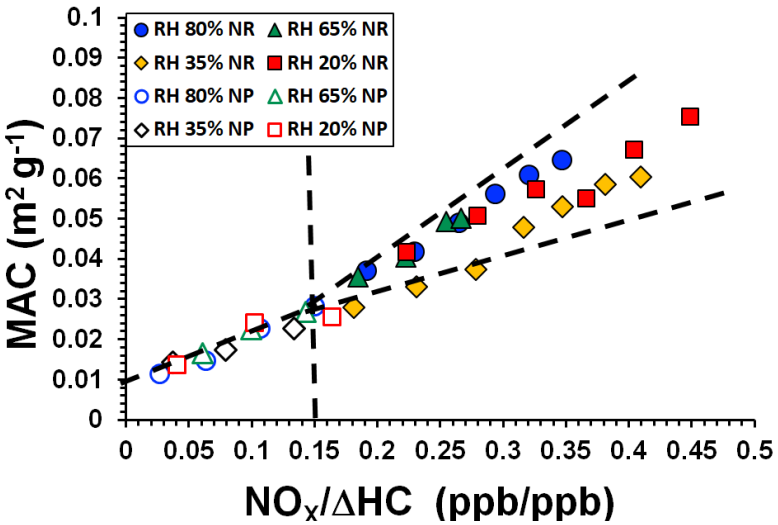

Figure 18: MAC (mass absorption cross-section) as a function of the [NOx]/[ΔHC] ratio at 80%, 65%, 35% and 20% RH. Empty and filled symbols show results for NP and NR SOA, respectively. The dashed lines are included to guide the eye.

At a given RH, the B_{abs} value of the SOA reflects only the amount of chromophores formed as a result of toluene-OH-NOx-water-mediated chemistry. The increase in B_{abs} with [NOx]/[ΔHC] indicates that NOx-water chemistry has an important effect on MAC at high RH levels. At the same time, hygroscopic growth at high RH enhances the contribution of aerosol liquid water i.e. ALW, to the SOA mass measured by the SMPS, which is calculated using the SOA density functions of Ng et al. [160]. This in turn leads to underestimation of the MAC at high RH. These two processes may have opposing effects on the MAC because hygroscopic growth increases SOA mass, while toluene-OH-NOx-water mediated chemistry promotes BrC formation. At high RH, hygroscopic growth reduces MAC, while toluene-OH-NOx-water-mediated chemistry increases B_{abs}.

4.4.3 Influence of NH_3 and NOx on SBrC formation and properties at high RH (Experiments: Tol-5 and Tol-6)

Two results shown in Figure 19 are particularly noteworthy: (i) the B_{abs} and MAC under low NOx conditions (Tol-5) showed a peak at $[NH_3]/[\Delta HC]$ ~0.11 – a similar behaviour as SOA mass (see *Figure 8 in paper IV*) in response to increasing $[NH_3]/[\Delta HC]$; (ii) the B_{abs} and MAC under high NOx conditions (Tol-6) were much higher than low NOx experiment (Tol-5). The similar behaviours of B_{abs} and MAC as functions of $[NH_3]/[\Delta HC]$ suggest that N-H-containing organic chromophores (e.g., cyclic amines) with similar light absorption profiles were formed under low NOx regime [48,49]. In the high NOx regime, SOA formation via the toluene-OH-NOx-water-mediated chemistry appears to dominate because the B_{abs} and MAC in this case behaved similar to those of the NR SOA formed in Tol-1.

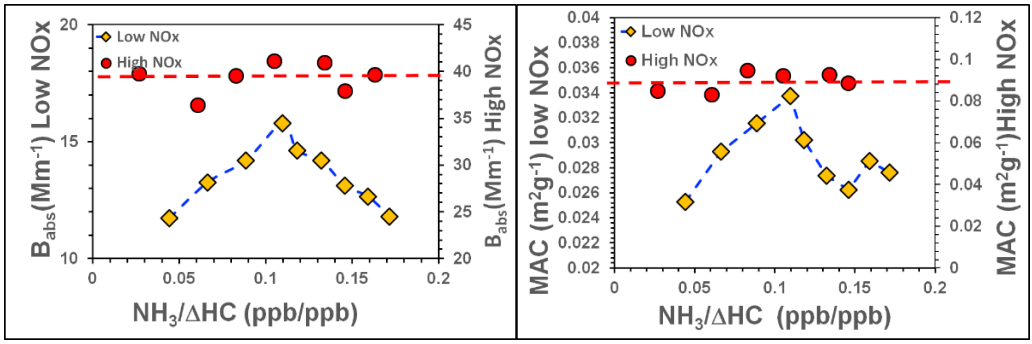

Figure 19: B_{abs} and MAC as a function of the ($[NH_3]/[\Delta HC]$) ratio at 80% RH under low and high NOx scenarios. Blue and red dotted lines are the eye guiding lines for low and high NOx scenarios, respectively. The dashed lines are to guide the eye.

Figure 20 compares the effects of NH_3 on the optical characteristics of toluene SOA. Finally, the presence of NH_3 enhanced B_{abs} and MAC values under both the low and high NOx conditions. These results indicate that NH_3 increases the N:C ratio of the SOA under high NOx conditions.

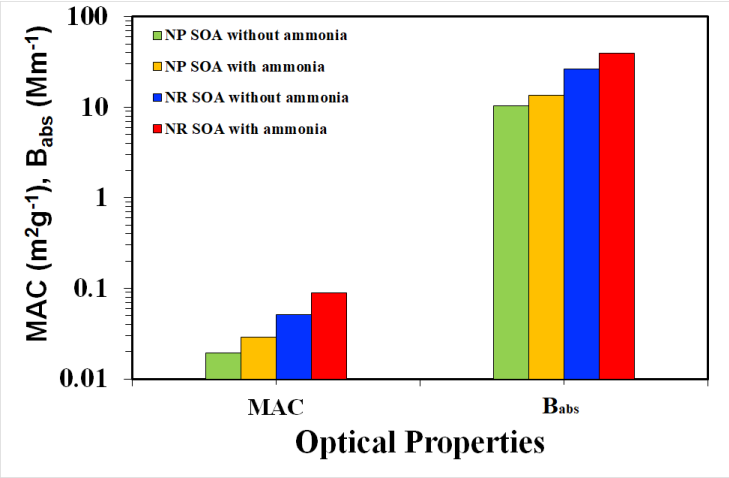

Figure 20: Compare the effects of NH_3 on the optical characteristics of toluene SOA. Finally, the presence of NH_3 enhanced B_{abs} and MAC values under both the low and high NOx conditions. These results indicate that NH_3 increases the N:C ratio of the SOA under high NOx conditions.

4.4.4 Influence of NOx, acidity and RH on SBrC formation and properties (Experiments: Tol-7 to Tol-9)

The key results of H_2SO_4 seeded experiments are:
(i) alike the non-seeded experiments, B_{abs} increased with [NOx]/[ΔHC] in the H_2SO_4 seeded experiments, but, with slightly steeper slopes in the seeded case at all RH values except at 80% RH (See *Figure 13 (a) –(f) in paper IV*). At 80% RH, the B_{abs} trends in the non-seeded (Tol-1) and H_2SO_4 seeded (Tol-7) experiments were almost identical, indicating that acidity had no obvious effect on B_{abs} under either the NP or the NR regime.
(ii) MAC of the all H_2SO_4 seeded experiments was higher than non-seeded experiments at all RH, signifying that acidity promoted the browning of the SOA (refer to *Figure 14 (a–c) in paper IV*).
(iii) MAC in the H_2SO_4-seeded experiments was higher than that in the corresponding non-seeded experiments and increased as the RH decreased. (refer to *Figure 14 (a–c) in paper IV*).
(iv) The higher MAC of acidic SOA at lower RH values is tentatively linked to the formation of organo-sulphate chromophores, which is suggested to be governed by two major parameters: (a) the pH of the SOA aqueous phase, and (b) the ratio of $[H^+]_{free}$ (the concentration of free protons in the aqueous phase) to the SOA mass.

Under NP conditions, the highest acidity i.e. the lowest pH (see *Figure S10 in Supplementary Information of paper IV*) and the highest $[H^+]_{free}$/ SOA mass ratio (see *Figure 14(c) in paper IV*) were both observed with H_2SO_4 seeding, supporting our hypothesis. In addition, a modelling study conducted by *McNeill et al.* [161] suggested that organo-sulphate formation was maximized at low pH and low RH (<60%), i.e., when the aerosol was more concentrated. Conversely, under NR conditions the MAC of non-seeded

SOA reached a minimum at an intermediate RH (65%), whereas the MAC of the H_2SO_4 seeded SOA peaked at the same RH (65%) and was lowest at 80% RH (see *Figure 14 (b) in paper IV*). These contrasting trends for seeded and non-seeded SOA under NR conditions are interesting and suggest that NOx has a strong influence on light absorption at the intermediate RH (65%). These observations indicate that the browning of toluene SOA is driven by complex interactions between the effects of acidity, NOx, and water vapor.
Influence of reactive nitrogen, acidity and water-on molecular composition of SBrC in toluene SOA

4.4.5 Identification of BrC molecules containing chromophores

The molecular characterization of toluene SOA experiments discussed in the previous section i.e. 4.4, was performed using their FIGAERO-HR-ToF-CIMS data. Here, I considered only 7 out of previous 9 experiments (i.e. Tol-1, Tol-3 to Tol-7 and Tol-9). The mass spectra data from HR-ToF-CIMS provided the mass to charge ratio for peaks/ions i.e. m/z representing the BrC molecules containing chromophores. In the light of the facts discussed in the section 4.4 of this thesis – the bulk B_{abs} increased against the increase of $[NO_x/\Delta HC]$ ratio, a criterion was set up to identify the key BrC molecules containing chromophores (i.e. m/z). The counts per seconds (CPS) signal of the peaks with a specific m/z must exhibit a positive correlation with both bulk B_{abs} and $[NO_x/\Delta HC]$ ratio and mimic the trend of B_{abs} against $[NO_x/\Delta HC]$ ratio. The detailed methods, calculations and results of m/z identification are provided in the *section 3.1 and supplementary Information of paper V* and the finally identified key m/z are listed in Table 3.

Table 3: BrC composition i.e. identified key m/z that mimic bulk B_{abs} trends in various experiments under the influence of RH, reactive nitrogen and acidity

Sr. no.	Experiment ID						
	Tol-1 key m/z (Av.CPS range)	**Tol-3 key m/z (Av.CPS range)**	**Tol-4 key m/z (Av.CPS range)**	**Tol-5 key m/z (Av.CPS range)**	**Tol-6 key m/z (Av.CPS range)**	**Tol-7 key m/z (Av.CPS range)**	**Tol-9 key m/z (Av.CPS range)**
1.	**281.929 (11-30)**	**295.946 (47-59)**	**226.918 (57-75)**	257.931 (34-36)	252.078 (1-2)	260.922 (19-27)	**226.924 (62-89)**
2.	293.942 (5-10)	**311.938 (8-11)**	227.925 (4-6)		348.061 (1-2)	274.939 (57-79)	289.921 (3-5)
3.	**295.942 (13-99)**	**315.985 (17-24)**			402.001 (2-3)	**281.922 (20-53)**	**295.947 (32-67)**
4.	**311.934 (4-13)**	**363.960 (8-13)**			519.010 (1-2)	286.942(71-101)	327.941 (3-7)
5.	**313.957 (10-21)**	435.991(4-6)			570.985 (1-2)	**295.937 (75-273)**	**329.956 (10-28)**
6.	**315.983 (7-23)**				638.985 (0-1)	299.932 (14-21)	345.956 (7-15)
7.	**329.948 (6-19)**					**311.930 (8-21)**	**361.957 (5-8)**
8.	333.944 (6-11)					**313.951 (11-22)**	
9.	**361.939 (3-12)**					314.971 (26-36)	
10.	**363.958 (4-17)**					342.991 (17-21)	

It was observed that the sets of key BrC molecules containing chromophores (m/z) in each experiment were different, which indicates that BrC composition was influenced by RH i.e. Tol-1, Tol-3 and Tol-4; NH_3 i.e. Tol-5 and Tol-6, and acidity i.e. Tol-7 and Tol-9. Further, as outlined above, a significant influence of NOx on the B_{abs} suggest that NOx also promoted the growth of key BrC molecules containing chromophores.

4.4.6 Influence of NOx, NH_3, acidity and RH on the m/z formation

As outlined in the section 4.4, NOx has a positive influence on the BrC formation and its composition i.e. m/z (see Table 3). NOx not only positively enhanced m/z CPS, but also significantly influenced their relative abundance at higher [NO_x/ΔHC] ratio as shown in Figure 21 for Tol-1. In Tol-1, the m/z 296 increased from about 20% to 40%, while relative distributions of other m/z was decreased, .e.g. the relative abundance of m/z 282 decreased from 16% to 11%. Thus, in Tol-1, m/z 296 significantly dominated the BrC composition at the higher [NO_x/ΔHC] ratio. Similar characteristics of m/z 296 dominance were also observed in the Tol-3, Tol-7 and Tol-9.

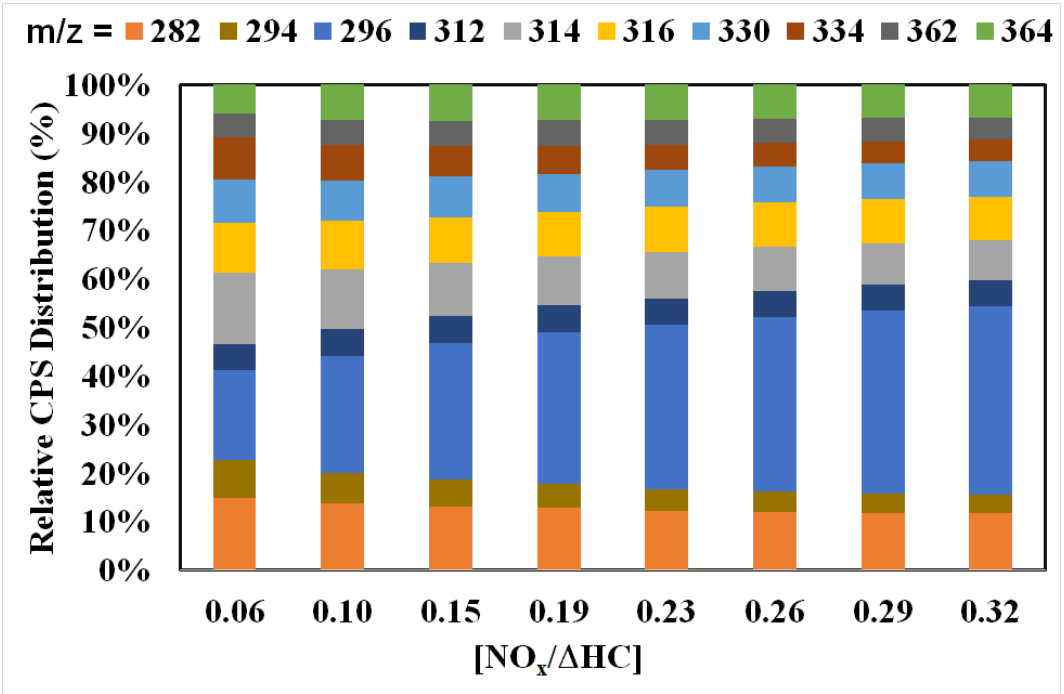

Figure 21: Abundance of m/z CPS to total sum of the all identified m/z (see Table 3) CPS during the NOx ramping in the Exp. Tol-1

The influence of RH on the BrC molecular composition i.e. relative distributions of the key m/z, was clearly visible. For instance, as shown in Table 3, at the higher RH, the number of key m/z contributing to BrC was higher (e.g. Tol-1: 10 key m/z at 80% RH; while for Tol-3: 5 key m/z at 35% RH and for Tol-4: merely 2 key m/z at 20%RH). Tol-1 and Tol-3 had several common m/z i.e. 296, 312, 316 and 364, which indicated similar chemical pathways of their formation. However, in the Tol-4, no common m/z were observed with either Tol-1 or Tol-3. These show that RH below 35% critically suppressed the formation of BrC molecules containing chromophores such as 296, 312, 316 and 364 etc. Interestingly, despite that experimental conditions of Tol-7 and Tol-9 (in presence of H_2SO_4 seeds) were chemically different than Tol-1 and Tol-3 (no acid), there were several common m/z among these four experiments. Tol-1 and Tol-7 were similar experiments at 80% except that Tol-7 has low concentration of H_2SO_4 seeds. Hence, Tol-1 and Tol-7 had significant (50% or 5 key m/z) overlap of m/z in the BrC composition. On the other hand, only two m/z of Tol-9 were common with Tol-1 i.e. m/z 296 and 362 and only one m/z common with Tol-3 and Tol-7, i.e. 296 and Tol-4 i.e. 227 (see Table 3). These suggest irrespective of acidity, RH played vital role in the formation of m/z 296. It can be inferred that even under the drier condition i.e. 20% RH (Tol-9) the formation of m/z 296 was feasible in the presence of acidity.

Although Exp. Tol-5 and Tol-6 were also performed under high RH (80%), their key m/z distributions for BrC were completely different than rest of the other experiments. This indicates that presence of ammonia significantly altered the chemical pathways of

formation of m/z i.e. BrC molecules containing chromophores. For instance, as outlined in Table 3, many higher numbered m/z were prevalent especially in Tol-6. In Tol-5, at low NOx (i.e. [NO_x/ΔHC] ratio = 0.052) and significantly low NH_3 (i.e. [NH_3/ΔHC] ratio = 0.05), B_{abs} was 13.5) which is higher almost by a factor of 2 relative to the B_{abs} of Tol-1 at the similar [NO_x/ΔHC] ratio (B_{abs} ~7; see *Figure 6 in paper V*). This suggests that presence of ammonia enhanced the formation of stronger light absorbing chromophores. In Tol-5, only one key m/z 258 was found to exactly match the B_{abs} pattern as shown in *Figure 8 of paper V*. Unlike NOx, this non-linear behaviour of ammonia indicates complex chemistry of toluene-OH-NH_3. There were also found other m/z in Tol-5, which were also found in Tol-1 e.g. 296, 282, 312, 314, 316, 362 and 364 (see *Figure 9 in paper V*). These potentially resulted from the toluene oxidation chemistry in the presence of low NO_x i.e. [NO_x/ΔHC] ratio = 0.052, and high RH (80%) and contributed to the observed B_{abs} in Tol-5.

In the Exp. Tol-6 at high NOx i.e. [NO_x/ΔHC] ratio = 0.32, and high RH (80%) during the ammonia ramping (42 to 203 ppb), the distribution of the key m/z were significantly different than low NOx scenario i.e. Tol-5, that matched the observed B_{abs} patterns as shown in Table 3. Alike Tol-5, presence of low NH_3 under high NOx i.e. [NO_x/ΔHC] ratio = 0.32 in Tol-6, significantly enhanced (e.g. ~20% higher) B_{abs} than Tol-1 under the similar [NO_x/ΔHC] ratio = 0.32. Further increasing ammonia, B_{abs} also increased; and also the m/z CPS increased and alike Tol-5, both B_{abs} and all m/z CPS peaked at [NH_3/ΔHC] ratio = 0.13 (see *Figure 10 in paper V*). Further increasing [NH_3/ΔHC] ratio, the B_{abs} and all m/z decreased. These are very similar patterns as discussed above for Tol-5. Thus, ammonia has positively enhanced the formation of light absorbing m/z in both Tol-5 and Tol-6. Similar to Tol-5, there were also found several m/z in Tol-6, which did not exactly match with B_{abs} pattern e.g. m/z 296, 282, 312, 314, 316, 362 and 364 as shown *in Figure 11 in paper V*. These potentially contributed to the observed high B_{abs} in Tol-6.

The experimental conditions of Tol-7 were similar to Tol-1 except that Tol-7 used the H_2SO_4 seeds. Therefore, I focus to discuss similarities and differences in the BrC composition i.e. m/z distribution in these two experiments. First the final B_{abs} values and its correlation with [NO_x/ΔHC] ratio were similar in Tol-1 (see *Figure 5 in paper V*) and Tol-7 (see *Figure 13 in paper V*). There was observed a significant overlap in the m/z distribution in Tol-1 and Tol-7 as shown in Table 3.

The effect of acidity on the key m/z distribution i.e. BrC composition was much prominent at low RH (20%). Here Tol-9 was similar to Tol-4 except that Tol-9 used the H_2SO_4 seeds. The B_{abs} values have similar patterns in both Tol-9 and Tol-4. However, the BrC composition in Tol-9 was drastically affected by acidity. As outlined in Table 3, the m/z in the BrC composition of Tol-4 was dominated by the m/z 227, while in presence of H_2SO_4 seeded experiment along with m/z 227 many other m/z contributed to BrC composition of Tol-9. These include m/z 296, 330, 346, 290, 362 and 324 (see *Figure 15 in paper V*).

4.4.7 Potential molecular tagging to m/z and their formation Pathways

Although the BrC composition (i.e. distribution of key m/z) was distinct for each experiment, there were also several common m/z in the similar set of experiments (See Table 3). For instance, Tol-1 and Tol-3 had four common m/z i.e. 296, 312, 316 and 364. In the Tol-1 and Tol-3, the primary difference was the RH and commonality was the similar ramping of [NO_x/ΔHC] ratio during each experiment. Out of these, m/z 296 was the most prominent BrC molecule containing chromophores. The m/z 296 i.e. 295.942 is potentially an iodide adduct of 3-methyl 4-nitrocatechol (3M4NC) or its isomers i.e. 5M4NC or 6M4NC or 4 nitro-guaiacol (4NG). In fact, 4NG and 3M4NC have been identified as products in atmospheric aerosol and toluene oxidation products by several previous studies [162-167]. Formation of nitro-aromatic compounds (NAC) are thought to be the key players in the BrC in the urban areas due to high NOx scenarios [168]. Formation of these NACs has been described in previous studies involving the oxidation of toluene leading to formation of nitro-catechol derivatives in presence of NOx [110,169-173].
Ji et al. [171] outlined the key pathways for toluene OH oxidation for the formation of o-cresol (MW=108) and further leading to formation of derivatives of catechol or Guaiacol (MW =124) as shown in Figure 22. *Frka et al.* [170] has outlined that nitration of *catechol* derivatives in aqueous phase leads to the formation of light absorbing *nitro-catechol* derivatives as shown in Figure 23. The enhancement of m/z 296 CPS with increase of NOx in several experiments e.g. Tol-1, Tol-3, Tol-7 and Tol-9, indicates the formation of nitro-catechol derivatives as the key BrC molecules containing chromophores in these experiments (see Table 3). Similarly other m/z such as 282, 294, 312, 314 and 330 also appeared to be derivatives of *nitro-catechol* during the processes of OH oxidation, demethylation or nitration processes as shown in Figure 22-Figure 25 [168,170,171,174].

The potential empirical formulae of several m/z and their corresponding structures are proposed here e.g. e.g. *Pyridine, 4-methoxy-1-oxide-* (m/z 252); *Benzonitrile, 4-formyl-* (m/z 258); *5-Methylbenzofurazan* (m/z 261); *2-nitro-Benzonitrile* (m/z 275); *4-nitro Catechol* (m/z 282); *3-nitro Benzoic acid* (m/z 294); *3M4NC / 4 NG* (m/z 296); *6-hydroxy 3 methyl 4-nitro Catechol* (m/z 312); *3,5-dihydroxy 4-nitro Catechol* (m/z 314); *3,5,6-trihydroxy 4-nitro Catechol* (m/z 330). These are also popular BrC molecules reported in the previous studies and are listed in [110,162-178] *Table 4 in paper V*. These are derivatives of aromatic nitro-compounds formed under the influence of reactive nitrogen, acidity and water.

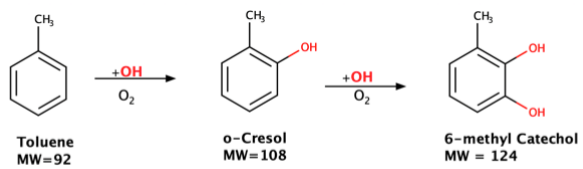

Figure 22: Dominant pathways of Toluene OH reaction leading to formation of Catechol [171] **(*Ji et al. 2017*)**

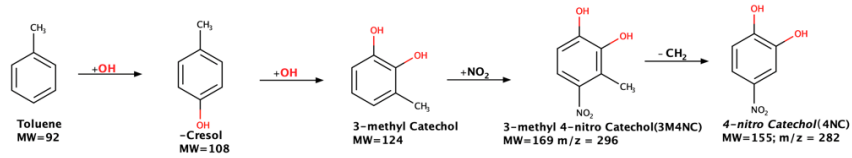

Figure 23: Dominant pathways of Toluene OH reaction leading to formation of nitro Catechol derivatives [170] (*Frka et al. 2016*)

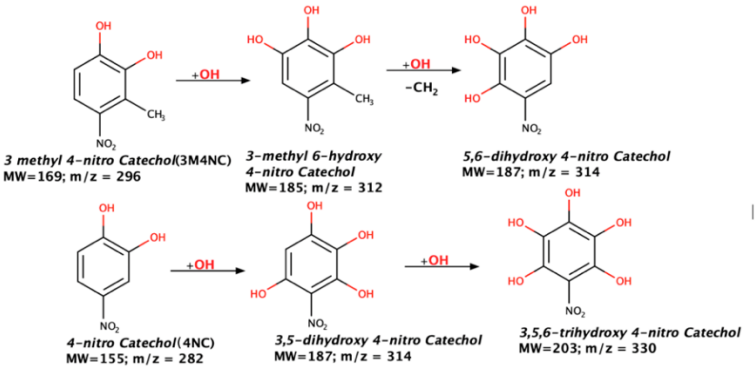

Figure 24: Proposed pathways of nitro Guaiacol and nitro-Catechol OH reaction leading to formation of Catechol derivatives [171] **(*Ji et al.* 2017)**

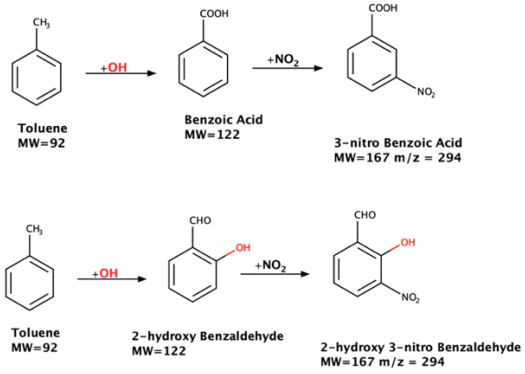

Figure 25: Proposed formation pathways of nitro-aromatic compounds (NAC) Chromophores via toluene photooxidation chemistry mediated by NOx and water **[179,180]**

5 Conclusions

This thesis is comprised of five research papers published or in process of publication. Studies of primary BrC formation and transformation are reported in Papers I, II and III and studies of secondary BrC formation and transformation are reported in Papers IV and V: These lab and field studies provided a holistic understanding of the formation and transformation processes and properties of atmospheric BrC. Final conclusions are summarized as following:

HR-ToF-CIMS data from the Swedish residential biomass burner were analysed using PMF, resulting in the identification of six factors: lignin pyrolysis products, cellulose/hemicellulose pyrolysis products, nitrogen-containing compounds, volatile molecules, semi-volatile compounds, and a factor related to instrument behaviour. Based on the optical properties and factor time series, the *lignin* and *cellulose* factors appeared to be the main contributors to PBrC emissions from biomass burning under the tested conditions.

At the IGP-CARE, thirteen episodic events (E1–E13) of elevated BC and BrC concentrations were characterized. The observed elevated concentrations of BC and BrC can be attributed to the local biomass burning (wood, agricultural residues, and dung cakes) for cooking and heating by the surrounding rural neighbourhoods. The high concentrations of BrC observed are suggested to be primary in nature and thought to be co-emitted with BC from biomass burning. The BrC/BC ratio decreased sharply during daylight hours (08:00–17:00 IST) and slowly increased at night (18:00–23:00 IST), especially in the winter and autumn; this may have been associated with BrC bleaching, which is thought to be affected by temperature, solar radiation, and ozone/radical chemistry.

The AAE at 405/781 nm of soot mixtures in the exhaust of three propane fuelled flames were higher than 1.5 in all the selected sizes i.e. 75, 100, 150, 200 and 250 nm. This suggested the highly absorptive nature of POA. Extremely high MAC values of POA (2–5 $m^2\ g^{-1}$) were measured at 405 nm. This strong light-absorbing POA containing BrC, is thought to be co-produced with BC and was attributed to the incomplete combustion of fuel. The flame settings, i.e., premixing and diffusion air flows, have a significant influence on the MAC values of POA containing BrC.

In the toluene photooxidation experiments, I observed that the pattern of SOA mass formation at [NOx]/[ΔHC] molar ratios below 0.15 differed markedly from that seen at higher [NOx]/[ΔHC] ratios. I therefore distinguish between nitrogen-poor (NP) SOA formed under conditions with low initial NOx concentrations and nitrogen-rich (NR) SOA, which has a higher content of compounds such as organo-nitrates. In addition, NOx promoted SOA browning under both regimes. Under the NP regime, MAC increased with [NOx]/[ΔHC] independently of the RH. However, for NR SOA, the MAC depended significantly on both [NOx]/[ΔHC] and the RH. The RH also had a complex effect on SOA browning (measured in terms of the MAC) under NR conditions but did not promote

browning under NP conditions. Both B_{abs} and MAC increased with the $[NH_3]/[\Delta HC]$ ratio, suggesting that NH_3 promotes the formation of N-H-containing organic chromophores such as cyclic amines and azo compounds with similar peak B_{abs} values under low NOx conditions. Acidity strongly promoted SOA mass formation. The results show that acidity has complex effects on S BrC formation that depend on both the NOx concentration and the RH. The MAC was significantly enhanced in both NP and NR regimes in the H_2SO_4 seeded SOA, indicating that acidity plays an important role in SOA browning. In addition, the MACs of the H_2SO_4-seeded SOA were higher at intermediate and low RH than at high RH (80%). This finding was rationalized by suggesting that the MAC enhancement of acidic SOA is linked to the formation of organosulphate chromophores and governed by two major parameters: the pH of the SOA aqueous phase and the ratio of the free hydrogen ion concentration in the aqueous phase ($[H^+]_{free}$) to the SOA mass.

The BrC composition i.e. set of the m/z contributing to the B_{abs} were different for different experimental conditions. However, within the same experiment, NOx affected the relative distributions of various m/z because the growth rate of different m/z were different. However, I found m/z 296 as a common dominant BrC molecule containing chromophore, under several experimental conditions. The RH played a vital role in determining the BrC composition i.e. m/z distribution under the influence of reactive nitrogen and acidity. The BrC molecules corresponding to various m/z identified are suggested to be nitro-aromatic compounds (NAC), which are primarily formed via OH oxidation of toluene followed by the nitration and/or demethylation processing of the oxidized aromatic ring. The suggested key BrC chromophores are the nitro-derivatives of the phenols, catechol and benzonitriles.

6 Acknowledgements

First and foremost, I would like to express my sincere gratitude to my supervisor Docent, Senior Lecturer Dr. Ravi Kant Pathak for guiding me and influencing me in many aspects during my PhD studies, for his patience, motivation, enthusiasm, and immense knowledge. I thank him for introducing me to the area of atmospheric BrC studies and for fruitful discussions and scientific support. My sincere thanks also go to my assistant supervisor, Prof. John Fletcher, for his encouragement, insightful comments. I am grateful to Prof. Mattias Hallquist for being my examiner and helping me greatly in many many intellectual and practical aspects during my studies.

My great appreciation also goes to Prof. Johan Boman, Prof. Jan B.C. Pettersson, and Dr. Xiangrui Kong, Dr. Xiangyu Pei, Dr. Christian Mark Salvador and Harsh Raj Mishra, Dr. Jai Prakash, Dr. Epameinondas Tsiligiannis. It has been an honor to work with them. I also owe earnest and sincere thanks to all the current and former members of the Atmospheric Science group, including Dr. Anna Lutz, Dr. Michael Le Breton, Dr. Samuel Mwaniki Gaita, Dr. Michael Priestley, Dr. Dimitri Castarède, Luis Filipe Escusa Dos Santos, Viktor Andersson, Dr. Yaxin Ge, Linjie Li, Veronica Geretti, Dr. Sofia Johansson, Dr. Julia Hammes, Dr. Erik Thomson. I am grateful to you all for your understanding and encouraging gestures!

All collaborators during my PhD studies are also owed many thanks for all their help and support: Mr. Staffan Carlsson and Dr. Kent O. Davidsson from RISE Research Institutes of Sweden AB (RISE); Dr. Åsa M. Hallquist from IVL Swedish Environmental Research Institute.

I want to express my deep deep gratitude to Prof. Aldo Jesorka at Chalmers University of Technology and Prof. Jonas Bergquist, MD at Uppsala University, Dr. Jens Herbig CTO of Ionicon Analytik Ges.m.b.H., who nurtured and who collaborated with me in my key motivation and research topic and without that collaboration and final results that helped me received multiple Swedish state and central government grants, and without that past I may not be considered for my PhD position. First Aldo, after Aldo getting convinced, he connected me with Jonas and finally Jens with whom I initiated and established a life time friendship, their initial support actually opened many future wonderful relations including, with Senior Researcher (currently retired) Dr Alex Schmid of University of Innsbruck, Dr. Veronika Ruzsányi of Innsbruck Medical University, Dr. Wojciech Filipiak of University of Innsbruck (currently Senior Researcher at Nicolaus Copernicus University), DI(FH) Helmut Wiesenhofer of University of Innsbruck, Clemens Ager of University of Innsbruck.

I am really thankful to Dr. Bo Norrman, Innovation Advisor of Chalmers University of Technology, Mr. Erik Bengtson CEO of Sahlgrenska Science Park (currently Investment Manager at Södra Ädla AB) both of whom I first met as my client and then they turned out to be as my most trusted friends since 2008 till today and helped me all through in every possible way. Once in 2011 Erik actually told me go back to university and invent

something wonderful; you can do wonders, then just helping researchers with novelty and techno-commercial innovation analysis. I actually take his words seriously and then joined Chalmers in 2012 to invent what I cherished in my mind for years!

I am really grateful to my current corporate friend and boss at Dr. Joel Kullberg, Owner, inventor, VP Innovation & Patents, Department of Innovation & Patents at Antraos Medical AB, a Docent and senior Lecturer (soon to be full Professor) at Uppsala University, my colleague Dr. Alexander Korenyushkin MD, Radiology Specialist, and Mr. Adam Maen, Machine Learning Specialist, Department of Innovation & Patents at Antraos Medical AB. I am thankful to all of them, we are within our small and beautiful close-knit-team in our department. I cherish their wonderful companionship. They help me in all possible ways during my double responsibility days both with my PhD and with corporate responsibility.

The person whom I never knew before personally, but she came to me directly after a University conference was over (where I was not even a speaker or presenter), in 2018. She is our Rektor Professor Eva Wiberg, who told me do not ever get stuck with any barrier in life, you must prevail, irrespective of whatever problems you face. I salute you Eva!

I am in debt for the kind cooperation I received directly from Dr. Markus J. Tamás, our ex-Department head who did his absolute best in collaboration with my PhD supervisor for my planned visit for our field experiments at IGP-CARE India. I am in debt for the kind cooperation I received from Dr. Kristina Hedfalk when she was temporarily Head of Department, Department of Chemistry and Molecular Biology at University of Gothenburg and afterwards when she immediately became Deputy Head of Department, Department of Chemistry and Molecular Biology, at University of Gothenburg. I am similarly in debt for the kind cooperation I received from Professor Marica Ericson, as current Head of Department, Department of Chemistry and Molecular Biology, University of Gothenburg.

I cannot acknowledge enough for Dr. Saswati Ghosal, (ex) Senior Synthetic Chemistry Scientist at AstraZeneca (Currently at Cambrex Karlskoga AB), who had kept me economically floating during my long economical worst years (but intellectually wonderful and exciting years) and days when I forget the real world that rightfully demanded from me every day economic responsibility. She is a friend who stayed and helped every way she could and still ready to help whenever she can. I really cannot thank you enough Saswati!

I cannot forget my first Swedish friend and houseowner Mr. Peter Lundin, for his uncountable helps in kind over the years, since I first reach Sweden in 2005, leaving my corporate job as Global IPR head for Indian biggest Electrical Engineering company. Then I had zero knowledge about Swedish Society, and without his continuous support from 2005 till date, I could not navigate the complex my new-found Swedish society with confidence. Peter is example of highly self-educated human in multiple fields in true sense, who never bothered to finished his school. Peter explored all 7 continents and world's most countries since he is 13 years old, each country for months and sometime years, to learn from his life experience in different cultures, new products and technologies. Peter is a

practicing mechanical engineer, whereas I am just a degree holding mechanical engineer and over the years get excited and truth seeker in molecular chemistry. Peter is not inhibited by any social doctrine/schooling with a theoretical preaching, but a free thinker with keenly observant mind who can see that what is truth and what is false with a very open mind- a minefield essential for all kind of new innovations.

I am thankful for Mr. Tobias Wirthensohn [whom I lovingly called my first Austrian Liar (lawyer) friend, sorry I already communicate my personal apology to him in our first moment, as my pronunciations are wrong and till date I cannot pronounce lawyer correctly] very supportive friend & flat mate at Innsbruck who also supported me all way during my serious experiment days spanning over 12 hours a day, 6 days a week, for months at Innsbruck University. I cherish his friendship. I also cherish also another friendship extended by Lisa Marie Gassner of Innsbruck University (currently Business Development Manager at Servify), whom I first time I lovingly called my kid friend. She is a friend, but she is my kid's age (if I had kid).

I will also fondly remember Dr. Gayathri Chaturvedi, who is kind enough to be on my side in thick and thin, in many ways possible to see through silently so that I could finish my PhD. I can really see her sacrifice in many ways to help me out.

I sincerely thank Mr, Ashutosh Tripathi & Ms. Yogita Parab to be with me in thick and thin since decades.

I sincerely want to thank my father and sister, for their all encouragement and support me throughout my life, and most importantly believing in me.

My early 16+ years when I lived with my mother, was wonderful for me and I cannot thank my mother enough for all the positive energy she infected me with! I lost my loving mother (in medically wrong diagnosis and matching with wrong treatments for years) when I was barely 16 years old. If she lived today, this day could be her day! In my adult life, I deliver uncountable pin-pointed diagnosis in multiple topics, related to inventions, patents and/or business for multiple companies in India, Europe & Canada. Soon after my mother's death, I promise to myself never be arrogant in topics where I do not know the truth and [say clearly only what I know, better self-learn new topics before guiding an industry/academic (national/European) expert on their topics], and never sell ignorance as truth, unlike what medical doctors confidently did with my mother for years! I love you mother! I wish you are here with me today!

7 References

1. IPCC. *Climate Change 2013: The Physical Science Basis. Contribution of Working Group I to the Fifth Assessment Report of the Intergovernmental Panel on Climate Change*; Stocker, T.F., Qin, D., Plattner, G.-K., Tignor, M., Allen, S.K., Boschung, J., Nauels, A., Xia, Y., Bex, V., Midgley, P.M., Eds.; Cambridge University Press: Cambridge, United Kingdom and New York, NY, USA, 2013; p. 1535.
2. Forrister, H.; Liu, J.; Scheuer, E.; Dibb, J.; Ziemba, L.; Thornhill, K.L.; Anderson, B.; Diskin, G.; Perring, A.E.; Schwarz, J.P.; et al. Evolution of brown carbon in wildfire plumes. *Geophys. Res. Lett.* **2015**, *42*, 4623-4630, doi:10.1002/2015GL063897.
3. Zhang, X.; Lin, Y.H.; Surratt, J.D.; Zotter, P.; Prévôt, A.S.H.; Weber, R.J. Light-absorbing soluble organic aerosol in Los Angeles and Atlanta: A contrast in secondary organic aerosol. *Geophys. Res. Lett.* **2011**, *38*, doi:10.1029/2011GL049385.
4. Lack, D.A.; Bahreini, R.; Langridge, J.M.; Gilman, J.B.; Middlebrook, A.M. Brown carbon absorption linked to organic mass tracers in biomass burning particles. *Atmos. Chem. Phys.* **2013**, *13*, 2415-2422, doi:10.5194/acp-13-2415-2013.
5. Mohr, C.; Lopez-Hilfiker, F.D.; Zotter, P.; Prévoît, A.S.H.; Xu, L.; Ng, N.L.; Herndon, S.C.; Williams, L.R.; Franklin, J.P.; Zahniser, M.S.; et al. Contribution of nitrated phenols to wood burning brown carbon light absorption in detling, united kingdom during winter time. *Environmental Science and Technology* **2013**, *47*, 6316-6324, doi:10.1021/es400683v.
6. Laskin, J.; Laskin, A.; Nizkorodov, S.A.; Roach, P.; Eckert, P.; Gilles, M.K.; Wang, B.; Lee, H.J.; Hu, Q. Molecular selectivity of brown carbon chromophores. *Environmental Science and Technology* **2014**, *48*, 12047-12055, doi:10.1021/es503432r.
7. Prakash, J.; Mishra, H.R.; Mitra, K.; Chandra, B.; Hallquist, M.; Habib, G.; Tiwari, G.; Pettersson, J.B.C.; Boman, J.; Pleijel, H.; et al. Characterization, sources, and atmospheric transformation of a few key short-lived climate pollutants (SLCPs) at a rural super-site in the Indo-Gangetic Plain (IGP) of India. *Environmental Science: Atmospheres* **2022**, doi:10.1039/d1ea00083g.
8. Kong, X.; Salvador, C.M.; Carlsson, S.; Pathak, R.; Davidsson, K.O.; Le Breton, M.; Gaita, S.M.; Mitra, K.; Hallquist, Å.M.; Hallquist, M.; et al. Molecular characterization and optical properties of primary emissions from a residential wood burning boiler. *Sci. Total Environ.* **2021**, *754*, doi:10.1016/j.scitotenv.2020.142143.
9. Mitra, K.; Mishra, H.R.; Pei, X.; Pathak, R.K. Secondary Organic Aerosol (SOA) from Photo-Oxidation of Toluene: 1 Influence of Reactive Nitrogen, Acidity and Water Vapours on Optical Properties. *Atmosphere* **2022**, *13*, doi:10.3390/atmos13071099.
10. Bougiatioti, A.; Stavroulas, I.; Kostenidou, E.; Zarmpas, P.; Theodosi, C.; Kouvarakis, G.; Canonaco, F.; Prévôt, A.S.H.; Nenes, A.; Pandis, S.N.; et al. Processing of biomass-burning aerosol in the eastern Mediterranean during summertime. *Atmos. Chem. Phys.* **2014**, *14*, 4793-4807, doi:10.5194/acp-14-4793-2014.
11. Washenfelder, R.A.; Attwood, A.R.; Brock, C.A.; Guo, H.; Xu, L.; Weber, R.J.; Ng, N.L.; Allen, H.M.; Ayres, B.R.; Baumann, K.; et al. Biomass burning dominates brown carbon absorption in the rural southeastern United States. *Geophys. Res. Lett.* **2015**, *42*, 653-664, doi:10.1002/2014GL062444.
12. Fuzzi, S.; Baltensperger, U.; Carslaw, K.; Decesari, S.; Denier Van Der Gon, H.; Facchini, M.C.; Fowler, D.; Koren, I.; Langford, B.; Lohmann, U.; et al. Particulate matter, air quality and climate: Lessons learned and future needs. *Atmos. Chem. Phys.* **2015**, *15*, 8217-8299, doi:10.5194/acp-15-8217-2015.

13. Lee, H.J.; Aiona, P.K.; Laskin, A.; Laskin, J.; Nizkorodov, S.A. Effect of solar radiation on the optical properties and molecular composition of laboratory proxies of atmospheric brown carbon. *Environmental Science and Technology* **2014**, *48*, 10217-10226, doi:10.1021/es502515r.
14. Zhong, M.; Jang, M. Dynamic light absorption of biomass-burning organic carbon photochemically aged under natural sunlight. *Atmos. Chem. Phys.* **2014**, *14*, 1517-1525, doi:10.5194/acp-14-1517-2014.
15. Zhao, R.; Lee, A.K.Y.; Huang, L.; Li, X.; Yang, F.; Abbatt, J.P.D. Photochemical processing of aqueous atmospheric brown carbon. *Atmos. Chem. Phys.* **2015**, *15*, 6087-6100, doi:10.5194/acp-15-6087-2015.
16. Lin, P.; Bluvshtein, N.; Rudich, Y.; Nizkorodov, S.A.; Laskin, J.; Laskin, A. Molecular Chemistry of Atmospheric Brown Carbon Inferred from a Nationwide Biomass Burning Event. *Environmental Science and Technology* **2017**, *51*, 11561-11570, doi:10.1021/acs.est.7b02276.
17. Pan, X.; Ichoku, C.; Chin, M.; Bian, H.; Darmenov, A.; Colarco, P.; Ellison, L.; Kucsera, T.; Da Silva, A.; Wang, J.; et al. Six global biomass burning emission datasets: Intercomparison and application in one global aerosol model. *Atmos. Chem. Phys.* **2020**, *20*, 969-994, doi:10.5194/acp-20-969-2020.
18. Budisulistiorini, S.H.; Riva, M.; Williams, M.; Chen, J.; Itoh, M.; Surratt, J.D.; Kuwata, M. Light-Absorbing Brown Carbon Aerosol Constituents from Combustion of Indonesian Peat and Biomass. *Environmental Science and Technology* **2017**, *51*, 4415-4423, doi:10.1021/acs.est.7b00397.
19. Fleming, L.T.; Lin, P.; Laskin, A.; Laskin, J.; Weltman, R.; Edwards, R.D.; Arora, N.K.; Yadav, A.; Meinardi, S.; Blake, D.R.; et al. Molecular composition of particulate matter emissions from dung and brushwood burning household cookstoves in Haryana, India. *Atmos. Chem. Phys.* **2018**, *18*, 2461-2480, doi:10.5194/acp-18-2461-2018.
20. Simoneit, B.R.T.; Rogge, W.F.; Mazurek, M.A.; Standley, L.J.; Hildemann, L.M.; Cass, G.R. Lignin pyrolysis products, lignans, and resin acids as specific tracers of plant classes in emissions from biomass combustion. *Environ. Sci. Technol.* **1993**, *27*, 2533-2541, doi:10.1021/es00048a034.
21. Iinuma, Y.; Böge, O.; Herrmann, H. Methyl-nitrocatechols: Atmospheric tracer compounds for biomass burning secondary organic aerosols. *Environmental Science and Technology* **2010**, *44*, 8453-8459, doi:10.1021/es102938a.
22. Simoneit, B.R.T. Biomass burning - A review of organic tracers for smoke from incomplete combustion. *Applied Geochemistry* **2002**, *17*, 129-162, doi:10.1016/S0883-2927(01)00061-0.
23. Sedlacek, A.J.; Buseck, P.R.; Adachi, K.; Onasch, T.B.; Springston, S.R.; Kleinman, L. Formation and evolution of tar balls from northwestern US wildfires. *Atmos. Chem. Phys.* **2018**, *18*, 11289-11301, doi:10.5194/acp-18-11289-2018.
24. Tóth, A.; Hoffer, A.; Nyiro-Kósa, I.; Pósfai, M.; Gelencsér, A. Atmospheric tar balls: Aged primary droplets from biomass burning? *Atmos. Chem. Phys.* **2014**, *14*, 6669-6675, doi:10.5194/acp-14-6669-2014.
25. Chakrabarty, R.K.; Moosmüller, H.; Chen, L.W.A.; Lewis, K.; Arnott, W.P.; Mazzoleni, C.; Dubey, M.K.; Wold, C.E.; Hao, W.M.; Kreidenweis, S.M. Brown carbon in tar balls from smoldering biomass combustion. *Atmos. Chem. Phys.* **2010**, *10*, 6363-6370, doi:10.5194/acp-10-6363-2010.
26. Girotto, G.; China, S.; Bhandari, J.; Gorkowski, K.; Scarnato, B.V.; Capek, T.; Marinoni, A.; Veghte, D.P.; Kulkarni, G.; Aiken, A.C.; et al. Fractal-like Tar Ball Aggregates from Wildfire Smoke. *Environmental Science and Technology Letters* **2018**, *5*, 360-365, doi:10.1021/acs.estlett.8b00229.

27. Li, C.; He, Q.; Schade, J.; Passig, J.; Zimmermann, R.; Meidan, D.; Laskin, A.; Rudich, Y. Dynamic changes in optical and chemical properties of tar ball aerosols by atmospheric photochemical aging. *Atmos. Chem. Phys.* **2019**, *19*, 139-163, doi:10.5194/acp-19-139-2019.
28. Pósfai, M.; Gelencsér, A.; Simonics, R.; Arató, K.; Li, J.; Hobbs, P.V.; Buseck, P.R. Atmospheric tar balls: Particles from biomass and biofuel burning. *Journal of Geophysical Research: Atmospheres* **2004**, *109*, D06213 06211-06219, doi:10.1029/2003jd004169.
29. Selimovic, V.; Yokelson, R.J.; McMeeking, G.R.; Coefield, S. In situ measurements of trace gases, PM, and aerosol optical properties during the 2017 NW US wildfire smoke event. *Atmos. Chem. Phys.* **2019**, *19*, 3905-3926, doi:10.5194/acp-19-3905-2019.
30. Di Lorenzo, R.A.; Washenfelder, R.A.; Attwood, A.R.; Guo, H.; Xu, L.; Ng, N.L.; Weber, R.J.; Baumann, K.; Edgerton, E.; Young, C.J. Molecular-Size-Separated Brown Carbon Absorption for Biomass-Burning Aerosol at Multiple Field Sites. *Environmental Science and Technology* **2017**, *51*, 3128-3137, doi:10.1021/acs.est.6b06160.
31. Hinks, M.L.; Brady, M.V.; Lignell, H.; Song, M.; Grayson, J.W.; Bertram, A.K.; Lin, P.; Laskin, A.; Laskin, J.; Nizkorodov, S.A. Effect of viscosity on photodegradation rates in complex secondary organic aerosol materials. *Phys. Chem. Chem. Phys.* **2016**, *18*, 8785-8793, doi:10.1039/c5cp05226b.
32. Hems, R.F.; Abbatt, J.P.D. Aqueous Phase Photo-oxidation of Brown Carbon Nitrophenols: Reaction Kinetics, Mechanism, and Evolution of Light Absorption. *ACS Earth and Space Chemistry* **2018**, *2*, 225-234, doi:10.1021/acsearthspacechem.7b00123.
33. Gelencsér, A.; Hoffer, A.; Kiss, G.; Tombácz, E.; Kurdi, R.; Bencze, L. In-situ formation of light-absorbing organic matter in cloud water. *Journal of Atmospheric Chemistry* **2003**, *45*, 25-33, doi:10.1023/A:1024060428172.
34. Chang, J.L.; Thompson, J.E. Characterization of colored products formed during irradiation of aqueous solutions containing H2O2 and phenolic compounds. *Atmos. Environ.* **2010**, *44*, 541-551, doi:10.1016/j.atmosenv.2009.10.042.
35. Tang, H. Light-Absorbing Products Form during the Aqueous Phase Reaction of Phenolic Compounds in the Presence of Nitrate and Nitrite with UV Illumination. *Open Journal of Air Pollution* **2012**, *1*, 13-21, doi:http://dx.doi.org/10.4236/ojap.2012.12002.
36. Smith, J.D.; Kinney, H.; Anastasio, C. Phenolic carbonyls undergo rapid aqueous photodegradation to form low-volatility, light-absorbing products. *Atmos. Environ.* **2016**, *126*, 36-44, doi:10.1016/j.atmosenv.2015.11.035.
37. Kaur, R.; Labins, J.R.; Helbock, S.S.; Jiang, W.; Bein, K.J.; Zhang, Q.; Anastasio, C. Photooxidants from brown carbon and other chromophores in illuminated particle extracts. *Atmos. Chem. Phys.* **2019**, *19*, 6579-6594, doi:10.5194/acp-19-6579-2019.
38. Smol, M.; Włodarczyk-Makuła, M. The Effectiveness in the Removal of PAHs from Aqueous Solutions in Physical and Chemical Processes: A Review. *Polycyclic Aromatic Compounds* **2017**, *37*, 292-313, doi:10.1080/10406638.2015.1105828.
39. Shankar, R.; An, J.G.; Loh, A.; Yim, U.H. A systematic study of the effects of solvents on phenanthrene photooxidation. *Chemosphere* **2019**, *220*, 900-909, doi:10.1016/j.chemosphere.2018.12.206.
40. Miller, J.S.; Olejnik, D. Photolysis of polycyclic aromatic hydrocarbons in water. *Water Research* **2001**, *35*, 233-243, doi:10.1016/S0043-1354(00)00230-X.
41. Fleming, L.T.; Lin, P.; Roberts, J.M.; Selimovic, V.; Yokelson, R.; Laskin, J.; Laskin, A.; Nizkorodov, S.A. Molecular composition and photochemical lifetimes of brown carbon chromophores in biomass burning organic aerosol. *Atmos. Chem. Phys.* **2020**, *20*, 1105-1129, doi:10.5194/acp-20-1105-2020.
42. Tomaz, S.; Cui, T.; Chen, Y.; Sexton, K.G.; Roberts, J.M.; Warneke, C.; Yokelson, R.J.; Surratt, J.D.; Turpin, B.J. Photochemical Cloud Processing of Primary Wildfire Emissions

as a Potential Source of Secondary Organic Aerosol. *Environmental Science and Technology* **2018**, *52*, 11027-11037, doi:10.1021/acs.est.8b03293.
43. Saleh, R.; Hennigan, C.J.; McMeeking, G.R.; Chuang, W.K.; Robinson, E.S.; Coe, H.; Donahue, N.M.; Robinson, A.L. Absorptivity of brown carbon in fresh and photochemically aged biomass-burning emissions. *Atmos. Chem. Phys.* **2013**, *13*, 7683-7693, doi:10.5194/acp-13-7683-2013.
44. Liu, J.M.; Lin, P.; Laskin, A.; Laskin, J.; Kathmann, S.M.; Wise, M.; Caylor, R.; Imholt, F.; Selimovic, V.; Shilling, J.E. Optical properties and aging of light-absorbing secondary organic aerosol. *Atmos. Chem. Phys.* **2016**, *16*, 12815-12827, doi:10.5194/acp-16-12815-2016.
45. Sumlin, B.J.; Pandey, A.; Walker, M.J.; Pattison, R.S.; Williams, B.J.; Chakrabarty, R.K. Atmospheric Photooxidation Diminishes Light Absorption by Primary Brown Carbon Aerosol from Biomass Burning. *Environmental Science and Technology Letters* **2017**, *4*, 540-545, doi:10.1021/acs.estlett.7b00393.
46. Feng, Y.; Ramanathan, V.; Kotamarthi, V.R. Brown carbon: A significant atmospheric absorber of solar radiation. *Atmos. Chem. Phys.* **2013**, *13*, 8607-8621, doi:10.5194/acp-13-8607-2013.
47. Bahadur, R.; Praveen, P.S.; Xu, Y.; Ramanathan, V. Solar absorption by elemental and brown carbon determined from spectral observations. *Proc. Natl. Acad. Sci. U. S. A.* **2012**, *109*, 17366-17371, doi:10.1073/pnas.1205910109.
48. Chung, C.E.; Ramanathan, V.; Decremer, D. Observationally constrained estimates of carbonaceous aerosol radiative forcing. *Proc. Natl. Acad. Sci. U. S. A.* **2012**, *109*, 11624-11629, doi:10.1073/pnas.1203707109.
49. Laskin, A.; Laskin, J.; Nizkorodov, S.A. Chemistry of Atmospheric Brown Carbon. *Chem. Rev.* **2015**, *115*, 4335-4382, doi:10.1021/cr5006167.
50. Ramanathan, V.; Li, F.; Ramana, M.V.; Praveen, P.S.; Kim, D.; Corrigan, C.E.; Nguyen, H.; Stone, E.A.; Schauer, J.J.; Carmichael, G.R.; et al. Atmospheric brown clouds: Hemispherical and regional variations in long-range transport, absorption, and radiative forcing. *Journal of Geophysical Research Atmospheres* **2007**, *112*, doi:10.1029/2006JD008124.
51. Jiang, X.; Wiedinmyer, C.; Carlton, A.G. Aerosols from fires: An examination of the effects on ozone photochemistry in the Western United States. *Environmental Science and Technology* **2012**, *46*, 11878-11886, doi:10.1021/es301541k.
52. Li, G.; Bei, N.; Tie, X.; Molina, L.T. Aerosol effects on the photochemistry in Mexico City during MCMA-2006/MILAGRO campaign. *Atmos. Chem. Phys.* **2011**, *11*, 5169-5182, doi:10.5194/acp-11-5169-2011.
53. Ervens, B.; Turpin, B.J.; Weber, R.J. Secondary organic aerosol formation in cloud droplets and aqueous particles (aqSOA): a review of laboratory, field and model studies. *Atmos. Chem. Phys.* **2011**, *11*, 11069-11102, doi:10.5194/acp-11-11069-2011.
54. McNeill, V.F. Aqueous organic chemistry in the atmosphere: Sources and chemical processing of organic aerosols. *Environmental Science and Technology* **2015**, *49*, 1237-1244, doi:10.1021/es5043707.
55. Kroll, J.H.; Seinfeld, J.H. Chemistry of secondary organic aerosol: Formation and evolution of low-volatility organics in the atmosphere. *Atmos. Environ.* **2008**, *42*, 3593-3624, doi:10.1016/j.atmosenv.2008.01.003.
56. Jacobson, M.Z. Isolating nitrated and aromatic aerosols and nitrated aromatic gases as sources of ultraviolet light absorption. *Journal of Geophysical Research Atmospheres* **1999**, *104*, 3527-3542, doi:10.1029/1998JD100054.

57. Pitts, J.; Van Cauwenberghe, K.; Grosjean, D.; Schmid, J.; Fitz, D.; Belser, W.; Knudson, G.; Hynds, P. Atmospheric reactions of polycyclic aromatic hydrocarbons: facile formation of mutagenic nitro derivatives. *Science* **1978**, *202*, 515-519, doi:10.1126/science.705341.
58. Bones, D.L.; Henricksen, D.K.; Mang, S.A.; Gonsior, M.; Bateman, A.P.; Nguyen, T.B.; Cooper, W.J.; Nizkorodov, S.A. Appearance of strong absorbers and fluorophores in limonene-O3 secondary organic aerosol due to NH4+ -mediated chemical aging over long time scales. *Journal of Geophysical Research Atmospheres* **2010**, *115*, doi:10.1029/2009JD012864.
59. Sareen, N.; Schwier, A.N.; Shapiro, E.L.; Mitroo, D.; McNeill, V.F. Secondary organic material formed by methylglyoxal in aqueous aerosol mimics. *Atmos. Chem. Phys.* **2010**, *10*, 997-1016, doi:10.5194/acp-10-997-2010.
60. Updyke, K.M.; Nguyen, T.B.; Nizkorodov, S.A. Formation of brown carbon via reactions of ammonia with secondary organic aerosols from biogenic and anthropogenic precursors. *Atmos. Environ.* **2012**, *63*, 22-31, doi:10.1016/j.atmosenv.2012.09.012.
61. Flores, J.M.; Zhao, D.F.; Segev, L.; Schlag, P.; Kiendler-Scharr, A.; Fuchs, H.; Watne, A.K.; Bluvshtein, N.; Mentel, T.F.; Hallquist, M.; et al. Evolution of the complex refractive index in the UV spectral region in ageing secondary organic aerosol. *Atmos. Chem. Phys.* **2014**, *14*, 5793-5806, doi:10.5194/acp-14-5793-2014.
62. Nozière, B.; Esteve, W. Organic reactions increasing the absorption index of atmospheric sulfuric acid aerosols. *Geophysical Research Letters* **2005**, *32*, L03812, doi:10.1029/2004GL021942.
63. Nozière, B.; Esteve, W. Light-absorbing aldol condensation products in acidic aerosols: Spectra, kinetics, and contribution to the absorption index. *Atmospheric Environment* **2007**, *41*, 1150-1163, doi:http://dx.doi.org/10.1016/j.atmosenv.2006.10.001.
64. Hoffer, A.; Kiss, G.; Blazsó, M.; Gelencsér, A. Chemical characterization of humic-like substances (HULIS) formed from a lignin-type precursor in model cloud water. *Geophysical Research Letters* **2004**, *31*, L06115, doi:10.1029/2003GL018962.
65. Limbeck, A.; Kulmala, M.; Puxbaum, H. Secondary organic aerosol formation in the atmosphere via heterogeneous reaction of gaseous isoprene on acidic particles. *Geophys. Res. Lett.* **2003**, *30*, ASC 6-1 - ASC 6-4, doi:10.1029/2003GL017738.
66. Rincón, A.G.; Guzmán, M.I.; Hoffmann, M.R.; Colussi, A.J. Thermochromism of Model Organic Aerosol Matter. *The Journal of Physical Chemistry Letters* **2010**, *1*, 368-373, doi:10.1021/jz900186e.
67. Rincón, A.G.; Guzmán, M.I.; Hoffmann, M.R.; Colussi, A.J. Optical Absorptivity versus Molecular Composition of Model Organic Aerosol Matter. *The Journal of Physical Chemistry A* **2009**, *113*, 10512-10520, doi:10.1021/jp904644n.
68. Lin, G.; Penner, J.E.; Flanner, M.G.; Sillman, S.; Xu, L.; Zhou, C. Radiative forcing of organic aerosol in the atmosphere and on snow: Effects of SOA and brown carbon. *Journal of Geophysical Research: Atmospheres* **2014**, *119*, 7453-7476, doi:10.1002/2013JD021186.
69. Liu, J.; Bergin, M.; Guo, H.; King, L.; Kotra, N.; Edgerton, E.; Weber, R.J. Size-resolved measurements of brown carbon in water and methanol extracts and estimates of their contribution to ambient fine-particle light absorption. *Atmos. Chem. Phys.* **2013**, *13*, 12389-12404, doi:10.5194/acp-13-12389-2013.
70. Corr, C.A.; Hall, S.R.; Ullmann, K.; Anderson, B.E.; Beyersdorf, A.J.; Thornhill, K.L.; Cubison, M.J.; Jimenez, J.L.; Wisthaler, A.; Dibb, J.E. Spectral absorption of biomass burning aerosol determined from retrieved single scattering albedo during ARCTAS. *Atmos. Chem. Phys.* **2012**, *12*, 10505-10518, doi:10.5194/acp-12-10505-2012.
71. Doherty, S.J.; Warren, S.G.; Grenfell, T.C.; Clarke, A.D.; Brandt, R.E. Light-absorbing impurities in Arctic snow. *Atmos. Chem. Phys.* **2010**, *10*, 11647-11680, doi:10.5194/acp-10-11647-2010.

72. Chen, Y.; Li, N.; Li, X.; Tao, Y.; Luo, S.; Zhao, Z.; Ma, S.; Huang, H.; Chen, Y.; Ye, Z.; et al. Secondary organic aerosol formation from 3C∗-initiated oxidation of 4-ethylguaiacol in atmospheric aqueous-phase. *Sci. Total Environ.* **2020**, *723*, doi:10.1016/j.scitotenv.2020.137953.
73. Huang, D.D.; Zhang, Q.; Cheung, H.H.Y.; Yu, L.; Zhou, S.; Anastasio, C.; Smith, J.D.; Chan, C.K. Formation and Evolution of aqSOA from Aqueous-Phase Reactions of Phenolic Carbonyls: Comparison between Ammonium Sulfate and Ammonium Nitrate Solutions. *Environmental Science and Technology* **2018**, *52*, 9215-9224, doi:10.1021/acs.est.8b03441.
74. Slikboer, S.; Grandy, L.; Blair, S.L.; Nizkorodov, S.A.; Smith, R.W.; Al-Abadleh, H.A. Formation of Light Absorbing Soluble Secondary Organics and Insoluble Polymeric Particles from the Dark Reaction of Catechol and Guaiacol with Fe(III). *Environ. Sci. Technol.* **2015**, *49*, 7793-7801, doi:10.1021/acs.est.5b01032.
75. Xu, F.; van Harten, G.; Diner, D.J.; Davis, A.B.; Seidel, F.C.; Rheingans, B.; Tosca, M.; Alexandrov, M.D.; Cairns, B.; Ferrare, R.A.; et al. Coupled Retrieval of Liquid Water Cloud and Above-Cloud Aerosol Properties Using the Airborne Multiangle SpectroPolarimetric Imager (AirMSPI). *Journal of Geophysical Research: Atmospheres* **2018**, *123*, 3175-3204, doi:10.1002/2017JD027926.
76. Mabato, B.R.G.; Lyu, Y.; Ji, Y.; Li, Y.J.; Huang, D.D.; Li, X.; Nah, T.; Lam, C.H.; Chan, C.K. Aqueous secondary organic aerosol formation from the direct photosensitized oxidation of vanillin in the absence and presence of ammonium nitrate. *Atmos. Chem. Phys.* **2022**, *22*, 273-293, doi:10.5194/acp-22-273-2022.
77. Powelson, M.H.; Espelien, B.M.; Hawkins, L.N.; Galloway, M.M.; De Haan, D.O. Brown carbon formation by aqueous-phase carbonyl compound reactions with amines and ammonium sulfate. *Environmental Science and Technology* **2014**, *48*, 985-993, doi:10.1021/es4038325.
78. Herrmann, H.; Hoffmann, D.; Schaefer, T.; Bräuer, P.; Tilgner, A. Tropospheric aqueous-phase free-radical chemistry: Radical sources, spectra, reaction kinetics and prediction tools. *ChemPhysChem* **2010**, *11*, 3796-3822, doi:10.1002/cphc.201000533.
79. Smith, J.D.; Sio, V.; Yu, L.; Zhang, Q.; Anastasio, C. Secondary organic aerosol production from aqueous reactions of atmospheric phenols with an organic triplet excited state. *Environmental Science and Technology* **2014**, *48*, 1049-1057, doi:10.1021/es4045715.
80. Canonica, S.; Jans, U.; Stemmler, K.; Hoigné, J. Transformation Kinetics of Phenols in Water: Photosensitization by Dissolved Natural Organic Material and Aromatic Ketones. *Environmental Science and Technology* **1995**, *29*, 1822-1831, doi:10.1021/es00007a020.
81. Anastasio, C.; Faust, B.C.; Rao, C.J. Aromatic carbonyl compounds as aqueous-phase photochemical sources of hydrogen peroxide in acidic sulfate aerosols, fogs, and clouds. 1. Non- phenolic methoxybenzaldehydes and methoxyacetophenones with reductants (phenols). *Environmental Science and Technology* **1997**, *31*, 218-232, doi:10.1021/es960359g.
82. Vione, D.; Maurino, V.; Minero, C.; Pelizzetti, E.; Harrison, M.A.J.; Olariu, R.I.; Arsene, C. Photochemical reactions in the tropospheric aqueous phase and on particulate matter. *Chem. Soc. Rev.* **2006**, *35*, 441-453, doi:10.1039/b510796m.
83. George, C.; Brüggemann, M.; Hayeck, N.; Tinel, L.; Donaldson, J. Chapter 14 - Interfacial Photochemistry. In *Physical Chemistry of Gas-Liquid Interfaces*, Faust, J.A., House, J.E., Eds.; Elsevier: 2018; pp. 435-457.
84. Kaur, R.; Anastasio, C. First Measurements of Organic Triplet Excited States in Atmospheric Waters. *Environmental Science and Technology* **2018**, *52*, 5218-5226, doi:10.1021/acs.est.7b06699.

85. Smith, J.D.; Kinney, H.; Anastasio, C. Aqueous benzene-diols react with an organic triplet excited state and hydroxyl radical to form secondary organic aerosol. *Phys. Chem. Chem. Phys.* **2015**, *17*, 10227-10237, doi:10.1039/c4cp06095d.
86. Yu, L.; Smith, J.; Laskin, A.; Anastasio, C.; Laskin, J.; Zhang, Q. Chemical characterization of SOA formed from aqueous-phase reactions of phenols with the triplet excited state of carbonyl and hydroxyl radical. *Atmos. Chem. Phys.* **2014**, *14*, 13801-13816, doi:10.5194/acp-14-13801-2014.
87. Jiang, W.; Misovich, M.V.; Hettiyadura, A.P.S.; Laskin, A.; McFall, A.S.; Anastasio, C.; Zhang, Q. Photosensitized Reactions of a Phenolic Carbonyl from Wood Combustion in the Aqueous Phase - Chemical Evolution and Light Absorption Properties of AqSOA. *Environmental Science and Technology* **2021**, *55*, 5199-5211, doi:10.1021/acs.est.0c07581.
88. Rogge, W.F.; Hildemann, L.M.; Mazurek, M.A.; Cass, G.R.; Simoneit, B.R.T. Sources of fine organic aeresol. 9. Pine, oak, and synthetic log combustion in residential fireplaces. *Environmental Science and Technology* **1998**, *32*, 13-22, doi:10.1021/es960930b.
89. Nolte, C.G.; Schauer, J.J.; Cass, G.R.; Simoneit, B.R.T. Highly polar organic compounds present in wood smoke and in the ambient atmosphere. *Environmental Science and Technology* **2001**, *35*, 1912-1919, doi:10.1021/es001420r.
90. Schauer, J.J.; Kleeman, M.J.; Cass, G.R.; Simoneit, B.R.T. Measurement of emissions from air pollution sources. 3. C1-C29 organic compounds from fireplace combustion of wood. *Environmental Science and Technology* **2001**, *35*, 1716-1728, doi:10.1021/es001331e.
91. Bond, T.C.; Streets, D.G.; Yarber, K.F.; Nelson, S.M.; Woo, J.H.; Klimont, Z. A technology-based global inventory of black and organic carbon emissions from combustion. *Journal of Geophysical Research: Atmospheres* **2004**, *109*, doi:10.1029/2003JD003697.
92. Desyaterik, Y.; Sun, Y.; Shen, X.; Lee, T.; Wang, X.; Wang, T.; Collett Jr, J.L. Speciation of "brown" carbon in cloud water impacted by agricultural biomass burning in eastern China. *Journal of Geophysical Research Atmospheres* **2013**, *118*, 7389-7399, doi:10.1002/jgrd.50561.
93. Xiao, H.W.; Wu, J.F.; Luo, L.; Liu, C.; Xie, Y.J.; Xiao, H.Y. Enhanced biomass burning as a source of aerosol ammonium over cities in central China in autumn. *Environmental Pollution* **2020**, *266*, doi:10.1016/j.envpol.2020.115278.
94. Zielinski, T.; Bolzacchini, E.; Cataldi, M.; Ferrero, L.; Graßl, S.; Hansen, G.; Mateos, D.; Mazzola, M.; Neuber, R.; Pakszys, P.; et al. Study of chemical and optical properties of biomass burning aerosols during long-range transport events toward the arctic in summer 2017. *Atmosphere* **2020**, *11*, doi:10.3390/ATMOS11010084.
95. Munger, J.W.; Jacob, D.J.; Waldman, J.M.; Hoffmann, M.R. Fogwater chemistry in an urban atmosphere. *Journal of Geophysical Research* **1983**, *88*, 5109-5121, doi:10.1029/JC088iC09p05109.
96. Collett Jr, J.L.; Hoag, K.J.; Sherman, D.E.; Bator, A.; Richards, L.W. Spatial and temporal variations in San Joaquin Valley fog chemistry. *Atmos. Environ.* **1998**, *33*, 129-140, doi:10.1016/S1352-2310(98)00136-8.
97. Zhang, Q.; Anastasio, C. Conversion of fogwater and aerosol organic nitrogen to ammonium, nitrate, and NOx during exposure to simulated sunlight and ozone. *Environmental Science and Technology* **2003**, *37*, 3522-3530, doi:10.1021/es034114x.
98. Li, P.; Li, X.; Yang, C.; Wang, X.; Chen, J.; Collett, J.L. Fog water chemistry in Shanghai. *Atmos. Environ.* **2011**, *45*, 4034-4041, doi:10.1016/j.atmosenv.2011.04.036.
99. Giulianelli, L.; Gilardoni, S.; Tarozzi, L.; Rinaldi, M.; Decesari, S.; Carbone, C.; Facchini, M.C.; Fuzzi, S. Fog occurrence and chemical composition in the Po valley over the last twenty years. *Atmos. Environ.* **2014**, *98*, 394-401, doi:10.1016/j.atmosenv.2014.08.080.
100. Bianco, A.; Passananti, M.; Brigante, M.; Mailhot, G. Photochemistry of the cloud aqueous phase: A review. *Molecules* **2020**, *25*, doi:10.3390/molecules25020423.

101. Herrmann, H. On the photolysis of simple anions and neutral molecules as sources of O-/OH, SOx- and Cl in aqueous solution. *Phys. Chem. Chem. Phys.* **2007**, *9*, 3935-3964, doi:10.1039/b618565g.
102. Scharko, N.K.; Berke, A.E.; Raff, J.D. Release of nitrous acid and nitrogen dioxide from nitrate photolysis in acidic aqueous solutions. *Environmental Science and Technology* **2014**, *48*, 11991-12001, doi:10.1021/es503088x.
103. Minero, C.; Bono, F.; Rubertelli, F.; Pavino, D.; Maurino, V.; Pelizzetti, E.; Vione, D. On the effect of pH in aromatic photonitration upon nitrate photolysis. *Chemosphere* **2007**, *66*, 650-656, doi:10.1016/j.chemosphere.2006.07.082.
104. Klodt, A.L.; Romonosky, D.E.; Lin, P.; Laskin, J.; Laskin, A.; Nizkorodov, S.A. Aqueous Photochemistry of Secondary Organic Aerosol of α-Pinene and α-Humulene in the Presence of Hydrogen Peroxide or Inorganic Salts. *ACS Earth and Space Chemistry* **2019**, *3*, 2736-2746, doi:10.1021/acsearthspacechem.9b00222.
105. Zhang, X.; Zou, T.; Lassaletta, L.; Mueller, N.D.; Tubiello, F.N.; Lisk, M.D.; Lu, C.; Conant, R.T.; Dorich, C.D.; Gerber, J.; et al. Quantification of global and national nitrogen budgets for crop production. *Nature Food* **2021**, *2*, 529-540, doi:10.1038/s43016-021-00318-5.
106. Kahnt, A.; Behrouzi, S.; Vermeylen, R.; Safi Shalamzari, M.; Vercauteren, J.; Roekens, E.; Claeys, M.; Maenhaut, W. One-year study of nitro-organic compounds and their relation to wood burning in PM10 aerosol from a rural site in Belgium. *Atmos. Environ.* **2013**, *81*, 561-568, doi:10.1016/j.atmosenv.2013.09.041.
107. Teich, M.; Van Pinxteren, D.; Wang, M.; Kecorius, S.; Wang, Z.; Müller, T.; Močnik, G.; Herrmann, H. Contributions of nitrated aromatic compounds to the light absorption of water-soluble and particulate brown carbon in different atmospheric environments in Germany and China. *Atmos. Chem. Phys.* **2017**, *17*, 1653-1672, doi:10.5194/acp-17-1653-2017.
108. Li, M.; Wang, X.; Lu, C.; Li, R.; Zhang, J.; Dong, S.; Yang, L.; Xue, L.; Chen, J.; Wang, W. Nitrated phenols and the phenolic precursors in the atmosphere in urban Jinan, China. *Sci. Total Environ.* **2020**, *714*, doi:10.1016/j.scitotenv.2020.136760.
109. Liu, Y.; Liggio, J.; Staebler, R. Reactive uptake of ammonia to secondary organic aerosols: Kinetics of organonitrogen formation. *Atmos. Chem. Phys.* **2015**, *15*, 13569-13584, doi:10.5194/acp-15-13569-2015.
110. Xie, M.; Chen, X.; Hays, M.D.; Lewandowski, M.; Offenberg, J.; Kleindienst, T.E.; Holder, A.L. Light Absorption of Secondary Organic Aerosol: Composition and Contribution of Nitroaromatic Compounds. *Environmental Science and Technology* **2017**, *51*, 11607-11616, doi:10.1021/acs.est.7b03263.
111. Lopez-Hilfiker, F.D.; Mohr, C.; Ehn, M.; Rubach, F.; Kleist, E.; Wildt, J.; Mentel, T.F.; Lutz, A.; Hallquist, M.; Worsnop, D.; et al. A novel method for online analysis of gas and particle composition: description and evaluation of a Filter Inlet for Gases and AEROsols (FIGAERO). *Atmos. Meas. Tech.* **2014**, *7*, 983-1001, doi:10.5194/amt-7-983-2014.
112. Thornton, J.A.; Mohr, C.; Schobesberger, S.; D'Ambro, E.L.; Lee, B.H.; Lopez-Hilfiker, F.D. Evaluating Organic Aerosol Sources and Evolution with a Combined Molecular Composition and Volatility Framework Using the Filter Inlet for Gases and Aerosols (FIGAERO). *Accounts of Chemical Research* **2020**, *53*, 1415-1426, doi:10.1021/acs.accounts.0c00259.
113. Bertram, T.H.; Kimmel, J.R.; Crisp, T.A.; Ryder, O.S.; Yatavelli, R.L.N.; Thornton, J.A.; Cubison, M.J.; Gonin, M.; Worsnop, D.R. A field-deployable, chemical ionization time-of-flight mass spectrometer. *Atmos. Meas. Tech.* **2011**, *4*, 1471-1479, doi:10.5194/amt-4-1471-2011.

114. Kang, E.; Root, M.J.; Toohey, D.W.; Brune, W.H. Introducing the concept of Potential Aerosol Mass (PAM). *Atmos. Chem. Phys.* **2007**, *7*, 5727-5744, doi:10.5194/acp-7-5727-2007.
115. Watne, Å.K.; Psichoudaki, M.; Ljungström, E.; Le Breton, M.; Hallquist, M.; Jerksjö, M.; Fallgren, H.; Jutterström, S.; Hallquist, Å.M. Fresh and Oxidized Emissions from In-Use Transit Buses Running on Diesel, Biodiesel, and CNG. *Environmental Science and Technology* **2018**, *52*, 7720-7728, doi:10.1021/acs.est.8b01394.
116. Arnott, W.P.; Moosmüller, H.; Rogers, C.F.; Jin, T.; Bruch, R. Photoacoustic spectrometer for measuring light absorption by aerosol: Instrument description. *Atmos. Environ.* **1999**, *33*, 2845-2852, doi:10.1016/S1352-2310(98)00361-6.
117. McMurry, P.H.; Wang, X.; Park, K.; Ehara, K. The relationship between mass and mobility for atmospheric particles: A new technique for measuring particle density. *Aerosol Science and Technology* **2002**, *36*, 227-238, doi:10.1080/027868202753504083.
118. Huffman, J.A.; Ziemann, P.J.; Jayne, J.T.; Worsnop, D.R.; Jimenez, J.L. Development and characterization of a fast-stepping/scanning thermodenuder for chemically-resolved aerosol volatility measurements. *Aerosol Science and Technology* **2008**, *42*, 395-407, doi:10.1080/02786820802104981.
119. Burtscher, H.; Baltensperger, U.; Bukowiecki, N.; Cohn, P.; Hüglin, C.; Mohr, M.; Matter, U.; Nyeki, S.; Schmatloch, V.; Streit, N.; et al. Separation of volatile and non-volatile aerosol fractions by thermodesorption: Instrumental development and applications. *Journal of Aerosol Science* **2001**, *32*, 427-442, doi:10.1016/S0021-8502(00)00089-6.
120. Ziemann, P.J.; Atkinson, R. Kinetics, products, and mechanisms of secondary organic aerosol formation. *Chem. Soc. Rev.* **2012**, *41*, 6582-6605, doi:10.1039/c2cs35122f.
121. Jimenez, J.-L. *Laboratory Experiments and Modeling for Interpreting Field Studies of Secondary Organic Aerosol Formation Using an Oxidation Flow Reactor*; DOE/SC0006035-1; THE U.S. DEPARTMENT OF ENERGY OFFICE OF SCIENCE OFFICE OF BIOLOGICAL AND ENVIRONMENTAL RESEARCH ATMOSPHERIC SYSTEMS RESEARCH PROGRAM UNDER CONTRACT NO. DE-SC0006035: Colorado, 2016; pp. 1-46.
122. Mao, J.; Ren, X.; Brune, W.H.; Olson, J.R.; Crawford, J.H.; Fried, A.; Huey, L.G.; Cohen, R.C.; Heikes, B.; Singh, H.B.; et al. Airborne measurement of OH reactivity during INTEX-B. *Atmos. Chem. Phys.* **2009**, *9*, 163-173, doi:10.5194/acp-9-163-2009.
123. Laskin, J.; Laskin, A.; Nizkorodov, S.A. New mass spectrometry techniques for studying physical chemistry of atmospheric heterogeneous processes. *International Reviews in Physical Chemistry* **2013**, *32*, 128-170, doi:10.1080/0144235X.2012.752904.
124. Laskin, J.; Laskin, A.; Nizkorodov, S.A. Mass Spectrometry Analysis in Atmospheric Chemistry. *Analytical Chemistry* **2018**, *90*, 166-189, doi:10.1021/acs.analchem.7b04249.
125. Riemer, N.; Ault, A.P.; West, M.; Craig, R.L.; Curtis, J.H. Aerosol Mixing State: Measurements, Modeling, and Impacts. *Reviews of Geophysics* **2019**, *57*, 187-249, doi:10.1029/2018RG000615.
126. Huey, L.G. Measurement of trace atmospheric species by chemical ionization mass spectrometry: Speciation of reactive nitrogen and future directions. *Mass Spectrometry Reviews* **2007**, *26*, 166-184, doi:10.1002/mas.20118.
127. Ji, Y.; Gregory Huey, L.; Tanner, D.J.; Ro Lee, Y.; Veres, P.R.; Andrew Neuman, J.; Wang, Y.; Wang, X. A vacuum ultraviolet ion source (VUV-IS) for iodide-chemical ionization mass spectrometry: A substitute for radioactive ion sources. *Atmos. Meas. Tech.* **2020**, *13*, 3683-3696, doi:10.5194/amt-13-3683-2020.
128. Achad, M.; Caumo, S.; Vasconcellos, P.D.; Bajano, H.; Gomez, D.; Smichowski, P. Chemical Markers of Biomass Burning: Determination of Levoglucosan, and Potassium in Size-classified Atmospheric Aerosols Collected in Buenos Aires, Argentina by Different

Analytical Techniques. *Microchemical Journal* **2018**, *139*, 181-187, doi:10.1016/j.microc.2018.02.016.
129. Mashayekhy Rad, F.; Spinicci, S.; Silvergren, S.; Nilsson, U.; Westerholm, R. Validation of a HILIC/ESI-MS/MS method for the wood burning marker levoglucosan and its isomers in airborne particulate matter. *Chemosphere* **2018**, *211*, 617-623, doi:10.1016/j.chemosphere.2018.07.188.
130. Fourtziou, L.; Liakakou, E.; Stavroulas, I.; Theodosi, C.; Zarmpas, P.; Psiloglou, B.; Sciare, J.; Maggos, T.; Bairachtari, K.; Bougiatioti, A.; et al. Multi-tracer approach to characterize domestic wood burning in Athens (Greece) during wintertime. *Atmos. Environ.* **2017**, *148*, 89-101, doi:10.1016/j.atmosenv.2016.10.011.
131. Tao, J.; Zhang, L.M.; Zhang, R.J.; Wu, Y.F.; Zhang, Z.S.; Zhang, X.L.; Tang, Y.X.; Cao, J.J.; Zhang, Y.H. Uncertainty Assessment of Source Attribution of PM2.5 and its Water-soluble Organic Carbon Content using Different Biomass Burning Tracers in Positive Matrix Factorization Analysis - a Case Study in Beijing, China. *Science of the Total Environment* **2016**, *543*, 326-335, doi:10.1016/j.scitotenv.2015.11.057.
132. Nielsen, I.E.; Eriksson, A.C.; Lindgren, R.; Martinsson, J.; Nyström, R.; Nordin, E.Z.; Sadiktsis, I.; Boman, C.; Nøjgaard, J.K.; Pagels, J. Time-resolved analysis of particle emissions from residential biomass combustion – Emissions of refractory black carbon, PAHs and organic tracers. *Atmos. Environ.* **2017**, *165*, 179-190, doi:10.1016/j.atmosenv.2017.06.033.
133. Yang, H.; Yan, R.; Chen, H.; Lee, D.H.; Zheng, C. Characteristics of hemicellulose, cellulose and lignin pyrolysis. *Fuel* **2007**, *86*, 1781-1788, doi:10.1016/j.fuel.2006.12.013.
134. Kirchstetter, T.W.; Novakov, T.; Hobbs, P.V. Evidence that the spectral dependence of light absorption by aerosols is affected by organic carbon. *J. Geophys. Res.-Atmos.* **2004**, *109*, 12, doi:10.1029/2004jd004999.
135. Bergstrom, R.W.; Pilewskie, P.; Russell, P.B.; Redemann, J.; Bond, T.C.; Quinn, P.K.; Sierau, B. Spectral absorption properties of atmospheric aerosols. *Atmos. Chem. Phys.* **2007**, *7*, 5937-5943, doi:10.5194/acp-7-5937-2007.
136. Russell, P.B.; Bergstrom, R.W.; Shinozuka, Y.; Clarke, A.D.; Decarlo, P.F.; Jimenez, J.L.; Livingston, J.M.; Redemann, J.; Dubovik, O.; Strawa, A. Absorption Angstrom Exponent in AERONET and related data as an indicator of aerosol composition. *Atmos. Chem. Phys.* **2010**, *10*, 1155-1169, doi:10.5194/acp-10-1155-2010.
137. Lack, D.A.; Langridge, J.M.; Bahreini, R.; Cappa, C.D.; Middlebrook, A.M.; Schwarz, J.P. Brown carbon and internal mixing in biomass burning particles. *Proc. Natl. Acad. Sci. U. S. A.* **2012**, *109*, 14802-14807, doi:10.1073/pnas.1206575109.
138. Liu, C.; Chung, C.E.; Yin, Y.; Schnaiter, M. The Absorption Angstrom Exponent of Black Carbon: from Numerical Aspects. *Atmospheric Chemistry and Physics* **2018**, *18*, 6259-6273, doi:10.5194/acp-18-6259-2018.
139. Andreae, M.O.; Gelencsér, A. Black carbon or brown carbon? the nature of light-absorbing carbonaceous aerosols. *Atmos. Chem. Phys.* **2006**, *6*, 3131-3148, doi:10.5194/acp-6-3131-2006.
140. Sun, H.; Biedermann, L.; Bond, T.C. Color of brown carbon: A model for ultraviolet and visible light absorption by organic carbon aerosol. *Geophys. Res. Lett.* **2007**, *34*, doi:10.1029/2007GL029797.
141. Zhang, X.; Lin, Y.H.; Surratt, J.D.; Weber, R.J. Sources, composition and absorption Ångström exponent of light-absorbing organic components in aerosol extracts from the los angeles basin. *Environmental Science and Technology* **2013**, *47*, 3685-3693, doi:10.1021/es305047b.
142. Zhang, X.; Kim, H.; Parworth, C.L.; Young, D.E.; Zhang, Q.; Metcalf, A.R.; Cappa, C.D. Optical Properties of Wintertime Aerosols from Residential Wood Burning in Fresno, CA:

Results from DISCOVER-AQ 2013. *Environmental Science and Technology* **2016**, *50*, 1681-1690, doi:10.1021/acs.est.5b04134.
143. Bansal, O.; Singh, A.; Singh, D. Characteristics of Black Carbon aerosols over Patiala Northwestern part of the IGP: Source apportionment using cluster and CWT analysis. *Atmospheric Pollution Research* **2019**, *10*, 244-256, doi:10.1016/j.apr.2018.08.001.
144. Liakakou, E.; Stavroulas, I.; Kaskaoutis, D.G.; Grivas, G.; Paraskevopoulou, D.; Dumka, U.C.; Tsagkaraki, M.; Bougiatioti, A.; Oikonomou, K.; Sciare, J.; et al. Long-term variability, source apportionment and spectral properties of black carbon at an urban background site in Athens, Greece. *Atmos. Environ.* **2020**, *222*, doi:10.1016/j.atmosenv.2019.117137.
145. Dumka, U.C.; Kaskaoutis, D.G.; Devara, P.C.S.; Kumar, R.; Kumar, S.; Tiwari, S.; Gerasopoulos, E.; Mihalopoulos, N. Year-long variability of the fossil fuel and wood burning black carbon components at a rural site in southern Delhi outskirts. *Atmospheric Research* **2019**, *216*, 11-25, doi:10.1016/j.atmosres.2018.09.016.
146. Herich, H.; Hueglin, C.; Buchmann, B. A 2.5 year's source apportionment study of black carbon from wood burning and fossil fuel combustion at urban and rural sites in Switzerland. *Atmos. Meas. Tech.* **2011**, *4*, 1409-1420, doi:10.5194/amt-4-1409-2011.
147. Gani, S.; Bhandari, S.; Seraj, S.; Wang, D.S.; Patel, K.; Soni, P.; Arub, Z.; Habib, G.; Hildebrandt Ruiz, L.; Apte, J.S. Submicron aerosol composition in the world's most polluted megacity: The Delhi Aerosol Supersite study. *Atmos. Chem. Phys.* **2019**, *19*, 6843-6859, doi:10.5194/acp-19-6843-2019.
148. Srivastava, S.; Kumar, M.; Singh, R.S.; Rai, B.N.; Mall, R.K.; Banerjee, T. Long-term observation of black carbon aerosols at an urban location over the central Indo-Gangetic Plain, South Asia. *Atmosfera* **2019**, *32*, 95-113, doi:10.20937/ATM.2019.32.02.02.
149. Tiwari, S.; Dumka, U.C.; Hopke, P.K.; Tunved, P.; Srivastava, A.K.; Bisht, D.S.; Chakrabarty, R.K. Atmospheric heating due to black carbon aerosol during the summer monsoon period over Ballia: A rural environment over Indo-Gangetic Plain. *Atmospheric Research* **2016**, *178-179*, 393-400, doi:10.1016/j.atmosres.2016.04.008.
150. Alfoldy, B.; Mahfouz, M.M.; Gregorič, A.; Ivančič, M.; Ježek, I.; Rigler, M. Atmospheric concentrations and emission ratios of black carbon and nitrogen oxides in the Arabian/Persian Gulf region. *Atmos. Environ.* **2021**, *256*, doi:10.1016/j.atmosenv.2021.118451.
151. Mieville, A.; Granier, C.; Liousse, C.; Guillaume, B.; Mouillot, F.; Lamarque, J.F.; Grégoire, J.M.; Pétron, G. Emissions of gases and particles from biomass burning during the 20th century using satellite data and an historical reconstruction. *Atmos. Environ.* **2010**, *44*, 1469-1477, doi:10.1016/j.atmosenv.2010.01.011.
152. Dickau, M.; Olfert, J.; Stettler, M.E.J.; Boies, A.; Momenimovahed, A.; Thomson, K.; Smallwood, G.; Johnson, M. Methodology for quantifying the volatile mixing state of an aerosol. *Aerosol Science and Technology* **2016**, *50*, 759-772, doi:10.1080/02786826.2016.1185509.
153. Sgro, L.A.; Borghese, A.; Speranza, L.; Barone, A.C.; Minutolo, P.; Bruno, A.; D'Anna, A.; D'Alessio, A. Measurements of nanoparticles of organic carbon and soot in flames and vehicle exhausts. *Environ. Sci. Technol.* **2008**, *42*, 859-863.
154. Maricq, M.M. Examining the relationship between black carbon and soot in flames and engine exhaust. *Aerosol Sci. Technol.* **2014**, *48*, 620-629.
155. Kim, J.; Bauer, H.; Dobovičnik, T.; Hitzenberger, R.; Lottin, D.; Ferry, D.; Petzold, A. Assessing optical properties and refractive index of combustion aerosol particles through combined experimental and modeling studies. *Aerosol Science and Technology* **2015**, *49*, 340-350, doi:10.1080/02786826.2015.1020996.

156. Lu, Z.; Streets, D.G.; Winijkul, E.; Yan, F.; Chen, Y.; Bond, T.C.; Feng, Y.; Dubey, M.K.; Liu, S.; Pinto, J.P.; et al. Light absorption properties and radiative effects of primary organic aerosol emissions. *Environmental Science and Technology* **2015**, *49*, 4868-4877, doi:10.1021/acs.est.5b00211.
157. Moore, R.H.; Ziemba, L.D.; Dutcher, D.; Beyersdorf, A.J.; Chan, K.; Crumeyrolle, S.; Raymond, T.M.; Thornhill, K.L.; Winstead, E.L.; Anderson, B.E. Mapping the operation of the miniature combustion aerosol standard (Mini-CAST) soot generator. *Aerosol Science and Technology* **2014**, *48*, 467-479, doi:10.1080/02786826.2014.890694.
158. Presto, A.A.; Hartz, K.E.H.; Donahue, N.M. Secondary organic aerosol production from terpene ozonolysis. 2. Effect of NOx concentration. *Environ. Sci. Technol.* **2005**, *39*, 7046-7054, doi:10.1021/es050400s.
159. Takeuchi, M.; Ng, N.L. Organic Nitrates and Secondary Organic Aerosol (SOA) Formation from Oxidation of Biogenic Volatile Organic Compounds. In *Multiphase Environmental Chemistry in the Atmosphere*; ACS Symposium Series; American Chemical Society: 2018; Volume 1299, pp. 105-125.
160. Ng, N.L.; Kroll, J.H.; Chan, A.W.H.; Chhabra, P.S.; Flagan, R.C.; Seinfeld, J.H. Secondary organic aerosol formation from m-xylene, toluene, and benzene. *Atmos. Chem. Phys.* **2007**, *7*, 3909-3922, doi:10.5194/acp-7-3909-2007.
161. McNeill, V.F.; Woo, J.L.; Kim, D.D.; Schwier, A.N.; Wannell, N.J.; Sumner, A.J.; Barakat, J.M. Aqueous-Phase Secondary Organic Aerosol and Organosulfate Formation in Atmospheric Aerosols: A Modeling Study. *Environ. Sci. Technol.* **2012**, *46*, 8075-8081, doi:10.1021/es3002986.
162. Kroflič, A.; Anders, J.; Drventić, I.; Mettke, P.; Böge, O.; Mutzel, A.; Kleffmann, J.; Herrmann, H. Guaiacol Nitration in a Simulated Atmospheric Aerosol with an Emphasis on Atmospheric Nitrophenol Formation Mechanisms. *ACS Earth and Space Chemistry* **2021**, *5*, 1083-1093, doi:10.1021/acsearthspacechem.1c00014.
163. Kitanovski, Z.; Grgić, I.; Vermeylen, R.; Claeys, M.; Maenhaut, W. Liquid chromatography tandem mass spectrometry method for characterization of monoaromatic nitro-compounds in atmospheric particulate matter. *Journal of Chromatography A* **2012**, *1268*, 35-43, doi:10.1016/j.chroma.2012.10.021.
164. Bluvshtein, N.; Lin, P.; Michel Flores, J.; Segev, L.; Mazar, Y.; Tas, E.; Snider, G.; Weagle, C.; Brown, S.S.; Laskin, A.; et al. Broadband optical properties of biomass-burning aerosol and identification of brown carbon chromophores. *Journal of Geophysical Research* **2017**, *122*, 5441-5456, doi:10.1002/2016JD026230.
165. Sun, Y.L.; Zhang, Q.; Anastasio, C.; Sun, J. Insights into secondary organic aerosol formed via aqueous-phase reactions of phenolic compounds based on high resolution mass spectrometry. *Atmos. Chem. Phys.* **2010**, *10*, 4809-4822, doi:10.5194/acp-10-4809-2010.
166. Ofner, J.; Kŕuger, H.U.; Grothe, H.; Schmitt-Kopplin, P.; Whitmore, K.; Zetzsch, C. Physico-chemical characterization of SOA derived from catechol and guaiacol - A model substance for the aromatic fraction of atmospheric HULIS. *Atmos. Chem. Phys.* **2011**, *11*, 1-15, doi:10.5194/acp-11-1-2011.
167. Yee, L.D.; Kautzman, K.E.; Loza, C.L.; Schilling, K.A.; Coggon, M.M.; Chhabra, P.S.; Chan, M.N.; Chan, A.W.H.; Hersey, S.P.; Crounse, J.D.; et al. Secondary organic aerosol formation from biomass burning intermediates: Phenol and methoxyphenols. *Atmos. Chem. Phys.* **2013**, *13*, 8019-8043, doi:10.5194/acp-13-8019-2013.
168. Wang, Y.; Hu, M.; Wang, Y.; Zheng, J.; Shang, D.; Yang, Y.; Liu, Y.; Li, X.; Tang, R.; Zhu, W.; et al. The formation of nitro-aromatic compounds under high NOx and anthropogenic VOC conditions in urban Beijing, China. *Atmos. Chem. Phys.* **2019**, *19*, 7649-7665, doi:10.5194/acp-19-7649-2019.

169. Jenkin, M.E.; Saunders, S.M.; Wagner, V.; Pilling, M.J. Protocol for the development of the Master Chemical Mechanism, MCM v3 (Part B): Tropospheric degradation of aromatic volatile organic compounds. *Atmos. Chem. Phys.* **2003**, *3*, 181-193, doi:10.5194/acp-3-181-2003.
170. Frka, S.; Šala, M.; Kroflič, A.; Huš, M.; Čusak, A.; Grgić, I. Quantum Chemical Calculations Resolved Identification of Methylnitrocatechols in Atmospheric Aerosols. *Environmental Science and Technology* **2016**, *50*, 5526-5535, doi:10.1021/acs.est.6b00823.
171. Ji, Y.; Zhao, J.; Terazono, H.; Misawa, K.; Levitt, N.P.; Li, Y.; Lin, Y.; Peng, J.; Wang, Y.; Duan, L.; et al. Reassessing the atmospheric oxidation mechanism of toluene. *Proc. Natl. Acad. Sci. U. S. A.* **2017**, *114*, 8169-8174, doi:10.1073/pnas.1705463114.
172. Finewax, Z.; De Gouw, J.A.; Ziemann, P.J. Identification and Quantification of 4-Nitrocatechol Formed from OH and NO3 Radical-Initiated Reactions of Catechol in Air in the Presence of NOx: Implications for Secondary Organic Aerosol Formation from Biomass Burning. *Environmental Science and Technology* **2018**, *52*, 1981-1989, doi:10.1021/acs.est.7b05864.
173. Vidović, K.; Kroflič, A.; Jovanovič, P.; Šala, M.; Grgić, I. Electrochemistry as a Tool for Studies of Complex Reaction Mechanisms: The Case of the Atmospheric Aqueous-Phase Aging of Catechols. *Environmental Science and Technology* **2019**, doi:10.1021/acs.est.9b02456.
174. Lauraguais, A.; Coeur-Tourneur, C.; Cassez, A.; Deboudt, K.; Fourmentin, M.; Choël, M. Atmospheric reactivity of hydroxyl radicals with guaiacol (2-methoxyphenol), a biomass burning emitted compound: Secondary organic aerosol formation and gas-phase oxidation products. *Atmos. Environ.* **2014**, *86*, 155-163, doi:10.1016/j.atmosenv.2013.11.074.
175. NISTWebBook. NIST Chemistry WebBook. Available online: https://webbook.nist.gov/chemistry/mw-ser/ (accessed on 23 Nov).
176. Montoya-Aguilera, J.; Horne, J.R.; Hinks, M.L.; Fleming, L.T.; Perraud, V.; Lin, P.; Laskin, A.; Laskin, J.; Dabdub, D.; Nizkorodov, S.A. Secondary organic aerosol from atmospheric photooxidation of indole. *Atmos. Chem. Phys.* **2017**, *17*, 11605-11621, doi:10.5194/acp-17-11605-2017.
177. Etchie, T.O.; Etchie, A.T.; Sivanesan, S.; Adewuyi, G.O.; Krishnamurthi, K.; Pillarisetti, A.; George, K.V.; Rao, P.S. Dangerous organic chemicals identified in inhalable particulate matter air pollution. In Proceedings of the IOP Conference Series: Materials Science and Engineering, 2019.
178. Markus, B.; Kwon, C.H. in vitro metabolism of aromatic nitriles. *Journal of Pharmaceutical Sciences* **1994**, *83*, 1729-1734, doi:10.1002/jps.2600831216.
179. Wu, R.; Pan, S.; Li, Y.; Wang, L. Atmospheric oxidation mechanism of toluene. *Journal of Physical Chemistry A* **2014**, *118*, 4533-4547, doi:10.1021/jp500077f.
180. Bloss, C.; Wagner, V.; Jenkin, M.E.; Volkamer, R.; Bloss, W.J.; Lee, J.D.; Heard, D.E.; Wirtz, K.; Martin-Reviejo, M.; Rea, G.; et al. Development of a detailed chemical mechanism (MCMv3.1) for the atmospheric oxidation of aromatic hydrocarbons. *Atmos. Chem. Phys.* **2005**, *5*, 641-664, doi:10.5194/acp-5-641-2005.

PART- II

Appended Papers